Klinik für Orthopädie und Unfallchirurgie
des Klinikums rechts der Isar der
Technischen Universität München
(Direktor: Univ.-Prof. Dr. R. Gradinger)

„Biomechanical Evaluation of the Femoral Strain Patterns After Implantation of Cemented Stems in Comparison to the Strain Patterns After Implantation of Cementless Stems. A Photoelastic study“

Wahid Fahmy Deryas

Vollständiger Abdruck der von der Fakultät für **Medizin der Technischen Universität München** zur Erlangung des akademischen Grades eines
Doktors der Medizin (Dr. med.)
genehmigten Dissertation.

Vorsitzender:	Univ.- Prof. Dr. D. Neumeier
Prüfer der Dissertation:	1. Univ.- Prof. Dr. R. Gradinger
	2. apl. Prof. Dr. H.P. Rechl

Die Dissertation wurde am 10.08.2006 bei der Technischen Universität München
eingereicht und durch die Fakultät für Medizin am 15.11.2006 angenommen

Contents

1. Introduction

Total hip arthroplasty is the most commonly performed reconstructive hip procedure commonly used for pain relief and restoration of lifestyle due to the debilitating disease of Osteoarthritis and for disabling effects of rheumatoid arthritis, congenital deformities, and particular kinds of posttraumatic conditions. Osteoarthritis is the most frequent indication for joint replacement, comprising about 65% of the total volume [41 p. 375].

In the early 20th Century, the use of biological and inorganic materials for hip arthroplasty became popular. Deformed or ankylosed joint surfaces were contoured and an interpositional layer inserted to resurface the joint and allow motion.

In the United States and Europe, grafts of fascia lata and periarticular soft tissues were used in 1912. Sir Robert Jones used gold foil. Results remained unpredictable, with residual pain and stiffness being causes of failure. In 1923, Smith Peterson introduced the concept of "mould arthroplasty" as an alternative to the interpositional membrane. The procedure was intended to restore congruous articular surface by exposing bleeding cancellous bone of the femoral head and acetabulum, with subsequent metaplasia of the fibrin clot to fibrocartilage under the influence of gentle motion.

Glass was chosen as the material for the first mould, after Smith-Petersen discovered a smooth synovial membrane surrounding a glass foreign body removed from a patient back. Although all the glass molds implanted broke within a few months, the initial results were encouraged and promoted a search for more durable materials. Pyrex, viscalloid (a celluloid derivative) and Bakelite version also were discarded fragility or severe foreign body reaction. In 1937 after the development of Vitallium by Venable and Stuck, implants of sufficient durability became available [66 p. 297].

In 1960 Charnley demonstrated the use of an acrylic polymer for fixation, thus long-term stability of metal implants was realised. This concept of initial rigid fixation was an essential step in the improved viability of the interamedullary hip prosthesis [44 p. 1655].

The popularity of the Charnley technique is due to its very high rate of success in the older population [46 p. 130, 48 p. 61]. However, a much lower rate has been reported in younger patients [10 p. 713].

The Charnley total hip arthroplasty results are the benchmark for evaluating the performance of other arthroplasties. The laboratory and clinical contributions of Sir John Charnley have improved the quality of life for many patients. In total hip replacement the surgeon can use different techniques for fixation of the implants, cementless, cemented and hybrid by using a cementless porous-coated acetabular component and a cemented femoral component. In 1989, Davey and Harris proved the advantage of hybrid total hip in some patients [19 p. 152, 46 p. 130]. There is no doubt that primary total hip arthroplasty offers the best chance of success, therefore selection of the appropriate implants and technical precision are utmost important [66 p. 300].

The function of total hip arthroplasty is to transfer load from acetabulum to the femur and to provide an adequate range of motion and sufficient stability. In total hip arthroplasty, the surgeon should be familiar with the many technical details of the operations. However, to successfully contend with the various problems that occur and to evaluate new concepts and implants, a working knowledge of biomechanical principles, materials, and design also is necessary.

2. Objective

Regarding to the most common causes of failure of total hip arthroplasty, beside infection, dislocation of the joint and presence of polyethylene wear, aseptic loosening of the implant is considered as one of the most important causes. It is a gradual process in which the biomechanical integrity of the bone-implant interface will be affected. The main four causes of aseptic loosening are; mechanical failure of the implant or cement, presence of wear debris in the interface region, relative motion across the interface, and stress shielding. Each of these causes leads to bone remodelling and resorption with loosening of the implant [44 p. 1655]. The most common mechanism is the enlargement of the endosteal surface [33 p. 122]. The stem will act as a rigid body when fitted to the femur, as there is one order of different magnitude between the stiffness of the stem and that of the cortical bone [15 p. 412].

Stress shielding: is the alteration of the stress pattern induced by an endoprosthesis, with respect to the physiological conditions.

Bone remodelling: is the complex of concurring biological processes that lead to bone density and geometry adaptation.

Bone resorption: is alteration of bone density and geometry deriving from unbalanced bone remodelling toward bone loss [15 p. 410]. Bone resorption is the physical manifestation of the stress shielding according to Wolf's Law [6 p. 79]. In 1988 Engh remarked that bone resorption tends to stabilise after the first one or two years [23 p. 22].

A long-standing concern with total hip arthroplasty is the possibility of resorptive bone remodelling secondary to proximal stress shielding and in long term causes problems such as loss of implant support, implant subsidence, and implant or bone fracture [6 p. 79].

Normally and in the intact femur, the stress will occur as a result of forces coming through the hip joint to the neck and then transfers through the metaphyseal trabecular structure to the cortical bone of the diaphysis. In total hip replacement and after implantation of the femur by an implant of different mechanical properties, the stress and strain in the femur will be changed even with fixed external load. According to Wolf's Law, a strain-adaptive bone remodelling process will occur and changes the internal structural organisation and shape to

adapt to the new mechanical requirement. After intramedullary implantation of the stem, the implant will not adapt with the bone and the load-transfer mechanism will be changed [39 p. 118, 41 p. 398]. This remodelling, in turn will change the strain and stress in bone till an equilibrium state is eventually reached [75 p. 81]. After implantation, the load on the hip joint now is transferred to the artificial femoral head then through the stem and from the stem to the femoral shaft and what was carried before by the bone alone, is now shared with the stem. As a consequence, the bone is subjected to reduced stress, hence stress shielded [37 p. 124]. The bone is shielded by the stem from the stress it is normally subjected to. In the intact femur, stresses are the highest at the proximal part and are decreased distally. After stem implantation, the reverse will occur. In order to restore stress distribution to normal and according to the adaptive bone remodelling theory, bone resorption and remodelling will occur, and loss of cortical bone will be in areas of reduced stress and lead to bone fracture and stem failure with difficult problems for reconstruction in the future [39 p. 118].

3. Aim of the Project

Aim of this study is a biomechanical research, in which the femoral strain patterns before and after implantation was investigated by photo elastic analysis.

Aim of the project was divided into three sections according to following implants:

(A) Cemented and cementless stems with different sizes (Type GHE-ESKA Implants GmbH)

1. The femoral strain patterns after implantation of cemented stems, with different, sizes and neck lengths (offset).

2. The femoral strain patterns after implantation of cemented and cementless partial porous coated stems.

(B) Cementless "Custom-made" stems with different sizes and shapes (Adaptiva®- Individual endoprosthesis-System) from endoPro medical GmbH, where the femoral strain patterns were investigated after implantation of three different stems.

(C) Comparison between cementless standard, custom-made and GHE stems.

After this study it can be suggested, the proper implant selection for total hip arthroplasty by which more physiological stress in the proximal femur was obtained with less stress shielding. As mentioned before about the stress shielding, it is one of the important causes of failure of total hip arthroplasty particularly among younger patients and because it is considered as a major long-term problem related to the technical and biomechanical issues, therefore it has an interest in the biomechanics.
In this in vitro experimental study, the strain values that occur immediately after stem implantation are considered without the long-term bone adaptation, which requires many cycles of dynamic loads by gait.

4. Basic Anatomy of the Hip Joint

[57 p. 135-137,*]

4. 1. Bones and Ligaments of the Hip

The hip joint is a multi axial ball and socket synovial joint, composed of the head of the femur and the acetabulum of the pelvis. This articulation has a loose fibrous capsule and is surrounded by large and strong muscles.

The femoral head:

Is the convex component and constitutes two third of a sphere. It is covered by articular cartilage that is thick centrally and thin peripherally. It is composed mainly of cancellous bone covered by a very thin cortical layer of about 0.2 mm thickness [42 p. 161].

The acetabulum:

Is the concave component and is covered with articular cartilage that is thin centrally and thick peripherally. These differences in the mechanical properties from point to point on the femoral head cartilage may influence the transmission from the acetabulum through the femoral head to the femoral neck. The opposing surfaces are regular and reciprocally curved, and only 2/5 of the femoral head occupies the acetabulum.

The labrum:

Converts the bony acetabulum into a true hemisphere and thus is increasing joint stability.

The femoral neck:

The interior of the neck is formed of cancellous bone with trabeculae arranged into medial and lateral trabecular system. Two important angels are formed by the femoral neck and the femoral shaft.

* SUNY Upstate Medical University, (2000), Functional Anatomy of the hip joint, http://www.upstate.edu/cdb/grossanat/limbs7.shtml, Stand: 16.07.2006

The neck shaft angle:

Is the angle of inclination of the neck to the shaft in the frontal plane which offsets the femoral shaft from the pelvis laterally. In adults this angle is about 125 degrees, but it can vary from 90 to 135 degrees. An angle more than 125 degrees results in coxa valga, and less than 125 degrees results in coxa vara. With ageing, degenerative changes will occur where the cortical bone will be thinned and the trabeculae will be resorbed and these changes may cause fracture of the neck.

The angle of anteversion:

It is formed as a projection of the long axis of the head and the transverse axis of the femoral condyles. In adults it is about 12 degrees, but it varies a great deal. If it is more than 12 degrees, produces a tendency to internal rotation of the leg during gait to keep the femoral head in the acetabular cavity. If it is less than 12 degrees, produces a tendency to external rotation of the leg during gait.

The fibrous capsule:

It has proximal attachment where it encircles the rim of the acetabulum, distal attachment, anteriorly to the greater trochanter and inter trochanteric line and posteriorly to the neck of the femur. The capsule is incomplete posteriorly.

There are three ligaments around the hip joint:

1- Iliofemoral ligament, arises from anterior inferior iliac spine and inserts into inter trochanteric line where it covers the hip joint anteriorly.

2- Pubofemoral ligament arises from pubic bone and margin of obturator foramen and inserts into the femoral neck deep to the iliofemoral ligament where it covers the hip joint anteriorly.

3- Ischiofemoral ligament arises from the ischium and inserts into the greater trochanter of the femur where it covers the hip joint posteriorly.

These ligaments are very important for the stability of the hip and limitation of the movement where the iliofemoral ligament resists hyperextension. Its lateral band limits adduction and the medial band limits lateral rotation. The pubofemoral ligament limits abduction. The ischiofemoral ligament limits medial rotation.

Fractures / Dislocation:

1. **Fracture of femoral neck**

- could disrupt retinacula and blood supply to femoral head
- avascular necrosis of the femoral head
- limb outwardly rotated

2. **Dislocation**

- limb is shortened and inwardly rotated

Cruciate anastomosis:

(collateral circulation posterior to hip joint) from the inferior gluteal artery and the deep femoral artery by three branches, transverse branch of lateral femoral circumflex artery, medial femoral circumflex artery and recurrent branch of the first perforating artery.

4. 2. Movements and Muscles around the Hip

Flexion and extension are in sagittal plane. Transverse axis through the femoral head. Range of flexion is from zero to 140 degrees. The following muscles will initiate flexion, tensor fascia late, pectineus, sartorius and gracilis. Iliopsoas muscle will complete the flexion. Range of extension is from zero to 15 degrees. The following muscles produce extension, gluteus maximus, hamstring and the posterior part of the adductor magnus.

Adduction and abduction are in frontal planes. Rotations are around anterior posterior axis through the femoral head.

Adduction by the following muscles: adductors longus, adductor brevis, adductor magnus and gracilis. Range of adduction is from zero to 25 degrees.

Abduction by gluteus medius and gluteus minimus. Range of abduction is from zero to 30 degrees.

Internal and external rotation in transverse plane. Vertical axis through the femoral head and lateral femoral condyle.

Internal rotation by gluteus minimus and tensor fascia lata. Range of internal rotation is from zero to 70 degrees.

External rotation by the following muscles, gluteus maximus, piriformis, obturator externus, obturator internus, superior gemellus, inferior gemellus, quadratus femoris and gluteus medius. Range of external rotation is from zero to 90 degrees.

4. 3. Clinical Importance of the Hip Muscles during Gait

During acceleration and heel strike, eccentric contraction of hamstring and gluteus maximus muscles will restrain the lower limp forward and by this action, the hip will be in a flexed position. Contraction of the gluteus medius and gluteus minimus (abductors muscles) will abduct the reference limb from a weight bearing position. The iliac crest will move but the femur can not move because at heel strike, it is a weight bearing position and the foot is in contact with the ground. Concomitantly, the non weight bearing hip is “hiked“ upward and counterbalances the effect of the gravity. Without the concentric contraction of the abductor muscles of the weight bearing limb, the other limb would tilt downward. This is called “Trendelenburg Gait.”

During toe off to acceleration interval, the reference limp goes from weight bearing to non weight bearing. Concentric contraction of the hip flexors specially the iliopsoas muscle and also by contraction of the adductor, the hip will be in flexion. Also by contraction the adductors bring the swinging limp in an internal rotation, and the foot will be under the pelvis rather than parallel with the shoulder.

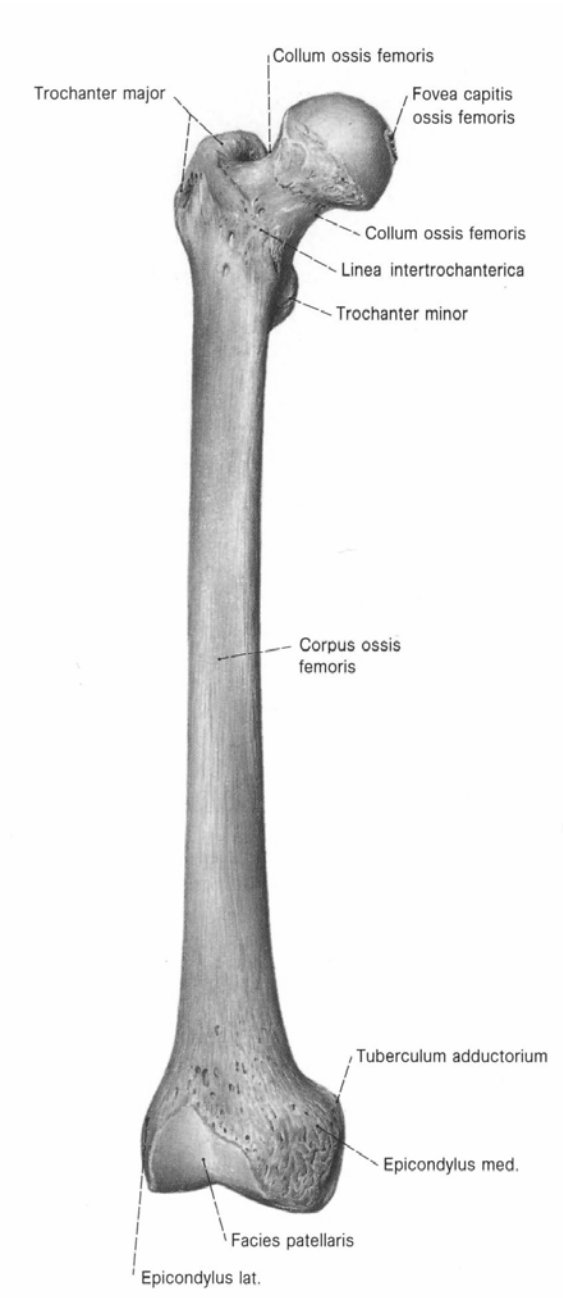

Fig. 1: Right femur (anterior view)

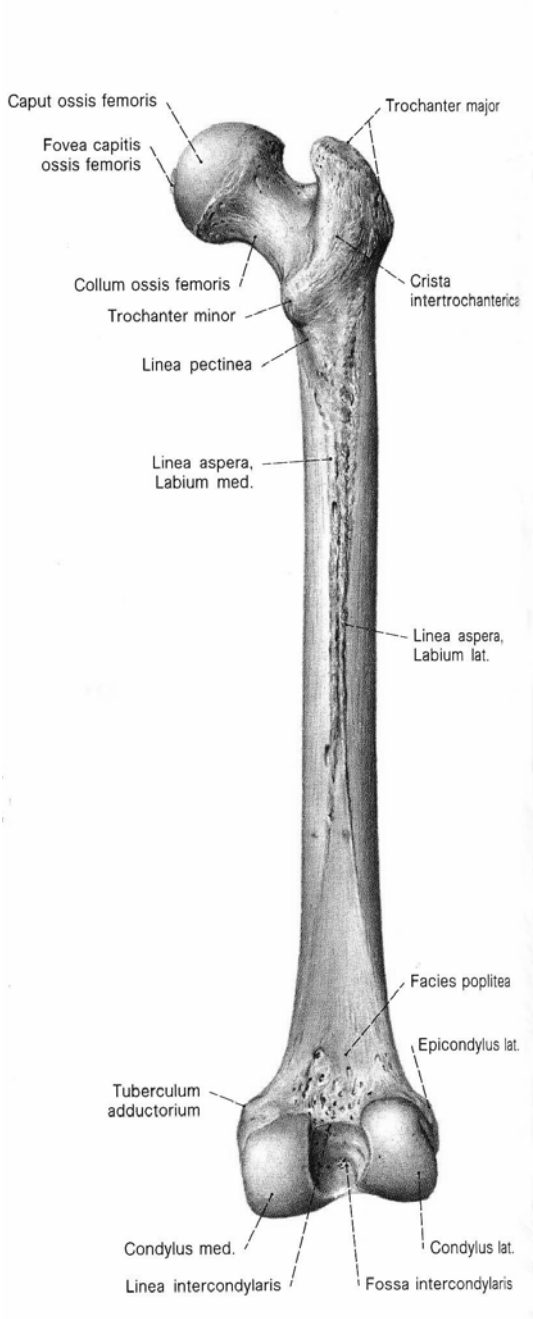

Fig. 2: Right femur (posterior view)

From [64 p. 256]

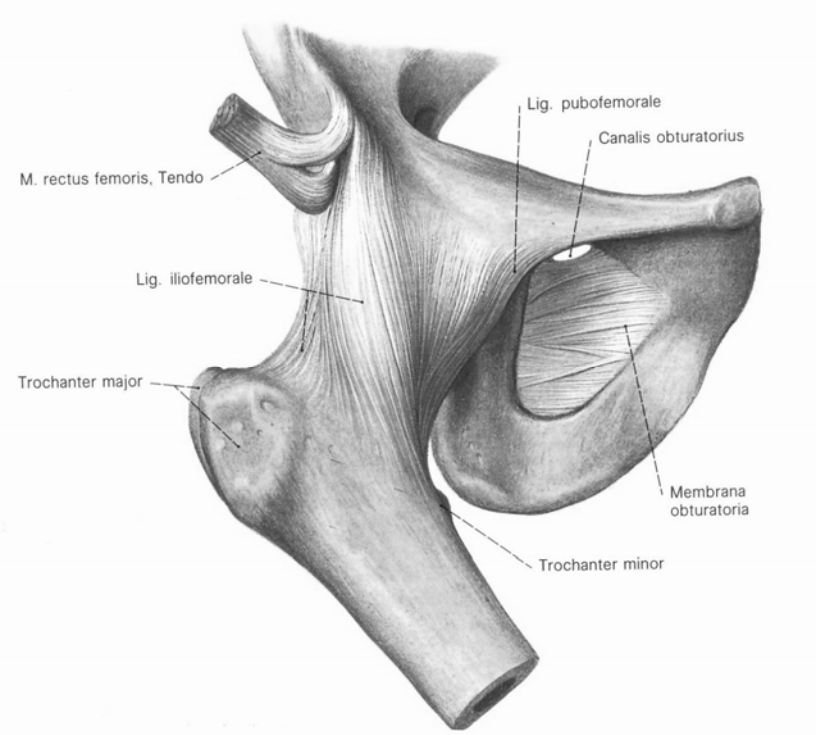

Fig. 3: The right articulatio coxae with the femur [os femoris] markedly adducted (anterior view).

From [64 P. 258]

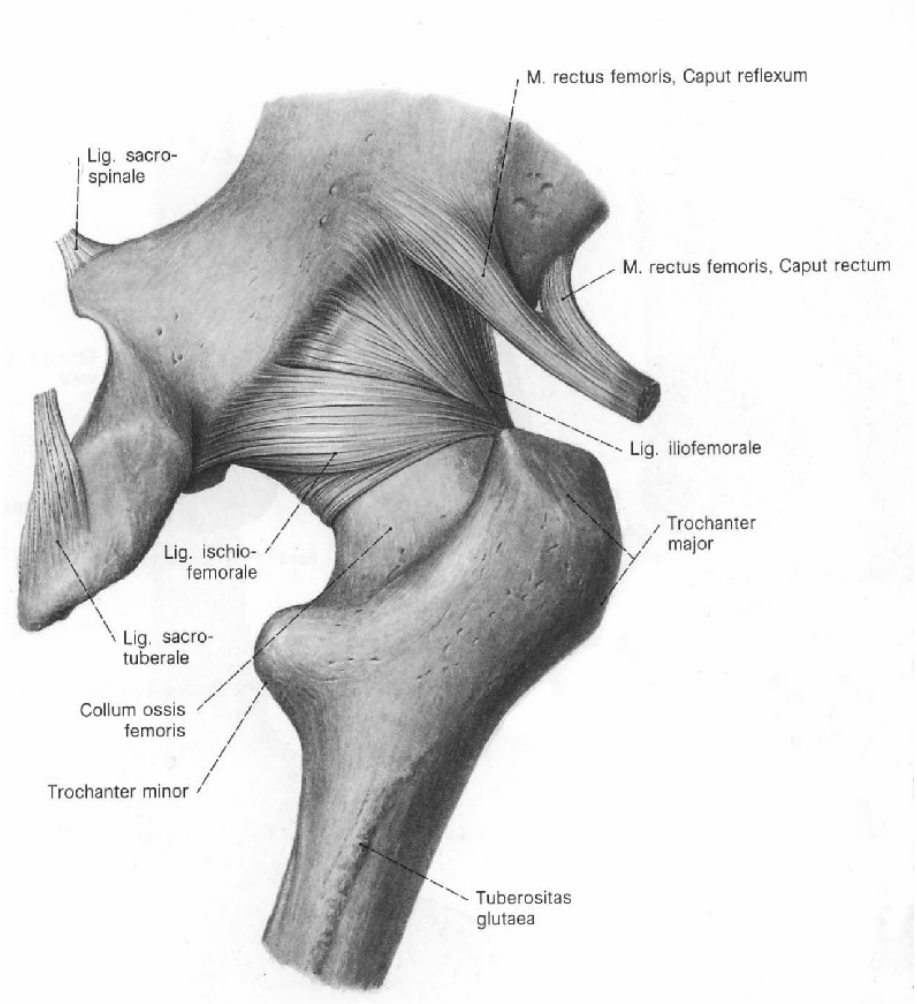

Fig. 4: The right articulatio coxae (posterior view). From [64 p. 258]

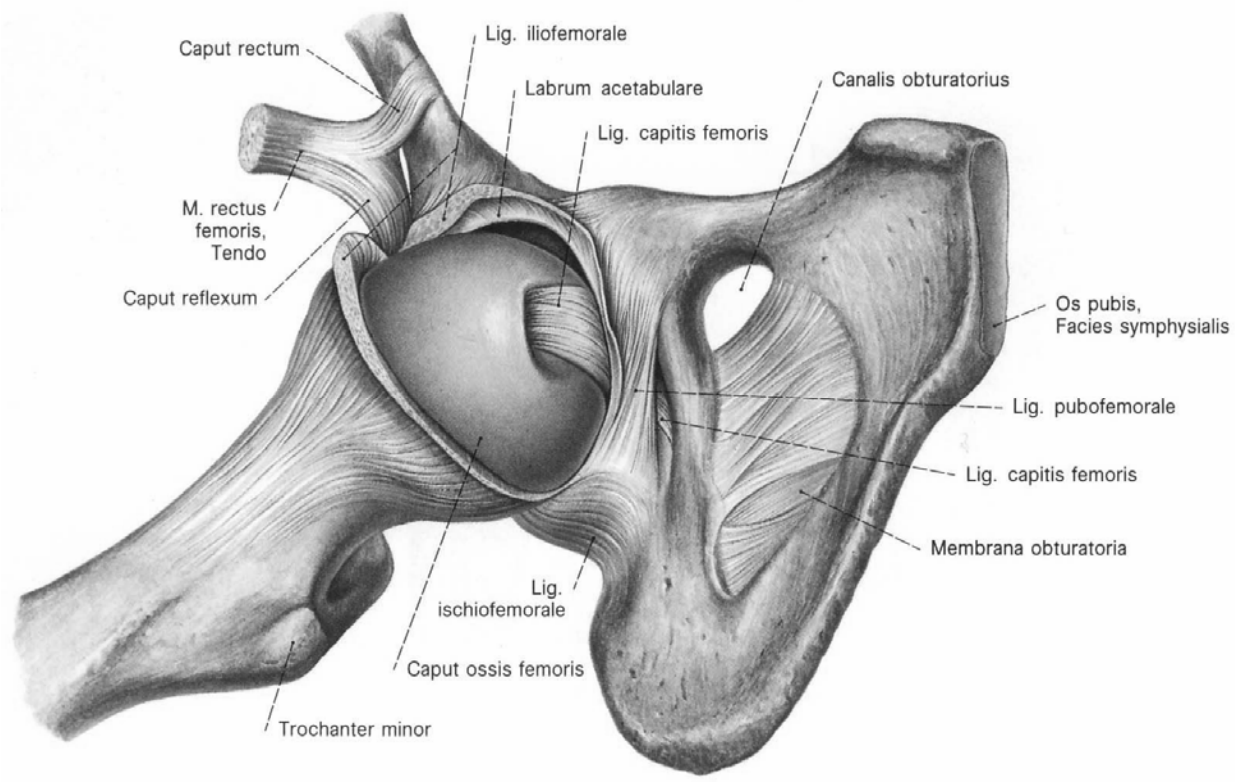

Fig. 5: Right articulatio coxae after opening the anterior aspect of the capsula articularis. To expose the ligamentum capitis femoris, the caput ossis femoris was pulled out from the acetabulum and forcibly rotated dorsolaterally [64 p. 258].

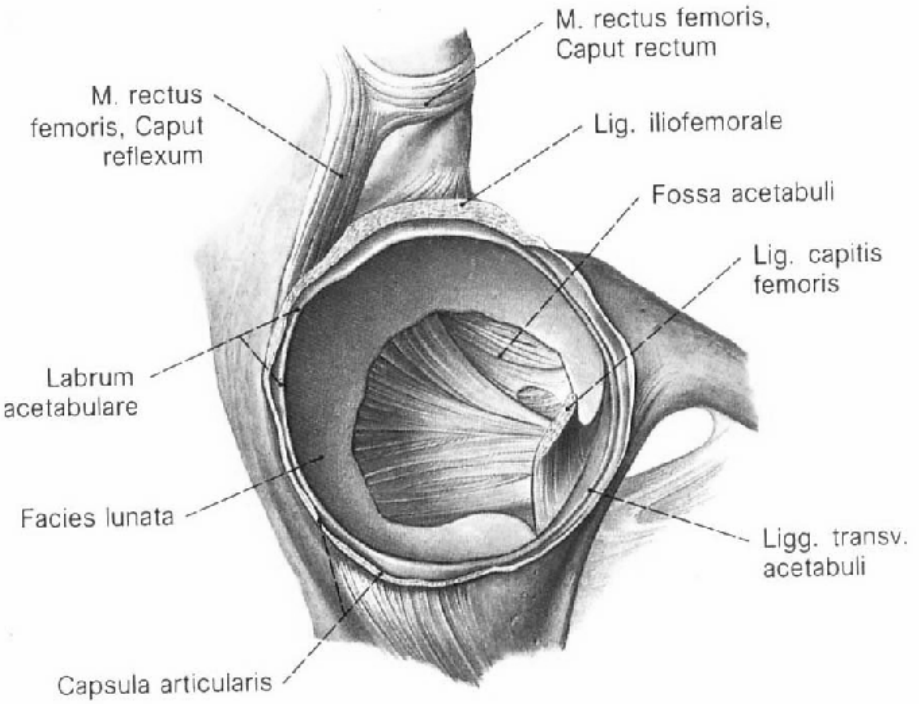

Fig. 6: The acetabulum of the right articulatio coxae after severing the capsula articularis and the ligamentum capitis femoris. The caput ossis femoris has been removed [64 p. 258].

5. Biomechanics of the Hip [57 p. 135-149]

5. 1. Stabilisation of the Hip Joint

The hip joint capsule and ligaments, specially the iliofemoral ligament, are the static stabilisers of the hip. In extension they help the joint to assume a stable position. The hip joint muscles, specially the abductors, are the dynamic stabilisers of the hip. Concerning the biomechanical analysis, the abductor muscles are the most important muscles where they affect the hip joint forces across the hip to stabilise the pelvis during walking [57 p. 141, 146]

5. 2. The Hip Joint Reaction Force in Stance Phases

During a two-leg stance phase, the line of gravity will be posterior to the symphysis pubes. The static stabilisers of the hip give stability to the joint and keep it in an erect stance without muscle contraction. The joint reaction force in each femoral head will equal to one half of the weight of the super incumbent body. Because each lower limp is one sixth of the body weight, the joint reaction force will equal to the remaining two thirds or one third of the body weight. In prolonged standing and by contraction of the hip joint muscles to maintain an upright position, the joint force will increase according to the muscle activity. Davy in 1988 measured 0.86 BW hip forces for double leg-stance phase and 2.1 BW for single leg-stance phase [57 p. 141, 20 p. 47]. During single-leg stance phase, there are three external forces acting on the body in equilibrium. The ground reaction force is equal to body weight (W). The gravitational force of the stance leg is equal to one sixth of the body weight (1/6 W) and the remaining force is equal to five sixth of the body weight (5/6 W). The joint reaction force will increase, due to shifting of the line of the gravity to all three planes and producing moments around the joint that should be antagonised by the joint force. Joint force depends on inclination of the pelvis, posture of the spine, position of the non-weight bearing leg and the upper extremities [51 p. 208]. McLeish and Charnley proved that the joint force is at an angle to the vertical varying from 7 to 10 degrees and with the femoral axis from 19 to 22 degrees [51 p. 207]. By inclination of the shoulders toward the supporting hip, the gravitational force lever arm (the perpendicular distance between the centre of rotation of the femoral head and the line of the gravity) will decrease and hence both moment and joint reaction force of the hip are also decreased.

5. 3. Simplified Free Body Technique for Coplanar Forces

This technique is used for estimation of the joint force with the pelvis in neutral position. The stance limp is considered as a free body. There are three main coplanar forces acting on the body.

The ground reaction force (W)

It is transmitted to the femoral condyles, through the tibia. It has a known magnitude equal to five sixth of the body weight, a known sense, line and point of application.

The abductor muscle force (M)

It has a known sense, a known line of application and point of application detected from the muscle origin and insertion on the x-ray, but it has an unknown magnitude. During stance phase of the gait, the abductor muscles (gluteus medius and minimus) are the primary supporters of the pelvis [26 p. 751].

The joint reaction force (J)

It has a known point of application on the surface of the femoral head, but an unknown magnitude, sense and line of application. By drawing and designating the three forces on the free body diagram and a triangle, it is found that the muscle force is approximately two times body weight and the joint reaction force is about 2.75 body weight. Although horizontal forces in sagittal plane are present, the main forces acting on the hip joint lie mainly in the frontal plane. However, McLeish and Charnley (1970) applied the static equilibrium approach to investigate the force and moments for different pelvis attitudes. They reported a 2.2 to 2.3 BW hip force at an angle of 20 to 25 degrees to the femoral axis and a 1.3 to 1.6 BW abducting force at 26 to 30 degrees to the femoral axis.

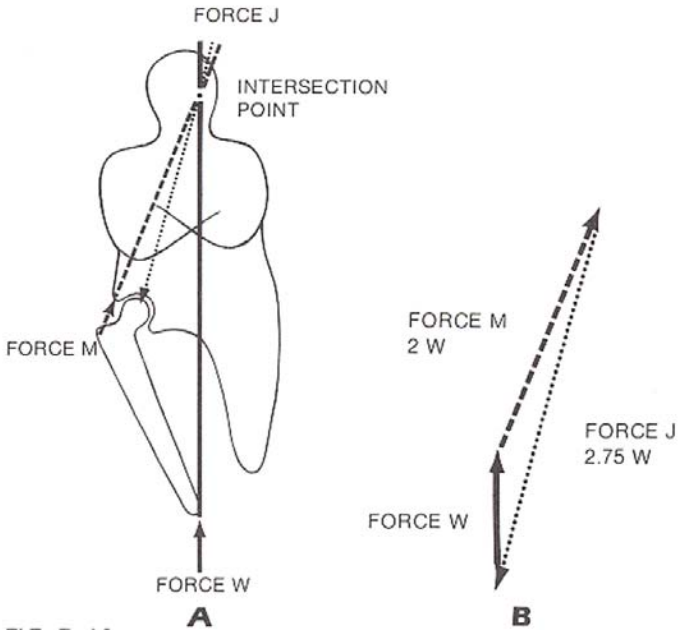

Fig. 7: [from 57 p. 142]

A. Diagram of the upper body and supporting lower extremity, the lines of application for W and M are extend till points of intersection. The line of application for J is then determined by connecting its point of application with the intersection point for W and M.

B. Triangle of forces. The magnitudes of M and J can be scaled from W (body weight).
Force M is about two times of the body weight, and force J is about 2.75 times of the body weight.

5. 4. Mathematical Method Utilising Equilibrium Equations.

When the body is in equilibrium, the ground reaction force is equal to the gravitational force of the body, where the gravitational force of the stance leg is equal to one sixth body weight and the remaining force is equal to five sixths of body weight [see below, fig. (8-A)].

The internal forces acting on the hip joint were found by separating the joint into an upper and lower free body. Regarding to the upper free body, the moment of equilibrium occurs by counterbalance between the moment arising from the abductor muscles force (M × C) and the moment arising from the gravitational force of the super incumbent body (5/6 W× b), which tilt the pelvis away from the supporting lower extremity [fig. (8-B)].

The direction of the abductor muscle force was found to be 30 degrees from the vertical. By vector analysis, it was proved that the horizontal component of (M_x) is equal to body weight and the vertical component (M_y) is about 1.7 times of body weight [fig. (8-C)].

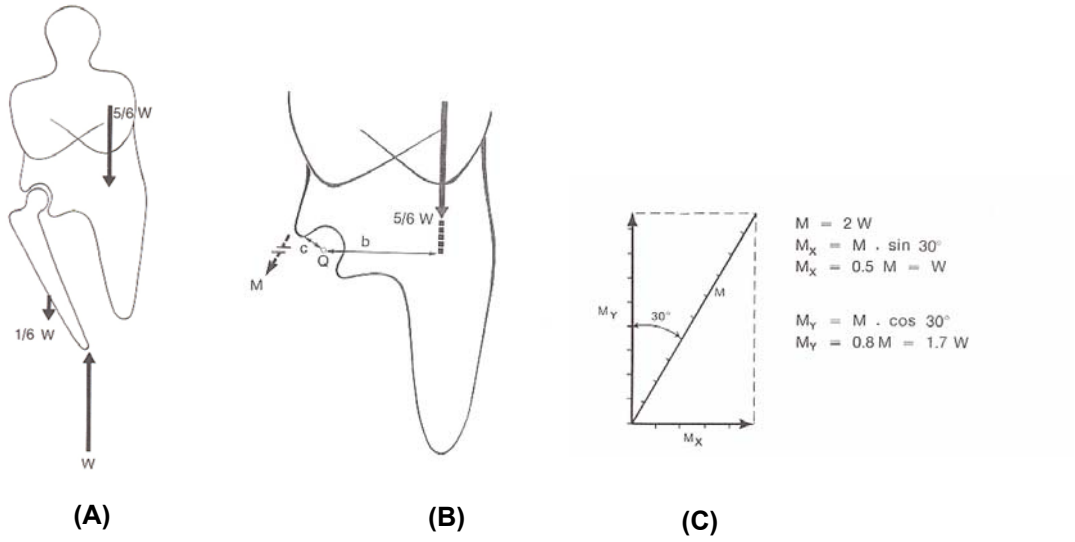

Fig. 8: [from 57 p. 143] (W) is equal to body weight. (M) Abductor muscle force. (C) Abductor force lever arm. (Q) Centre of rotation in the femoral head.
(B) Gravitational force lever arm. (5/6 W) Gravitational force of the body above the hip joint.
(M_x) and (M_y) represent the magnitudes of the abductor muscles components, horizontal and vertical respectively.

Regarding to the lower free body, because the body is in equilibrium, the sum of the horizontal forces must equal zero and also for what are in the vertical direction.

$M_x - J_x = 0$ $\qquad$ $M_y - J_y - 1/6\ W + W = 0$

$M_x = J_x$ $\qquad$ $M_y = 1.7\ W$

$M_x = W$ $\qquad$ $J_y = 1.7\ W + 5/6\ W$

$J_x = W$ $\qquad$ $J_y = 2.5\ W$

By vector analysis, it was proved that the joint reaction force on the femoral head in a single-leg stance is about 2.7 times of body weight, and its direction is 69 degrees from the horizontal. The joint reaction force depends on the relationship between the abductor muscle force lever arm and the gravitational force lever arm.
A small ratio (i.e., a small muscle force lever arm and a large gravitational force lever arm) will increase the joint reaction force, which will decrease with high ratio. This ratio was determined before and after joint replacement in a single-leg stance. After hip replacement, the line of gravity for the super incumbent body will shift laterally away from the affected side, resulting in increase of the gravitational force lever arm and increase of the joint reaction force.

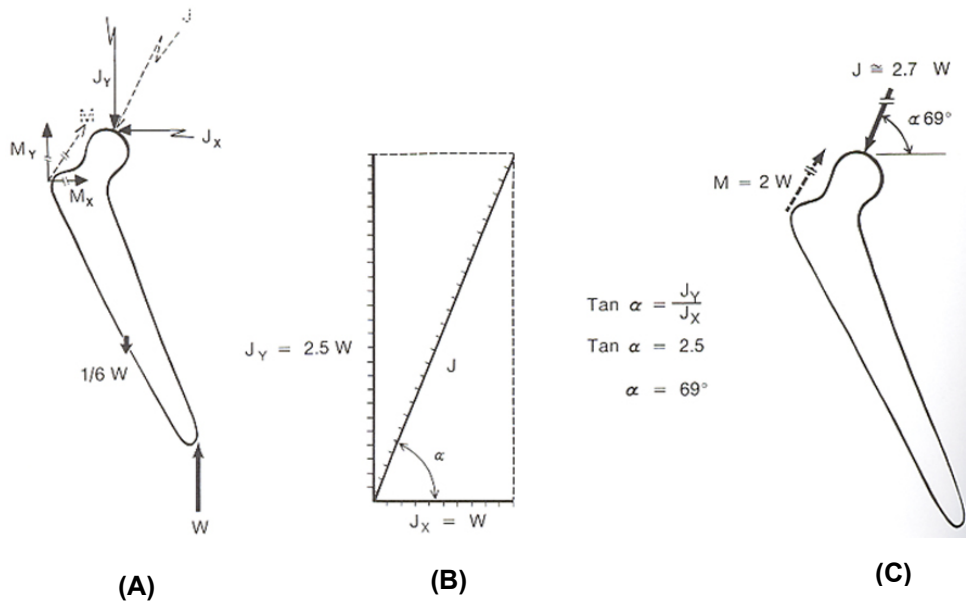

Fig. 9

A. Forces acting in the lower free body are divided into horizontal and vertical components. The magnitudes of J_y and J_x are found from force equilibrium equations.

B. Addition of the horizontal and vertical components J_y and J_x is performed graphically and the joint reaction force (J) is scaled off. The joint force direction is measured on the parallelogram of force, alternately trigonometry is used to find the direction of J.

C. The magnitude of the joint reaction force approximately 2.7 W and acts at an angle of 69 degrees from the horizontal [57 p. 144].

5. 5. Hip Joint Force during Dynamic Movements.

Bergmann in 1993, measured the resultant hip joint force, its orientation in two patients during walking and running in different speeds using telemetering total hip prostheses. One patient underwent bilateral joint replacement and a second patient, additionally suffering from a neuropathic disease and atactic gait patterns, received one instrumented hip implant. He found two maximum forces, the first one at the instant when the leg was about 5 degree before passing through the vertical position. This peak force R_{max} increased with the walking speed. The second maximum force, sometimes observed during the push-off phase of the gait cycle, decreased at higher walking speed but stayed about the same for fast walking and jogging at any speed [4 p. 973].

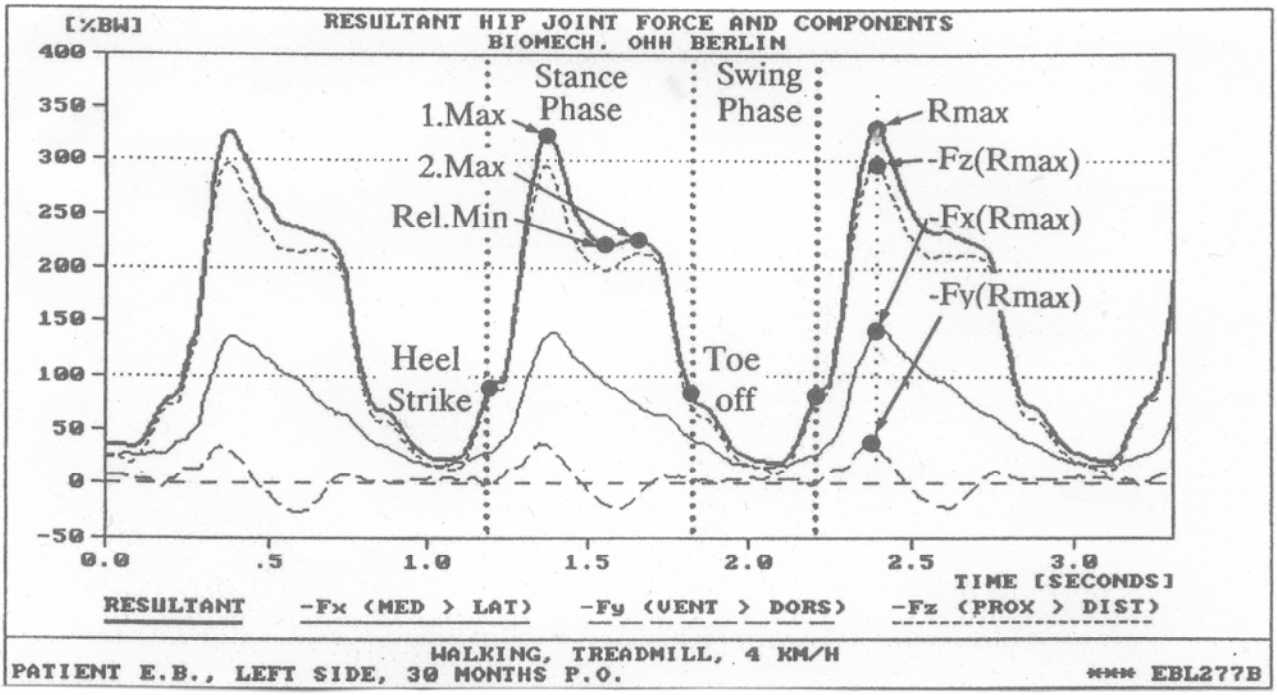

Fig. 10: showing first and second maximum hip joint forces [4 p. 976].

6. Strain Measurement Technique

6. 1. Introduction

There are four different methods used for measuring the strain distribution on the femur.

1. Strain gauging, which is relatively simple but the strain gauges provide local point-to-point information.
2. Finite element models have been used to evaluate the internal and the interface stress distribution, but in many cases no experimental validation was reported for F.E. [15 p. 451].
3. Brittle coating technique.
4. Photoelastic coating technique.

Each of these methods has limitations in its application to the study of bone, including directional and positional constrain, assumption of homogeneity, and sensitivity[*]. In this project, photoelastic coating technique was used. This technique overcomes the limitation and has the major advantage that a continuous strain pattern is determined for the entire bone surface [75 p. 72].

---

[*] Hank C. K. Wuh, Lynne C. Jones, and David S. Hungerford (1987), Strain Analysis of the Proximal Femur After Total Hip Replacement, http://www.aboutjoints.com/physicianinfo/topics/strain/strainanalysis.htm, Stand: 16.07.2006

6. 2. PhotoStress Measurement

PhotoStress* is an accurate technique used for measuring surface strains to determine the stress in a part or structure during static or dynamic testing, through a special, strain-sensitive plastic coating of the test part. Liquid plastic is cast on a flat-plate mould and allowed to partially polymerise. While still in a palpable state, the sheet is removed from the mould and formed by hand to the contours of the femur. When fully cured, the plastic coating is bonded in place with special reflective cement, and the femur is then ready for testing. When loads are applied to the femur, the coating is illuminated by polarised light from a reflection polariscope. When viewed through the polariscope, the coating layer will display the strain in a colourful, informative pattern which immediately reveals the over all strain distribution and pinpoint strained areas. Semi quantitative stress analysis is performed by using a compensator or optical transducer attached to the polariscope. Permanent records of the overall strain distribution can be made by photography or by video recording.

With PhotoStress technique it is possible to:

1. Measure the principal stresses and direction at any point on the coated femur.
2. Test the composite femur repeatedly with varying load combinations without recoating.
3. Measure assembly stresses and residual stresses.
4. Make stress measurements in laboratory or in field not affected by humidity or time.
5. Instantly identify critical areas, highlighting over stressed and under stressed regions.
6. Accurately measure peak stresses and determine stress concentration around holes, notches, fillets, and other potential failure areas.
7. Detect yielding, and observe redistribution of strain in the plastic range of deformation.

---

* Vishay Measurements Group (1997-2001), Technology, introduction to the PhotoStress Method http://www.vishay.com/brands/measurements_group/guide/pstress/tech/tn702/702index.htm, Stand: 16.07.2006

6. 3. Fundamentals of Polarised Light

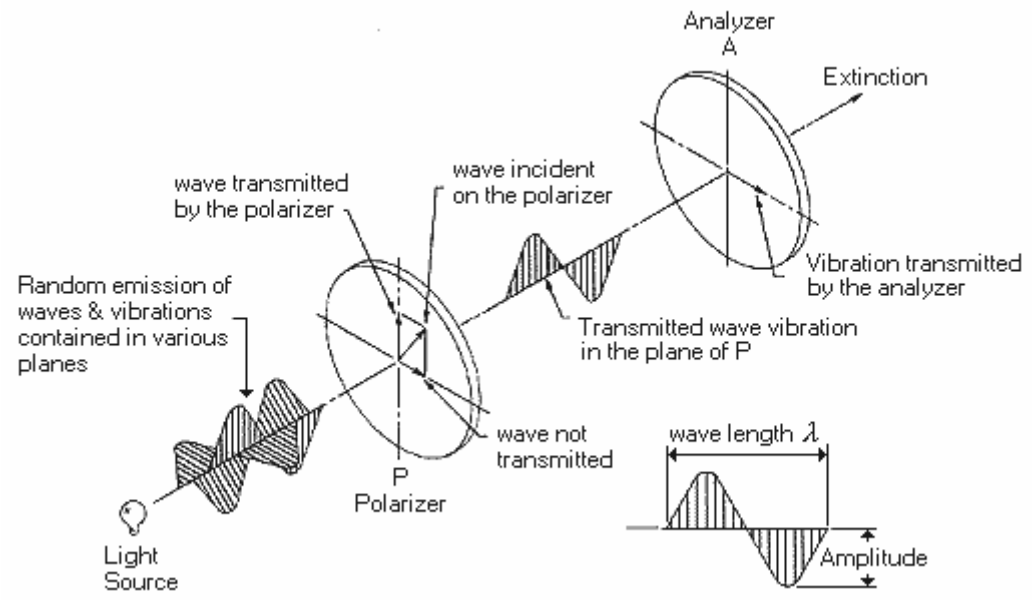

Fig. 11: Polarisation of the light

Light or luminous rays are electromagnetic vibrations similar to radio waves. An incandescent source emits radiant energy which propagates in all directions and contains a whole spectrum of vibrations of different frequencies or wavelengths. A portion of this spectrum, wavelengths between 400 and 800 nm (15 and 30 x 10^{-6} in), is useful within the limits of human perception. The vibration associated with light is perpendicular to the direction of propagation. A light source emits a train of waves containing vibrations in all perpendicular planes. However, by the introduction of a polarising filter **P** (see above) only one component of these vibrations will be transmitted (that which is parallel to the privileged axis of the filter). Such an organised beam is called polarised light or "plane polarised", because the vibration is contained in one plane. If another polarising filter **A** is placed in its way, complete extinction of the beam can be obtained when the axes of the two filters are perpendicular to each other. Light propagates in a vacuum or in air at a speed **C** of 3 x 10^{10} cm/sec. In other transparent bodies, the speed **V** is lower and the ratio **C/V** is called the index of refraction.

In a homogeneous body, this index is constant regardless of the direction of propagation or plane of vibration. However, in crystals the index depends upon the orientation of vibration with respect to index axis. Certain materials, notably plastics, behave isotropically when unstressed but become optically anisotropic when stressed. The change in index of refraction is a function of the resulting strain, analogous to the resistance change in a strain gage.

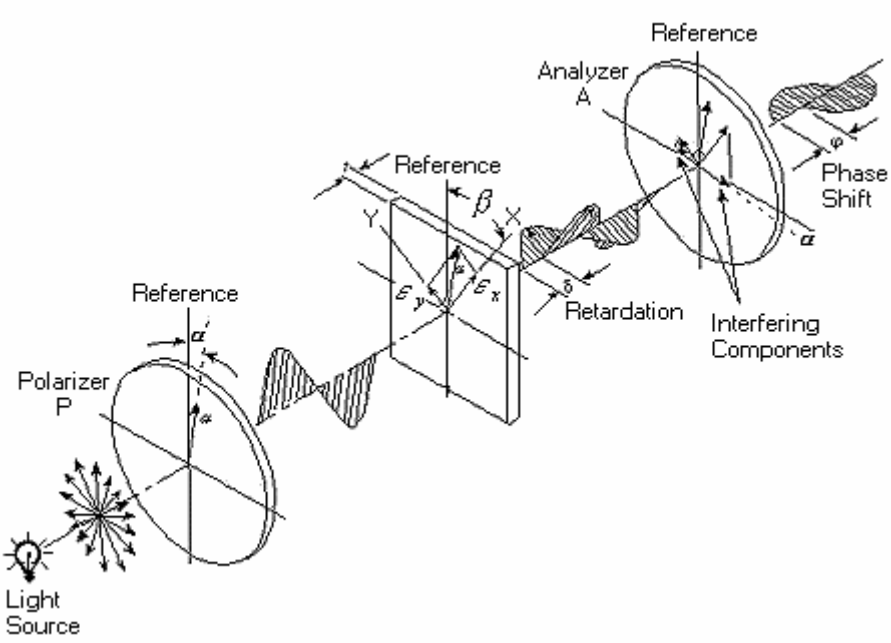

Fig. 12: Plane Polariscope

When a polarised beam **α** propagates through a transparent plastic of thickness ***T,*** where ***X*** and ***Y*** are the directions of principal strains at the point under consideration, the light vector splits and two polarised beams are propagated in planes ***X*** and ***Y*** (see above fig. 12). If the strain intensity along ***X*** and ***Y*** is $\boldsymbol{E}_x$ and $\boldsymbol{E}_y$, and the speed of the light vibrating in these directions is $\boldsymbol{V}_x$ and $\boldsymbol{V}_y$, respectively, the time necessary to cross the plate for each of them will be ***T/V***, and the relative retardation between these two beams is:

$$\delta = C\left(\frac{t}{V_x} - \frac{t}{V_y}\right) = t\left(n_x - n_y\right) \qquad (1)$$

Where: ***n*** = index of refraction

Brewster's law established that: "The relative change in index of refraction is proportional to the difference of principal strains", or:

$$\left(n_x - n_y\right) = K\left(\varepsilon_x - \varepsilon_y\right) \qquad (2)$$

The constant ***K*** is called the "strain-optical coefficient" and characterizes a physical property of the material. It is a dimensionless constant usually established by calibration and may be considered similar to the "gage factor" of resistance strain gages. Combining the expressions above:

$$\delta = tK\left(\varepsilon_x - \varepsilon_y\right) \quad \text{in transmission} \qquad (3)$$

$\delta = 2tK\left(\varepsilon_x - \varepsilon_y\right)$ in reflection (light passes through the plastic) (4)

Consequently, the basic relation for strain measurement using the PhotoStress (photoelastic coating) technique is:

$$\left(\varepsilon_x - \varepsilon_y\right) = \frac{\delta}{2tK} \quad (5)$$

Due to the relative retardation ***δ***, the two waves are no longer in phase when emerging from the plastic. The analyser **A** will transmit only one component of each of these waves (that parallel to **A**) as shown above. These waves will interfere and the resulting light intensity will be a function of:

The retardation **δ**

The angle between the analyser and direction of principal strains **(β − α)**

In the case of a plane polariscope, the intensity of light emerging will be:

$$I = a^2 \sin^2 2\left(\beta - \alpha\right) \sin^2 \frac{\pi\delta}{\lambda} \quad (6)$$

The light intensity becomes zero when the crossed polarizer/analyzer is parallel to the direction of the principal strains, or when **(β − α)** = 0. Thus we can measure the directions of the principal strain by using the plane polariscope set-up. By adding optical filters as quarter-wave plates (fig. 13) in the path of the light propagation produces circular polarised light, and the image observed is not influenced by the direction of principal strain.

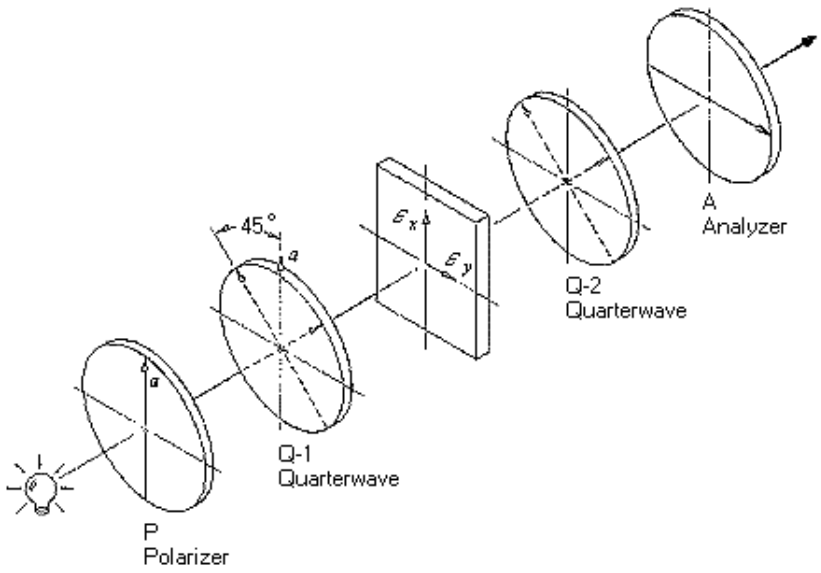

Fig. 13: Circular Polariscope

The intensity of emerging light thus becomes:

$$I = a^2 \sin^2 \frac{\pi \delta}{\lambda} \tag{7}$$

In a circular polariscope, the light intensity becomes zero when $\boldsymbol{\delta = 0, \delta = 1\lambda, \delta = 2\lambda}$ …, or in general:

$$\boldsymbol{\delta = N2}$$

where $\boldsymbol{N}$ is 1, 2, 3, etc. This number $\boldsymbol{N}$ is also called fringe order and expresses the size of $\boldsymbol{\delta}$.

The wavelength selected is:

$$\boldsymbol{\delta = 22.7 \times 10^{-6} \text{ in } (575 \text{ nm})}$$

The retardation, or photoelastic signal, is then simply described by $\boldsymbol{N}$. As an example:

If $\boldsymbol{N}$=2, ($\boldsymbol{\delta}$) Retardation = 2 Fringes or

$$\boldsymbol{\delta} = 2\boldsymbol{\lambda}$$

Once $\boldsymbol{\delta = N\lambda}$ is known, the principal strain difference is obtained by:

$$\varepsilon_x - \varepsilon_y = \frac{\delta}{2tK} = N\frac{\lambda}{2tK} = Nf \tag{8}$$

where the fringe value $\boldsymbol{f}$ contains all constants and $\boldsymbol{N}$ is the result of measurements.

6. 4. PhotoStress Instrumentation

Reflection Polariscope

In this project, a reflection polariscope, Model 031, s/n o69510, from Measurements Group, Raleigh, N.C. U.S.A was used.

Fig. 14
Photograph shows reflection polariscope model 031

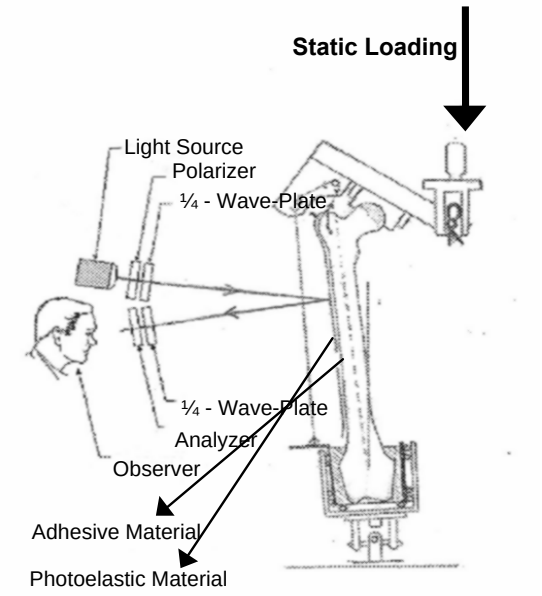

Fig. 15
Schematic representation of the reflection polariscope.

The main part of the reflection polariscope is the optical head, which consists of a polarisation filter and a quarter wave plate (see above fig. 14).

Polarizer: It consists of a polarization filter and a quarter wave plate, and acts as a source of polarized light.

Analyzer: Contains like wise polarization filter and a quarter wave plate, but has the task of analyzer by which one observes the photo layer during strain measurements.

These two components are linked together for a synchronous turn where they are running in a ball bearing set.

Manual Null-Balance Compensator Model 232

Consists of a pair of linear double breaking plates, which are one behind the other and arranged that the double refraction which is brought into the path of the rays proportionally to the mutual shift and uniform over the whole field of vision equal.

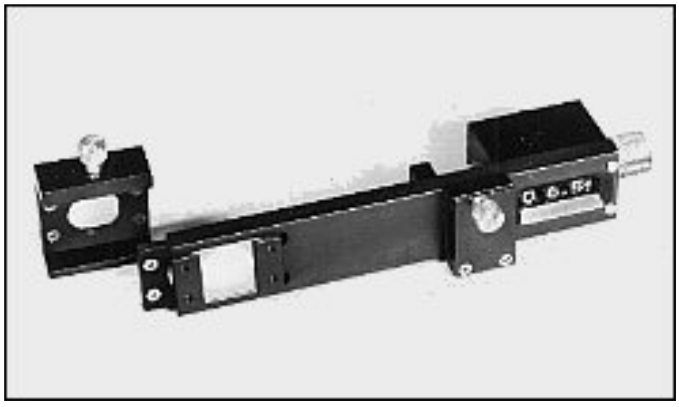

Fig. 16
Model 232 compensator

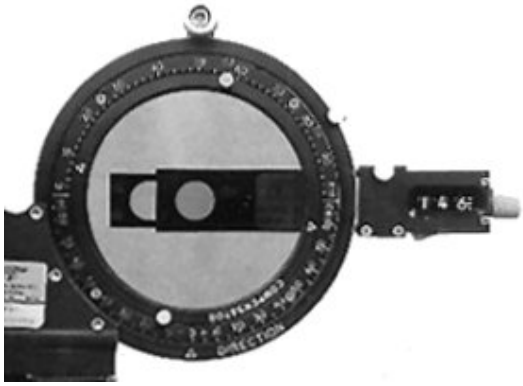

Fig. 17
Mounted on the 030 Series polariscope

- The compensator is used for determination of the ISO chromate order.
- It has a digital announcement, from which one receives the ISO chromate order by means of a calibration curve directly.
- The attitude of the control button on the compensator shifts the screw-driven, mobile plates and induces at the same time the speedometer to the indication of the shift.

6. 5. Analysis of the Photoelastic Fringe Patterns

Full-field interpretation of strain distribution

PhotoStress analysis gives the facility for immediate recognition of nominal strain and stress magnitudes, strain gradients, and strain distribution including identification of high and low stress areas. Its application depends on the recognition of fringe order by colour, and an understanding of the relationship between fringe order and strain magnitude. When a photoelastically coated composite femur is subjected to loads, the resulting stress causes strains to exist generally throughout the femur and over its surfaces.

Because the photoelastic coating is intimately and uniformly bonded to the femur, the femoral strains are transmitted to the photoelasting coating. The strains in the coating give proportional optical effects which appear as isochromatic fringes when viewed with reflection polariscope. Full-field observation of the stress distribution easily shows the effects of the varying modes of loading, as well as the relative significance of individual loads or load directions.

Fringe generation

By applying the load on a photoelastic coated composite femur, in increments, fringes will appear first at the highly stressed points. By increasing of the load, new fringes will appear and the earlier fringes are pushed toward the areas of lower stress. With further loading, other fringes are generated in the highly stressed regions and move towards regions of low stress or zero until the maximum load is reached. The fringes can be assigned ordinal numbers as they appear and they will retain their individual orders throughout the loading sequence. These fringes are not only ordered in the sense of serial numbering, but they are also orderly because they are continuous, and never cross or merge with one another and always maintain their respective position in the ordered sequence. With a reflection polariscope, the photoelastic fringe pattern appears as a series of successive and contiguous different-coloured bands (isochromatics) in which each band represents a different degree of birefringence corresponding to the underlying strain in the loaded coated composite femur. Thus, the colour of each band uniquely identifies the birefringence, fringe order (level of the strain) everywhere along the band.

With an understanding of the unvarying sequence in which the colour appears, the fringe pattern can be read much like a topographical map to visualise the stress distribution on the surface of the coated composite femur.

The photoelastic effect occurs as a result of alternately constructive and destructive interference between light rays which have undergone relative retardation, or phase shift, in the stressed photoelastic coating. With monochromatic light, the magnitude of the relative retardation along any fringe is an integral multiple of wave length **(λ, 2λ, 3λ etc.)**, the rays are 180 degrees out of the phase, and there is mutual cancellation, causing extinction of the light and producing a black band.

When the relative retardation is an odd multiple of **λ/2 (λ/2, 3λ/2, 5λ/2, etc.),** the rays are perfectly in phase and combine to cause maximum brightness. Intermediate magnitudes of relative retardation produce intermediate light intensities. However, because the light intensity is a sine-squared function of the relative retardation, the resulting photo elastic pattern appears to be made up of alternate light and dark fringes.

In PhotoStress testing, white light is used where it is composed of all wavelengths in the visible spectrum. The relative retardation causes extinction of one wavelength (colour) and does not extinguish others. With increasing birefringence, each colour in the spectrum is extinguished in turn according to the wavelength, starting with violet, which has the shortest wavelength and we can see the complementary colours. The complementary colours make up the visible fringe pattern in white light.

Fringe identification

By observing an unloaded PhotoStress-coated composite femur with a reflection polariscope, the coating layer will appear uniformly black. When the load is applied gradually on the femur, the most highly stressed region begins to take on colour - first grey, then white; and, when the violet is extinguished, yellow. By further load the blue is extinguished to produce orange, and then green, to give red. The next colour to vanish with increasing load is yellow, leaving a purple colour; and this is followed by extinction of orange, producing a deep blue fringe. The purple fringe is referred to as the tint of passage. Because of its distinctiveness and resolution, the purple tint of passage is selected to mark the increment in relative retardation equal to a fringe order of unity **(N = 1).** Subsequent recurrence of the tint of passage with greater relative retardation signifies the presence of higher integral fringe orders **(N = 2, N = 3, etc.).**

Additional relative retardation will occur by increasing of the load and the red is extinguished from the white light spectrum and blue-green is the resulting fringe colour. With greater load, the relative retardation will reach the level where it corresponds to twice the wavelength of violet, extinguishing this colour for the second time and starting the fringe cycle over again. Continuing to increase the load on the tested part and producing additional relative retardation, the red is extinguished from the white light spectrum, and the fringe colour is blue-green. With still greater load, the relative retardation reaches the level where it corresponds to twice the wavelength of the violet, extinguishing this colour for the second

time and starting the fringe cycle over again. However, the deep red colour at the far end of the white light spectrum also has twice the wavelength of the violet, and thus undergoes its first extinction simultaneously with the second extinction of the violet. The result is that the fringe colour is the combination of two complementary colours, yellow and green. As the load and the relative retardation continue to increase, the fringe colour cycle is repeated, but the colours are not exactly the same as in the first cycle because of simultaneous extinction of two or more colours. With each successive complete colour cycle the effect of increasing complex simultaneous extinction is to cause the fringe colour to become paler and less distinctive. Because of this effect, fringe orders above 4 or 5 are not distinguishable by colour in white light.

Quantitative significance of fringes

The black zero-order fringes are usually isolated spots, lines, or areas surrounded by or adjacent to higher-order fringes. The fringes never intersect therefore the fringe order and the strain level, are uniform at every point on a fringe. Furthermore the fringes always exist in a continuous sequence by both number and colour. In other words, if the first- and third-order fringes are identified, the second-order fringe must lie between them. The colour sequence in any direction establishes whether the fringe order and strain level increase or decrease in that direction. Zero-order fringe in the field view will be obvious by its black colour. When there is no zero-order fringe evident, the first-order fringe can be recognised because of the bright colours adjacent to the purple tint of passage. When the coated composite femur is loaded incrementally from an initially stress-free state, the starting zero-order fringe which covers the entire coating can usually be followed throughout the loading process as it recedes toward unstressed points and regions where the difference in principal stresses is zero.

Once one fringe has been identified, orders can be assigned to the other fringes, making certain that the direction of increasing fringe order corresponds to the correct colour sequence i.e., yellow-red-green, etc. By this process the observer can quickly locate the highest fringe orders and, generally, the most highly strained regions. Areas of closely spaced fine fringes will usually attract the attention, since regions of steep strain gradient ordinarily signify high strains as well. The stress analyst will also note any large areas where the pattern is almost uniformly black or grey, usually indicating a significantly understressed region.

6. 6. Measurements of Principal Strain Direction.

When a plane-polarised light traverses the photoelastic coating on a composite femur subjected to stress, it splits into waves propagating at different speeds along the direction of the principal strains. After emerging from the plastic, these two waves will be out of phase with one another and will not recombine into a single vibration parallel to the one entering the plastic. However, at points where the directions of the principal stresses are parallel to the axis of the polarising filter, the beam will be unaffected and the emerging vibration will be parallel to the entering vibration. An analyzing filter ***A*** with its axis perpendicular to the polarizing filter ***P*** will produce extinction of the vibrations at these points (see below).

Fig. 18

At every point where P - A are parallel to the principal stress, a black line or band is observed.

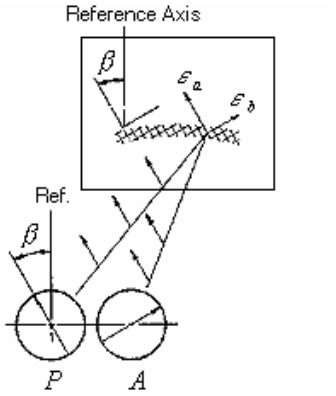

"Principal stress directions revealed by rotation of the polarizer / analyzer axes to produce complete extinction of light at the test point"

Fig. 19

When P - A are not parallel, the light is transmitted and colours are seen.

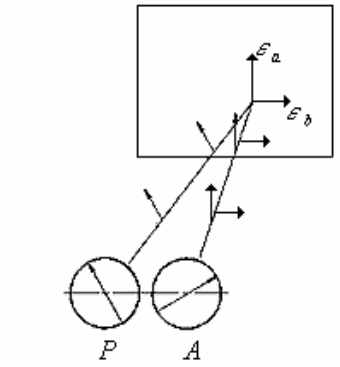

Fig. 20

Measurements of the strain direction with Model 031 Polariscope, where vertical axis and strain direction are seated from the calibrated dial

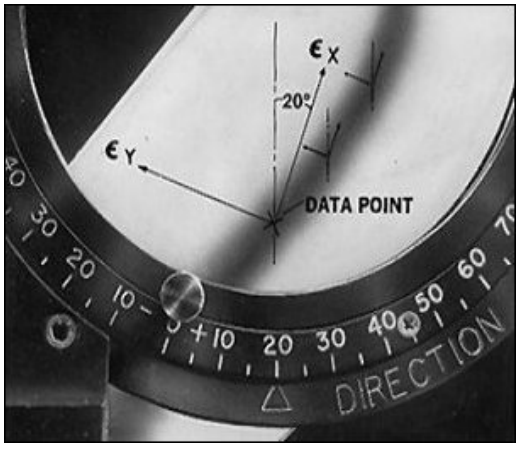

⇒ By looking through the reflection polariscope to the stressed point, black lines or areas will appear. These lines are called isoclinics.

⇒ By rotating the polarizer and analyzer together in small angular increment over the range from 0 to 90 degrees, the complete family of isoclinics will be generated.

⇒ To determine the principal strain direction at a specific point on a coated surface, an isoclinic line should be positioned at the point where the direction has to be measured.

⇒ By rotation of ***A*** and ***B*** together until the black isoclinic appears over each point and the direction is measured with respect to the established reference.

⇒ At every point on an isoclinic, the direction of the principal strain is parallel to the direction of the polarisation of *A* and *B*.

⇒ When the isoclinics are narrow and sharply defined, it means that the direction of E_x and E_y vary rapidly from one location to the other.

⇒ Isoclinics with broad black lines or areas indicate that E_x and E_y vary slowly in that region.

⇒ When this occurs, the boundary surrounding the entire isoclinic should be marked (not merely the centre).

6. 7. Measurements of Stress And Strain Magnitudes

(Relationships between fringe orders and magnitudes of strain and stress)

The fringe orders observed in photoelastic coating are proportional to the difference between the principal strain in the coating and in the surfaces of the composite femur. This can be expressed as follows

$$E_x - E_y = Nf \qquad (8)$$

where:

E_x , E_y = principal strains; N = fringe order

f = $\lambda / 2tK$ (fringe value of coating)

λ = wavelength (in white light, 22.7×10^{-6} in or 575 nm)

t = thickness of coating

K = strain optical coefficient of coating

The significance of the preceding is that the difference in the principal strains, or the maximum shear strain in the surface of the test part, can be obtained by simply recognising the fringe order and multiplying by the fringe value of the coating.

Measurements using the Null-Balance Compensator

The principal is, introducing a calibrated variable birefringence by the compensator into the light path of the polariscope and in opposite sign at that induced in the photoelastic coating by the strain field. When counter balance occurs between the strain-induces birefringence and the opposite sign variable birefringence from the compensator, the net birefringence in the light path will be zero. This resulting zero net birefringence is recognised easily where it produces a black fringe in the isochromatic pattern, where it was a coloured fringe before compensation.

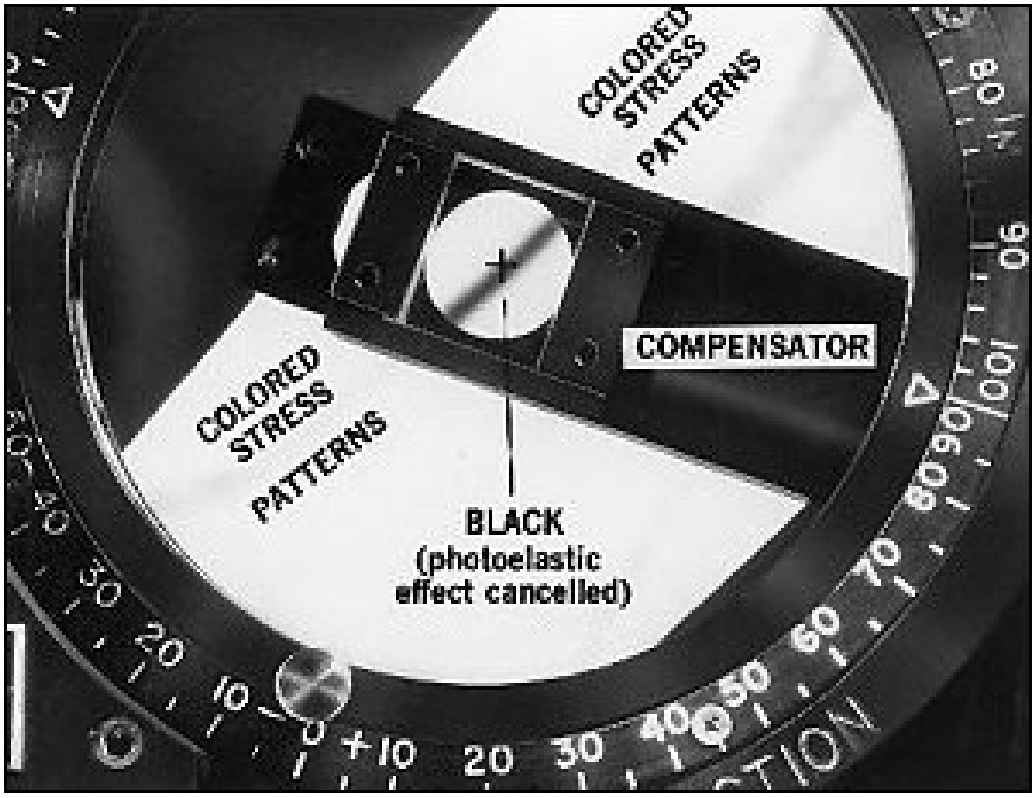

Fig. 21

Initially colored fringe is rendered black by null-balance compensation.

7. Characteristics of Human and Synthetic Femoral Bones

7. 1. Choice of Bone Specimen

In this project, synthetic composite femurs were used. Composite femurs are produced by Sawbones Europe AB**,** Malmö Sweden. These bone models were of size large left side and so called large left second-generation composite femurs [Vashon Island, Washington].

Composite femurs have the following advantages:

- They have physical properties similar to real bone.
- They have high reproducibility and low inter-specimen variability.
- They have been found with the range of cadaver specimens in axial and torsional tests.
- They provide a more reliable test bed than human cadaver femurs.
- They do not require special handling or preservation.
- There is no time restriction in testing.
- They are available in high quantity.

Because of its interest in biomechanical studies, many researches were done with the composite femurs, and now very good documents exist, regarding to their mechanical validity and success in experimental studies. Otani in 1993 investigated strain distribution in the proximal femur with flexible composite and metallic femoral components under axial and torsional loads in both composite and fresh cadaver femurs. He has reported that composite femurs showed similar longitudinal strain distribution to the fresh cadaver femurs both before and after implantation of the femoral stems in response to the axial load, thus using composite femurs for strain measurements and comparison studies in hip arthroplasty seemed to be a good alternative because many femurs with identical geometry and material properties could be used [59 p. 582].

Grecula in 2000 investigated the strain patterns on the femoral surfaces of four composite femurs coated by photoelastic method at each axial load interval (50, 1000, 1500, 2000 N). He found that there were no differences in the strain patterns between test runs for intact femurs.

The propagation of the strain gradients was consistent through each loading cycle and statistically there was no difference for each view and each load between the areas of strain across the three test runs.
He proved the intact strain and repeatability of the composite femurs (by repeated testing, performed by the same operator on the same specimen, disassembling the set-up each time) where composite femurs retain their material properties through repeated loading, as does the photoelastic coating [31 p. 929-931, 15 p. 457].

Harman in 1995 investigated and measured the proximal interface motion between cementless stems and synthetic composite femurs for comparison of the initial torsional stability. He concluded that multiple insertion of the stem in the composite femurs and load repetition does not appear to affect the resulting micromotion and that there was no visual evidence to the qualitative structural damage of the composite femurs [32 p. 164, 168].

Cristofolini et al. have shown that inter-femur variability of the composite femur was 20-200 times lower than that of the cadaver femurs where they have larger geometric differences and variability, that have always been a problem, as large sample sizes are difficult to obtain, maintain and expense to test [12 p. 533].

The inter-femur strain variability for cadaver specimens can be estimated from the literatures to be larger than 100% of the mean. To obtain a 95% confidence interval smaller than 10% of the mean would require a sample of several hundred femurs [15 p. 448]. Therefore smaller differences will be characterised as significant, if the composite femurs are used. The bending stiffness of the composite femurs was found to be similar to that of human femurs. Also composite femurs have high reproducibility for repeated testing on the same femur, thus satisfactory significant results do not require large number of repetitions as for human specimens.

Hydration of the bone tissue is a problem when using photoelastic coating on cadaver femur, where the coating layers are very sensitive to humidity [15 p. 452]. For these previous reasons, composite femurs are used now in biomechanical studies as an alternative to human cadaveric femurs for testing and comparisons of different stem geometry for design purposes where the actual strength properties of real bone are required [32 p. 168, 56 p. 249].

7. 2. Description of the Composite Femur *

It is formed of a glass fibre reinforced epoxy (cortical bone) around rigid polyurethane foam (trabecular area) which ranges in cell size between 0.5-1.0 mm and has 95% closed cells. The tensile and flexural strengths and moduli are consistent with the human bone, and its geometry has been reported to be agreeable as well.

- It is designed to be cut, drilled, and gauged by the standard orthopaedic instruments.
- There are two sizes available, both normally "left" femurs, in size medium and large.
- In this project we used the large femur.

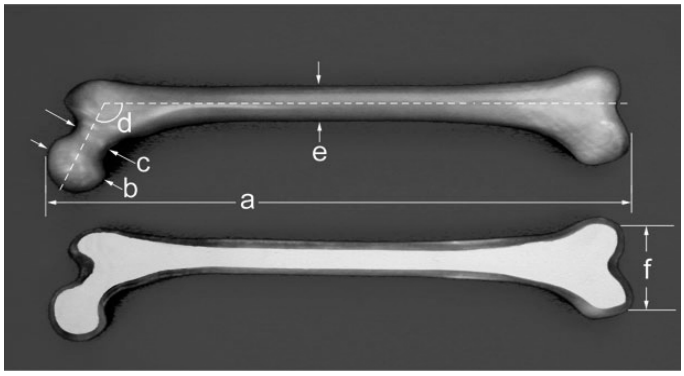

a) 485 mm d) 120 degrees
b) 52 mm e) 30 mm
c) 34 mm f) 86 mm

Fig. 22
Large left second-generation composite femur for mechanical testing. Model 3106

Typical properties

Table 1: Properties of composite bone, simulated cortical bone (E-glass / Epoxy Composite)

		Tensile		Flexural
Density	Strength	Modulus	Strength	Modulus
(g/cc)	(MPa)	(MPa)	(MPa)	(MPa)
2.08	172	18,615	275	14,200

Table 2: Properties of composite bone, simulated cancellous bone (Rigid Polyurethane Bone)

			Compressive
	Density	Strength	Modulus
	(g/ks)	(MPa)	(MPa)
Solid	0.27	4.8	104
Cellular	0.32	5.4	137

* Pacific Research Laboratories (2002), Biomechanical Test Materials, http://www.sawbones.com/products/bio/, Stand: 16.07.2006

8. Preparation and Photoelastic Coating of the Composite Femur

8. 1. Preparation of the Femur

The femoral condyles were resected longitudinally, and then the distal end of the femur was potted into a special steel container (cup) centrally, after sweeping the edges by oil to avoid adhesion of the container with the chemical materials. This cup was used latter for distal fixation of the femur. The container was filled with epoxy resin by mixture of ureol fc 52 ISO and ureol fc 52 polyol. The mixture gets hardened at least after one hour. Smoothing of the femoral surfaces with abrasive paper till the femur has very smooth surfaces, to avoid any artefacts during measurements. Then the femur was ready for coating.

8. 2. Coating of the Composite Femur [53]

8. 2. 1. Introduction

Coating application should be done in a clean area and at a temperature between 18 to 29 degrees. The presence of dust, moisture, and direct sun light or radiant heat, extreme drafts of hot or cold air should be avoided. Successful photostress analysis depends on the proper installation of the photoelastic coating on the femoral surface, and it requires good coating preparation, surface preparation, adhesive preparation and bonding procedures.

8. 2. 2. Coating Preparation

Soft, partially polymerised sheets are required to be contoured to the curved, irregular surfaces of the femur, then be allowed to fully polymerise while on the surface of the femur.

Preparation of the sheets

Firstly, by adjust the casting plate in an accurate horizontal position. Cleaning of the casting plate and the four rubber strands by acetone and alcohol. Prepare a rectangular coating sheet formed by the rubber strands on the casting plate, about 175 x 240 mm.

Preparation of the plastic (PL- 1) [54]

The amount of the plastic should be calculated according to the size and thickness of the sheet to be caste. The total amount of the plastic (resin and hardener) is determined by the following equations:

- $W = 18.5 \times A \times t$ (English units in inches) or
  $W = 1.13\ (10^{-3}) \times A \times t$ (metric unites in mm).
- Where W = the total amount of resin needed in grams.
- A = the area of the sheet to be cast.
- t = the desired thickness.
- Plastic density = 18.5 gm/in^3 or 1.13×10^{-3} g/mm^3.

Both the resin and the hardener should be warmed to at least 32 degrees, but never higher than 43 degrees, where warming will lower the viscosity of the resin and facilitate its mixture with hardener. The amount of hardener is calculated in parts per hundred or "pph". 10 pph means 10 grams of hardener for 100 grams of resin. For type PL-1 plastic, the amount of the hardener is 18 to 20 pph. The proper amount of resin PL-1 (about 79.25 g) was weighted in a plastic coated cup by using a balance scale. Accounting and remembering the weight of the plastic cup, then add about 15.85 g PLH-1 hardener to the resin and stir with a stem thermometer (part No. 012-6).

It is very important to achieve uniform mixture prior to pouring on the casting plate. Stir slowly using a circular motion without whipping action, as this will introduce excessive amount of air bubbles. Stir slowly but thoroughly, to achieve a clear non-streaking mixture. As stirring progresses, exothermic reaction will occur and the temperature rise and has to be monitored with the stem thermometer. When the temperature reaches to 52 degrees, the plastic will be ready to be poured into the casting plate. Immediately prior to pouring the mixed plastic, set the temperature control switch on the casting plate heat controller to the OFF poison. During pouring, keep the cup as close as possible to the surface of the casting plate to decrease the possibility of air bubble formation. Move the cup over the casting plate, to improve flow to all edges of the mould (see below). After pouring, resin will flow out and fill the mould. Use the stem thermometer to spread the resin evenly. The resin eventually

levels itself out with the time cover the mould with the Plexiglas cover to keep out dirt and to avoid dust settling on the plastic during its polymerisation. Cast PL-1 sheet takes about one to one and a half hours, according to size, thickness, and cure environment. When polymerization is near completion, remove the plastic from the plate and cut it into a propitiate shape by a cutter on wooden plate [48]. Contour the plastic around the composite femur. The coating is pressed on by hand over a period of 10-20 minutes to maintain intimate contact of the coating to the bone. This requires constant observation and application of pressure in different areas sequentially. Care should be taken not to produce local thinning by applying excessive pressure with the fingertips (see below fig. 25).

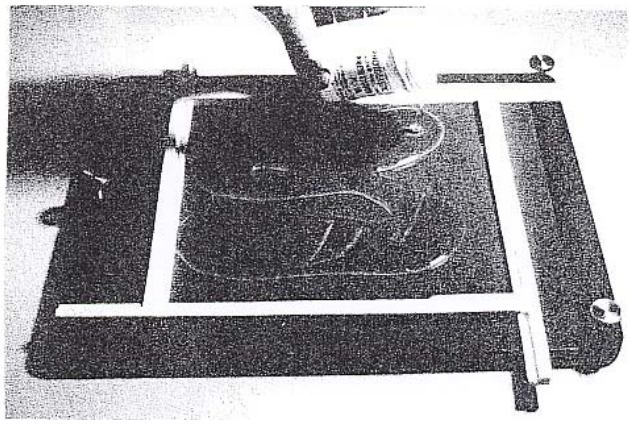

Fig. 23
Pouring of the plastic into the heating plate [52]

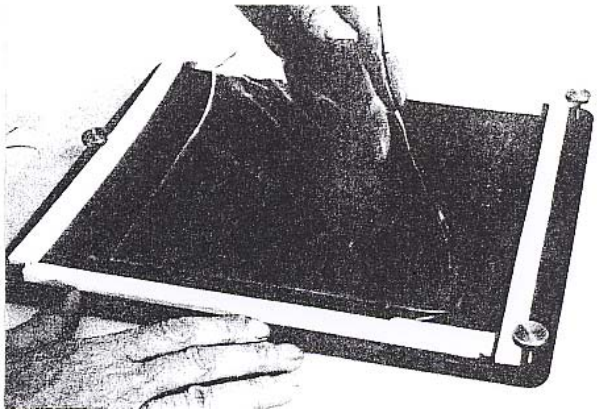

Fig. 24
Removal of the plastic from the casting plate [52]

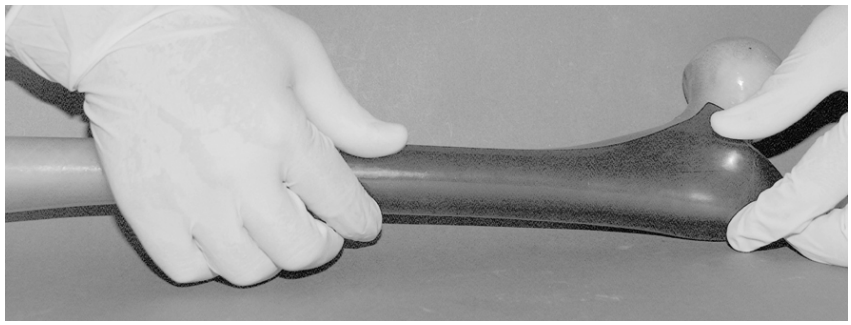

Fig. 25
Contouring of the plastic layer
on the femoral surface.

Each femur will be coated with a posterior-medial coat and an anterior-lateral coat, for both upper and lower half of the femur. Put mineral oil on the wooden plate of the plastic cut machine also on the femoral surfaces before contouring to avoid adhesion. Remove the contoured plastic from the bone after curing for 18 hours. After this time, the PL-1 will be hardened and has the same size and detailed contour as the femur. Saw the plastic by using an electric saw. During sawing of the plastic to fit different edges and boundaries, it is better to saw the plastic slightly oversize (1mm) and then trim to the final shape using files, abrasive paper or a hand router. Application of the coating required more than one sheet and it is very important to plan seam location between adjacent sheets, where properly prepared sheets cause little disturbance in photo elastic pattern. The seam should not cross the points of measurements and a gap about 1 to 2 mm should be between each two sheets.

8. 2. 3. Measurements of the Coating Thickness

Firstly draw the longitudinal axis for each femoral surface and also the identical axis on the corresponding surfaces of the coating plastic, using a stable marker pen. Mark the points of measurements over the photoelastic coating surfaces, 23 points starting at the calcar region and descending downwards. From point 1 to 16, the interval is 1 cm and from point 16 to 23 it is 2 cm. The reference points should be in the same site of location for all test femurs, where a specific ratio of distance from the head of the femur to the reference point over the length of the femur should be fixed. Measure the thickness of the photoelastic coating at each measuring point by using a micrometer apparatus. The average of the thickness is 1.80 mm. The thicknesses of all test specimens were relatively constant within 1.70-1.90 mm.

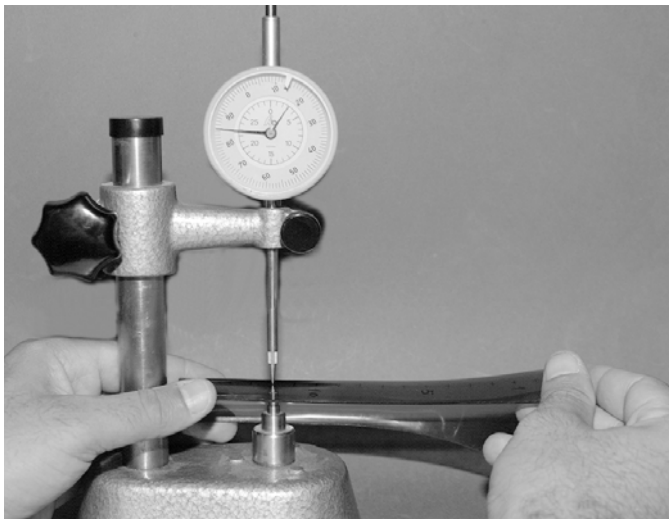

Fig. 26
Measurement of the thickness of photoelastic layer at each reference point by using a Micrometer apparatus.

Cleaning of the coating plastic

Clean the coating plastic sheet, thoroughly to be compatible with the cleaned surface of the femur. Cleaning of contoured sheets prepared from PL-1, by saturating a gauze sponge with the following solvent, metal cleaner, Neutra-sol, acetone and isopropyl alcohol, in that order [53 p. 3].

8. 2. 4. Preparation of the Femoral Surfaces

Preparing a smooth and clean femoral surface is very important to promote good adhesion. Clean the femoral surfaces with isopropyl alcohol, metal cleaner and Neutra-sol respectively.

8. 2. 5. Adhesive Preparation (PC-10)

Photoelastic adhesion material is formed of two components, resin and hardener mixed in a proper proportion. PC-10 is a fast curing room temperature adhesive used for bonding contoured sheets made from PL-1, and its cure time is four hours at room temperature. The temperature should be 21 to 24 degrees. Rubber gloves should be used during this procedure to avoid allergic reaction and dermatitis [55]. One gram of the adhesive material will cover approximately 10 cm^2. However, no more than 60 grams of adhesive should be prepared per mixture, because of very high temperatures at the exothermic reaction.

Resin-hardener preparation

The amount of the hardener required is calculated in parts per hundred or “pph”. The amount is 15 pph. In other words, 15 pph means 15 grams of hardener for 100 grams of resin. Add about 6.5 grams of hardener to 43.5 grams of resin in a container made of non absorbent material which can be discarded after using. Mix the two components thoroughly using wooden mixer and the mixing time required is about two to three minutes to ensure a homogenous blend. The container should not be cradled in the palm of the hand during mixing since the resulting body heat will accelerate the exothermic reaction and decrease the pot life. The curing time will be longer for lower temperature and shorter for higher temperature.

8. 2. 6. Bonding Procedures

Immediately after mixing of the adhesive materials, brush the adhesive onto the femoral surfaces in a uniform layer approximately 0.8 to 1.6 mm thick. Any adhesive left in the mixture container should be poured onto a clean paper towel and the mixing container discarded. By spreading of the adhesive in a thin layer after it has been mixed, its working time will be 10 to 15 minutes.

Place the coating plastic carefully over the adhesive, then press down on the plastic at one end with moderate finger pressure, and slowly toward the opposite end. This technique will allow any air bubbles that form to flow out with excessive adhesive. If air bubbles will return when finger pressure is relaxed, replay pressure and brush additional adhesive along the edge of the plastic. Then, after releasing the pressure, adhesive will flow instead of the air. The optimum thickness of the adhesive layer is approximately 0.076 to 0.13 mm.

After all of the excess is squeezed out, apply a thin coating of adhesive around the edges of the plastic to provide a seal against moisture absorption. The adhesive will become stiffer as it cures. After 30 minutes it will begin to develop the consistency of putty.

At this time adhesive bevels, if required, should be built and any remaining adhesive on the top of the coating should be cleaned off using the recommended solvent. After four hours of cure from the start of mixing the PC-10 adhesive, the femur will be ready for testing.

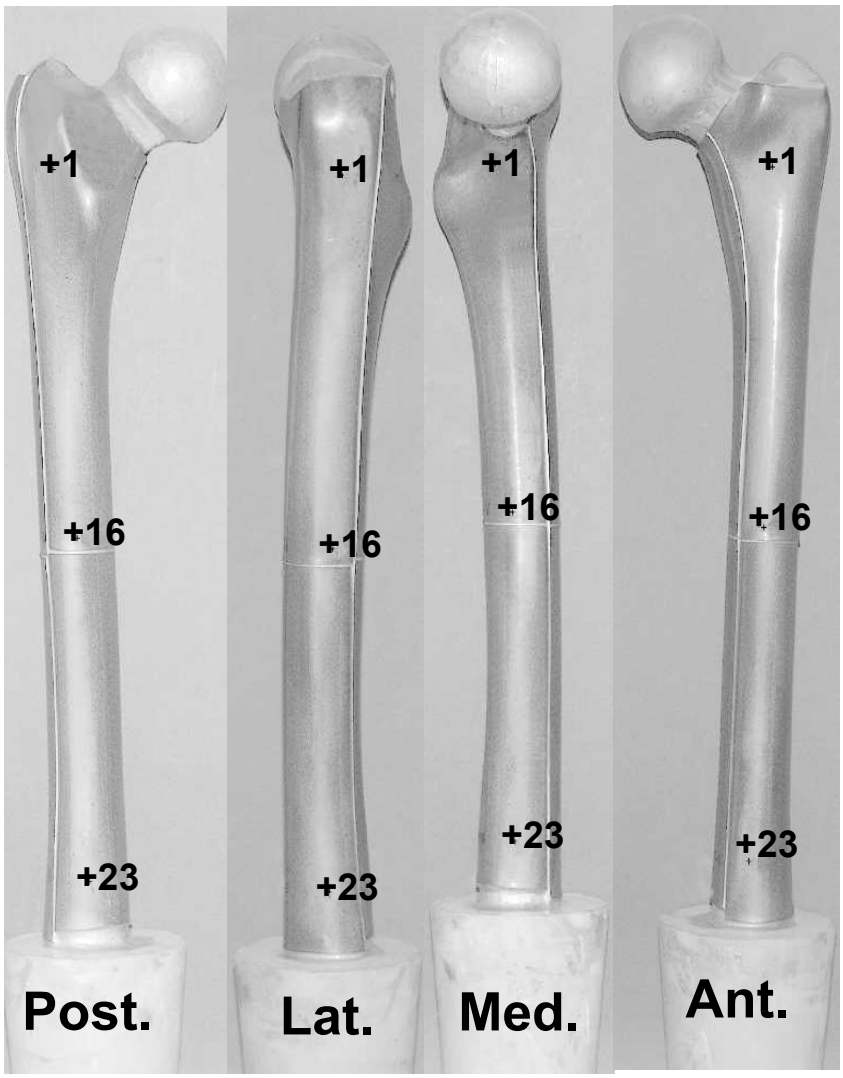

Fig. 27

Photographs showing the femoral surfaces of a coated composite femur with the reference points of measurements.

Fig. 28

Cross section through the neck of a coated Composite femur.

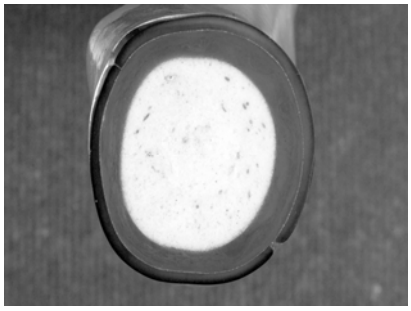

9. Experimental Set-Up (Fixed in all Experiments)

9. 1. General Explanation of the Experimental Set-Up

For testing purposes it is necessary to generate an isostatic set-up that allows replication of the physiological loads in a controlled fashion. Physiologically the femur is hyperstatically loaded and constrained by the joint reaction forces, muscle forces and ligaments [14 p. 215, 15 p. 432, 17 p. 76].

The test fixture in this project was designed to provide load simulating forces on the hip during weight bearing consisting of both, a compressive load to the femoral head and a tensile load to the trochanteric region causing bending as well as axial loading of the proximal femur [70 p. 277]. Load around the hip is in the form of hip joint force, muscles forces (abductor muscles and the ilio-tibial tract) and axial torsion moment. Each femur was loaded by a universal testing machine simulating single-legged stance phase and muscle forces simulating abductor muscles and the ilio-tibial tract, where the glutei are considered the principal muscles determining the vertical strain of the femur [13 p. 622]. The ilio-tibial tract acts as a lateral tension band and decreases the bending of the femur in the frontal plane. The abductor muscles and the ilio-tibial tract are simulated in this project by a strain, y-shaped tensile loading wire attached to the bone by a trans cortical bar (see fig. 30). This wire simulates the ilio-tibial tract and the abductor muscles will be at 12 and 15 degrees to the vertically, respectively (see fig. 31, A). The torsional moment was about 32 Nm, realised by a 20 kg weight which was applied to the femur by a pulley-system with lever arm 160 mm attached to the distal part of the femur (see fig. 32).

Proximally the femur is subjected to a compressive force to the femoral head through a polyethylene cup and a tensile force simulating the contraction of the abductor to the greater trochanter [70 p. 277]. The femur was fixed distally to the machine by a special designed steel cylinder for stabilisation in which the steel cup containing epoxy resin base of the composite femur will be potted and act as a rotating cup inside the cylinder. Constraining of the distal end of the femur in a cement block will give the most repeatable and reproducible constraining solution when the abductors are simulated, where it allows accurate control of the plane of application of the system of forces around the longitudinal axis of the femur if an anatomical reference has been used when cementing the femur [15 p. 436].

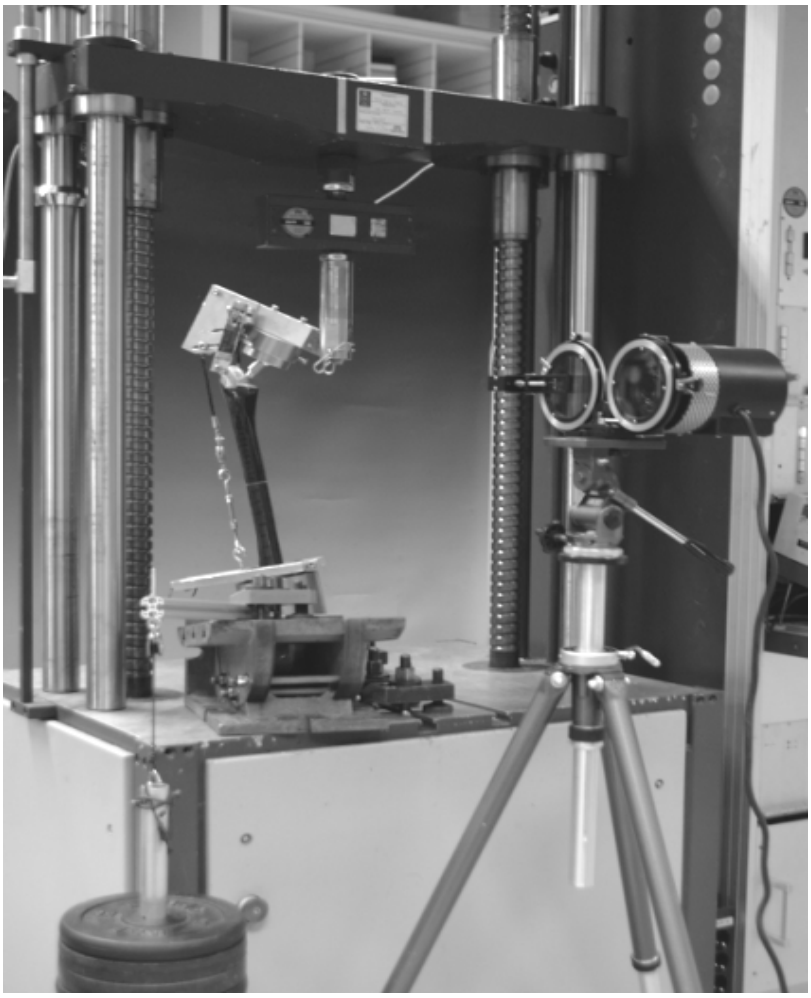

Fig. 29: Photograph showing experimental set-up.

The femoral shaft was positioned at a 12^0 angle laterally from the vertical in the frontal plane to simulate the proper anatomical axis and corresponds to the physiological inclination during single leg stance. Each femur was loaded by 1000 N, fixed in all experiments and applied to the femoral head by a lever arm connected to the testing machine simulating the single-leg stance of a subject weighting 102 kg. Loading transmitted although a polyethylene cup fixed to the lever arm. The cup articulated with the femoral head, causing bending of the proximal part of the femur with longitudinal deformation in the form of compression on the medial side and tension on the lateral side resulting in joint reaction force about 2.4 BW. According to Bergmann (1993) 2.4 x 1000 = 2.4 kN, which could vary with different medial offset. In order to insure that only an axial load was transmitted to the fixture at the location of the applied load, proximal loading sphere and distal support sphere were attached to the ends of the test fixture. Both proximal and distal spheres allow freely bending of the femur during loading with accurate load transmission as an isostatic method to constrain the femur [26 p. 757, 70 p. 278].

In addition to the application of axial load and loading component of the hip joint force, a torsional load of 32 Nm = 20 kg with 160 mm lever arm was applied to the femur by a weight-and-pulley system attached through a transverse plate to the rotating cup. Thus the torsional load was applied to the distal end of the femur and the moments was transmitted to the trochanteric wire (simulate the abductor muscles) and the polyethylene acetabular cup, which antagonise the rotating action of the femur.

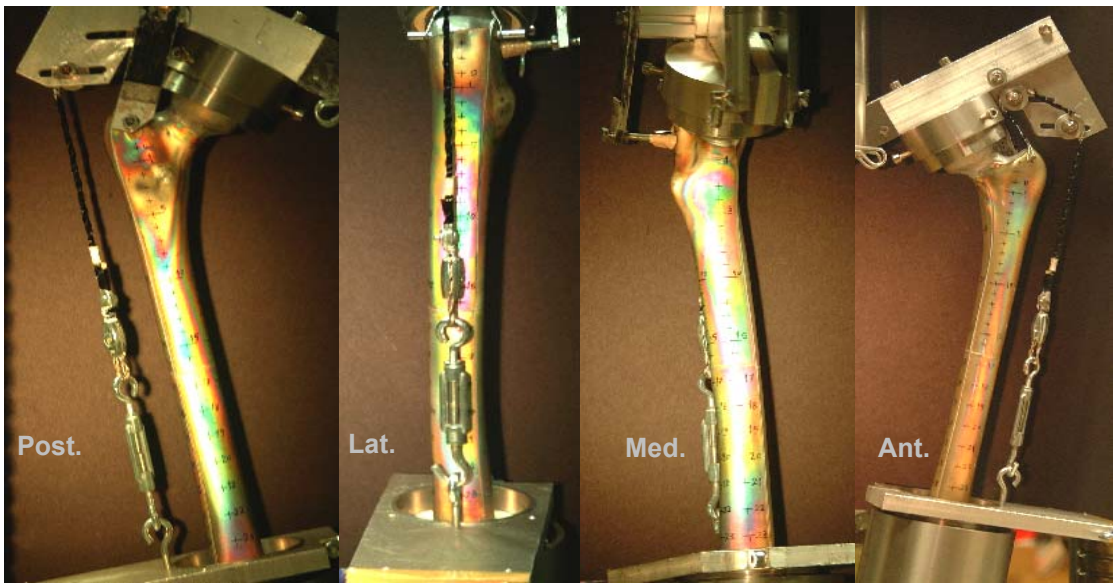

Fig. 30

Photographs showing the four femoral surfaces of an intact loaded photoelastic coated femur with muscles simulation (viewed through a reflection polariscope).

9. 2. Dimensions of the Proximal Loading Apparatus

The test set-up was arranged to simulate single-leg stance and to standardise several factors:

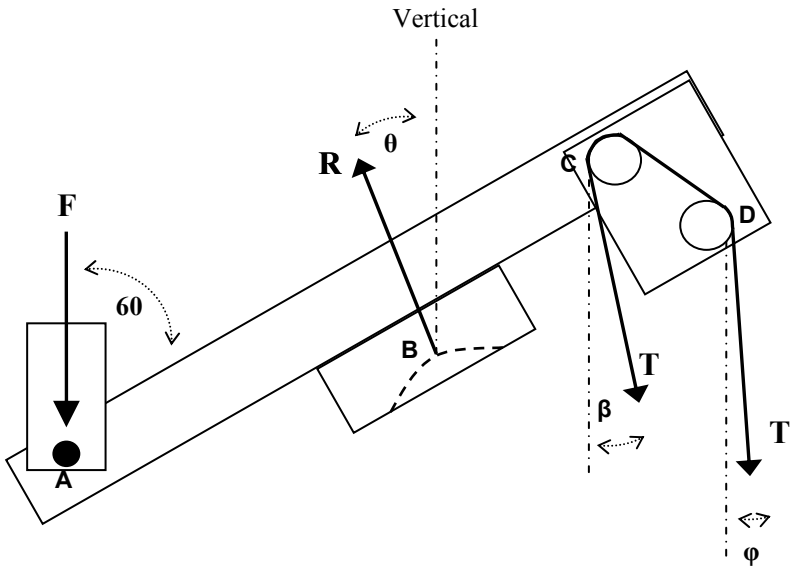

1. The hip joint force F_R = 2.4 kN
2. with the abductor strap in place, a 110 mm offset was maintained between the lines of action of the axial
3. The angle of the femoral axis was 12 degrees to the vertical.
4. The angle of the abductor band was 15 degrees to the vertical.
5. The angle between the abductor band and the femoral axis = 27 degrees.
6. The angle of the ilio-tibial band was 12 degrees to the vertical.
7. The distance between the ilio-tibial band and the femoral axis about 50 mm.
8. The torque moment = 32 Nm (20 kg x 160 mm)

Fig. 31 (A)

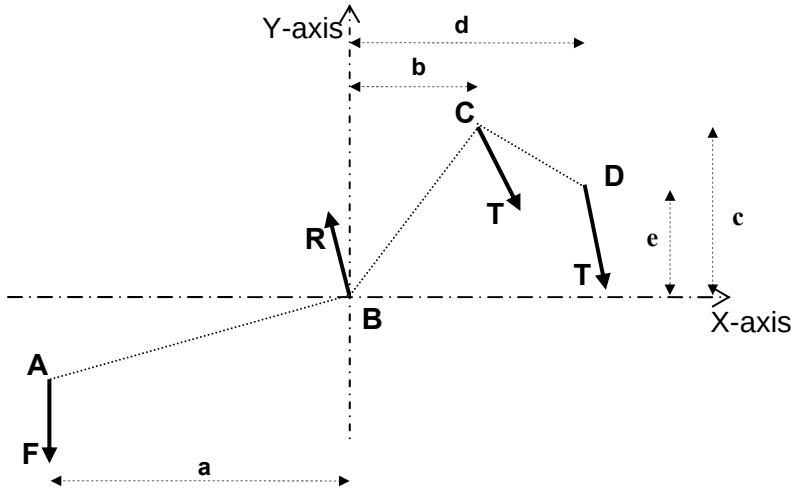

Experiment Set-up:

F: Applied load force
R: Joint reaction force
T: Tension force in the string
Θ: Reaction force angle with the vertical
ß: 15 degrees
φ:12 degrees
a: 108.2 mm
b: 53.7 mm
c: 51.8 mm
d: 91.6 mm
e: 29.3 mm

Fig. 31 (B)

Fig. 31
(A) and (B) represent the power-plan of the lever-arm.

9. 3. Dimensions of the Distal Loading Apparatus

The distal implanted fixation was used for application of the torsional load component. A weight of 20 kg was connected by a lever arm of 160 mm to the distal aluminium part.

In this study the femurs were examined in single-leg stance phase at the moment of heal strike when the highest hip joint load acts [4 p. 976]. The load situation at this moment was chosen for the experimental investigation because the worst loading of the femurs. Single-leg stance phase leads to substantial increase in the hip joint force, where the abductor muscles must generate sufficient power to neutralise the adduction moment about the hip exerted by the body weight [47 p. 94].

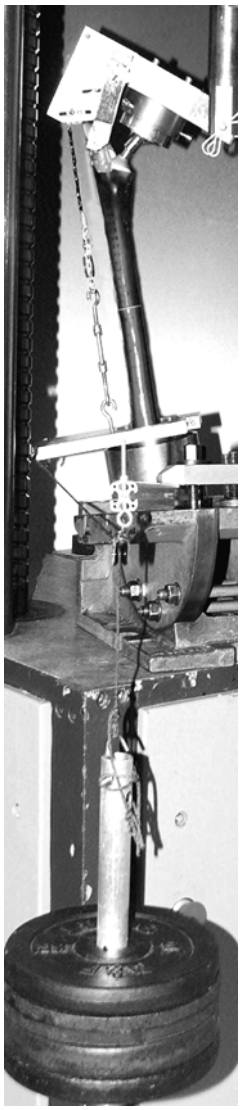

It was proved that, during stance phase of slow walking, the vertical floor reaction is constant for a period [11 p. 156, 157]. Hip endoprostheses are usually fitted to elderly patients who walk slowly, so study of the single-leg stance gives valuable information for the design of such endoprostheses [51 p. 191].

Femurs were examined in a 12 degree position of adduction, where it was proved from radiological examination of erect subjects that the femur is angulated 8-15 degrees to the frontal plane in single-leg stance and consequently an angle of 12 degrees was mimicked in our procedure [51 p. 205, 27 p. 338].

Fig. 32

Photograph showing experimental set-up. An implanted photoelastic coated femur loaded, proximally by 1000 n, distally by torsional load 32 Nm = 20 kg applied to the femur by a weight-and-pulley system attached through a transverse plate to the rotating cup.

In this project, the abductor muscles and ilio-tibial tract were simulated because applying a single load to the femoral head will represent a non physiological state of loading. Rohlmann and Mössner found that applying a single load on the femoral head parallel to the femoral

shaft was useful in experimental analysis where only the stresses in the diaphysis are to be considered [61 p. 732]. Duda in 1998 concluded, that simulation on bone modelling and remodelling processes distal to the lesser trochanter should consider the abductor, ilio-tibial band, adductor and hip joint force. If major muscles are neglected, the tensile and compressive strains are overestimated and torsional effects are underestimated. This may considerably influence mathematical simulations of bone remodelling or modelling processes as well as interpretations of stress shielding effects. Loading with only hip joint force, abductors and ilio-tibial band produced a strain pattern typical for bending. Due to unbalanced bending moment, the tension-compression pattern shifted between proximal and distal portion of the femur. In contrast, the tension compression pattern was relatively constant along the femoral shaft if all thigh muscles were included [21 p. 844, 845]. Without simulation of the abductors, the stress shielding on the lateral side of the femur will be overestimated where the hip joint force will transferred along the stem and the bone is loaded only distally at the tip of the stem. Conversely, the abductors will force the bone itself to strain and bend [15 p. 428, 62 p. 243].

Finlay et al. investigated and compared the principle direct strain for intact femora in three configurations (vertical shaft, after simulation of ilio-tibial band, after simulation of the abductors. The femoral shaft angled at 11 degrees to the vertical in the last two configurations. They proved that the mathematical analysis of the normal anatomically oriented femur indicates the presence of increased bending moments about the proximal femur compared with the femoral diaphysis. This suggests that a realistic load distribution in single-leg stance must take in account simulation of the muscles of the thigh [26 p. 757]. The lateral musculature of the thigh will apply additional compressive load to the femur to reduce the otherwise large tensile bending strain on the lateral aspect of the femur [26 p. 750, 61 p. 742, 62 p. 241]. The ilio-tibial tract has a tensile strength about five times of the body weight [62 p. 241]. The ilio-tibial tract is active and reduces bending, where it is postulated that the circular cross section of the femoral diaphysis is due to a compressive state of the stress rather than bending which could lead bone to adapt to an elliptic section [71 p. 122].

Gerlach in 1990 has considered the ilio-tibial tract as a part of the connective tissue systems of the lower limbs which is formed also by other components and reduces the bending force on the femur, like the femoral intermuscular septa, fascia lata, the crural fascia, the crural intermuscular system and the membrane introssea. However, he considered the ilio-tibial tract as the biomechanically effective element of this connective tissue system [29 p. 22)].

9. 4. Equilibrium Analysis

Studying the equilibrium of the upper part of the apparatus as shown in the figure 31 (A, B), there are four external forces balancing each other. Therefore the sum of the resultant force in any direction is zero. The sum of the resultant moment about any direction is zero.

Force equilibrium in x-direction:

$\sum F_x = 0$

$- R \cdot \sin \Theta + T \cdot \sin ß - T \cdot \sin \varphi = 0$

$R \cdot \sin \Theta = T \cdot (\sin ß - \sin \varphi)$ -----> 1

Force equilibrium in y-direction:

$\sum F_y = 0$

$- F + R \cdot \cos \Theta - T \cdot \cos ß - T \cdot \cos \varphi = 0$

$R \cdot \cos \Theta = F + T \cdot (\cos ß + \cos \varphi)$ -----> 2

Moment equilibrium about point B:

$\sum M_B = 0$

$- F \cdot a + T.\cos ß \cdot b + T \cdot \sin ß \cdot c + T \cdot \cos \varphi \cdot d - T \cdot \sin \varphi \cdot e = 0$

$F = T \cdot (b \cdot \cos ß + c \cdot \sin ß + d \cdot \cos \varphi - e \cdot \sin \varphi)/a$ -----> 3

From 3:

F = 1.375 * T i.e T = 0.7272 * F -----> 4

By substituting the value of F in equation 2 and then dividing equation 1 by equation 2:

$$\frac{R \cdot \sin \Theta}{R \cdot \cos \Theta} = \frac{T \cdot (\sin ß - \sin \varphi)}{1.375 * T + T \cdot (\cos ß + \cos \varphi)}$$

Therefore:

$\tan \Theta = (\sin \Theta / \cos \Theta) = (\sin ß - \sin \varphi) / (1.375 + \cos ß + \cos \varphi)$

Θ = 0.8787 degrees

From equation 2, using the value of Θ

$R \cdot \cos 0.8787 = F + 0.7272. F \cdot (\cos 15 + \cos 12)$

R = 2.414 F

F = 1. 0 kN

From equation 4, using the value of **F**

T = 0.72 kN

10. Experimental Analysis with ESKA-Implants.

10. 1. Characteristics of the Implant Design

The surface of the cementless ESKA endoprostheses* is a three-dimensional grid network structure, which is adapted to bone spongiosa. This interconnection bare is technically given and reproducible. Structure and implant core are manufactured as homogenous casting in one piece.

After primary fixation by press fit, secondary stability will occur due to bone integration into the implant surface. The three dimensional regional structure is successfully used for 20 years. For special indications, the metallic endoprostheses components on request can be supplied with the following layers:

Hydroxyapatite Coating:
The cementless endoprostheses can be cotaed with a bioactive hydroxyapatite ceramic (coating 70-80 µm thick) for improving the bony integration. The coating supports the bony integration into the structured implant surface.

Titan/Niobium Coating:
The non-articulating, metallic surfaces can be coated with a multi-layer metallic Titan/Niobium coating (12 µm in total) for allergy protection (Nickel, Cobalt, Chromium, Molybdenum). This coating shows self-passivation, is chemically and biologically non-reactive and prevents allergic reactions of the body to metallic components of the implant.

Titan/Niobium-Ceramic Coating:
The articulating, metallic surfaces can be coated with a multi-layer ceramic Titan/Niobiumoxinitride coating (8 µm in total) for allergy protection (Nickel, Cobalt, Chromium, Molybdenum). This coating offers outstanding tribiological and electrochemical properties, is chemically and biologically non-reactive and prevents allergic reactions of the body to metallic components of the implant.

* ESKA Implants GmbH & Co (2002), Hip Stem, Type GHE, Product Properties, http://www.eska-implants.de/index.php?lang=2&area=2&group=2&id=26 / coating, Stand: 16.07.2006

10. 2. Characteristics of the Implants used in This Project

Left cemented stems of type GHE with different sizes (see Fig. 33).

Characters:

- Material is cobalt chromium alloy
- Anteversion angle 10^0
- Euro taper 12/14 mm
- Stem with collar
- Different stem sizes. In this project size 3, 4, and 5 were used
- Lengths of the used stems were 110, 120, and 130 mm respectively
- Anatomically stem shape with duple curvatures
- High femur resection with preservation of the greater trochanter

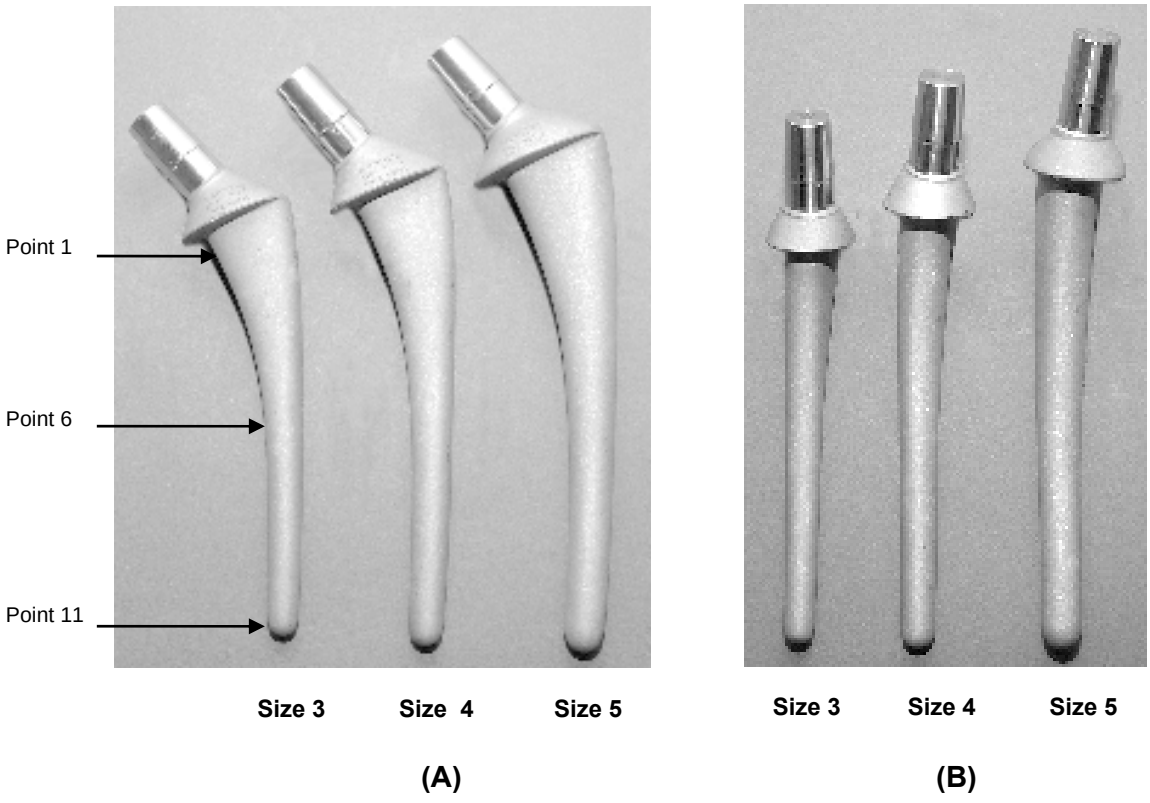

Fig. 33

Photographs showing anterior (A) and medial (B) views of the cemented GHE stems size 3, 4, 5 from left to right respectively.

Geometrical differences of the stems

Table 3: Lengths of the stems

Stem size 3	Stem size 4	Stem size 5
110 mm	120 mm	130 mm

Table 4: Mediolateral diameter

	Stem size 3	Stem size 4	Stem size 5
Point (1)	24.2 mm	25 .9 mm	29.3 mm
Point (6)	10.0 mm	11.1 mm	13.4 mm
Point (11)	8.3 mm	9.6 mm	11.4 mm

Table 5: Antero-posterior diameter

	Stem size 3	Stem size 4	Stem size 5
Point (1)	14.0 mm	15.8 mm	17.5 mm
Point (6)	10.0 mm	11.2 mm	13.2 mm
Point (11)	8.5 mm	9.7 mm	11.3 mm

NB: See fig. (33) for localisation of the three points (1, 6, and 11).

10. 3. Material and Methods

Three composite femurs were prepared and coated by photoelastic layers according to the instructions of Measurements Group as described before in the form of femur preparation, casting, contouring, measurements of the coating thickness and bonding procedure. Femurs were implanted by three different sizes of cemented stems (GHE stems) size 3, 4, and 5 with the following lengths 110, 120, and 130 mm, respectively.

Cutting of the femoral neck, reaming of the femoral canal, cementation technique and stem implantations were done for all femurs in the same situation and by an experienced orthopaedic surgeon (W.M.). Any technical variations during implantations were minimised by using the instruments recommended by ESKA Implants. Roentgenograms were done for each femur as documents for the right position of the implanted stem (fig. 34 and 35).

The implanted femurs were tested using the same loading protocol as employed for the intact femurs for the loading configuration which included the muscle simulations. As an option for increasing the power of comparisons, strains were measured in the intact femurs before implantation and used as a control, thus expressing the strains after implantations as percentages of the intact, where the variability will decrease by normalisation [15 P. 448].

In this project, we investigated the effect of the stem sizes on the femoral strain patterns with consideration to the influence of different offsets (from 32.2 to 51 mm).

The strain values after implantation of cemented stems were compared to those of cementless stems (the same type, GHE) and finally to those of a cementless custom-made stem.

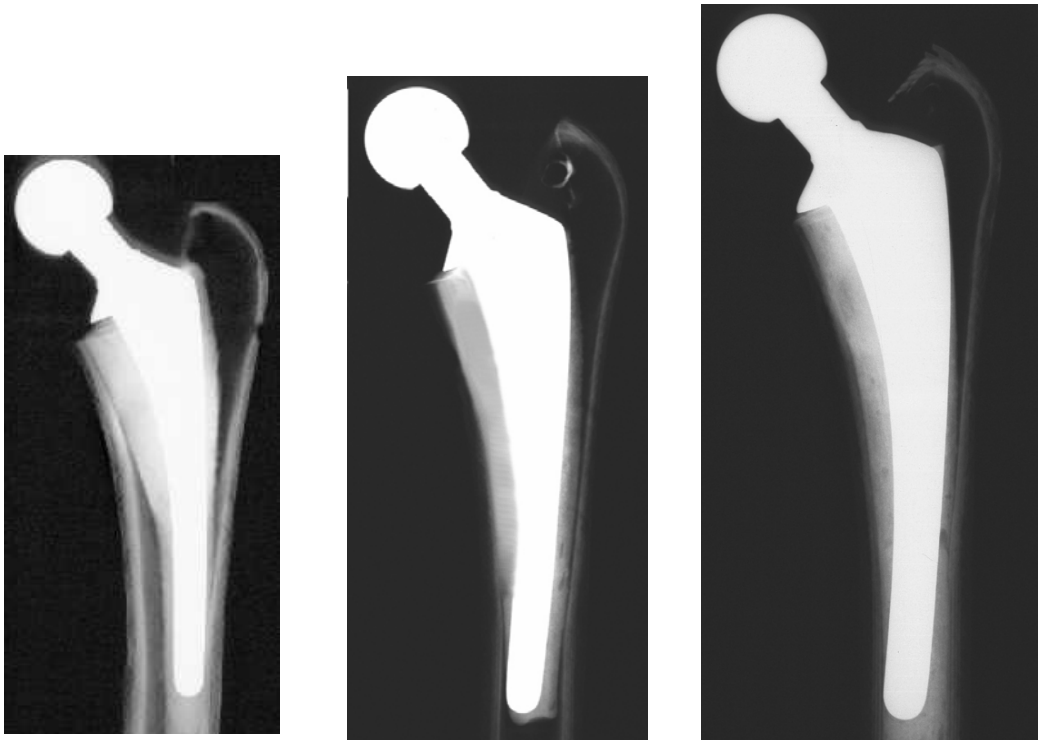

Fig. 34

Antero-posterior radiographs of the three coated composite femurs fitted with the three different sized cemented stems.

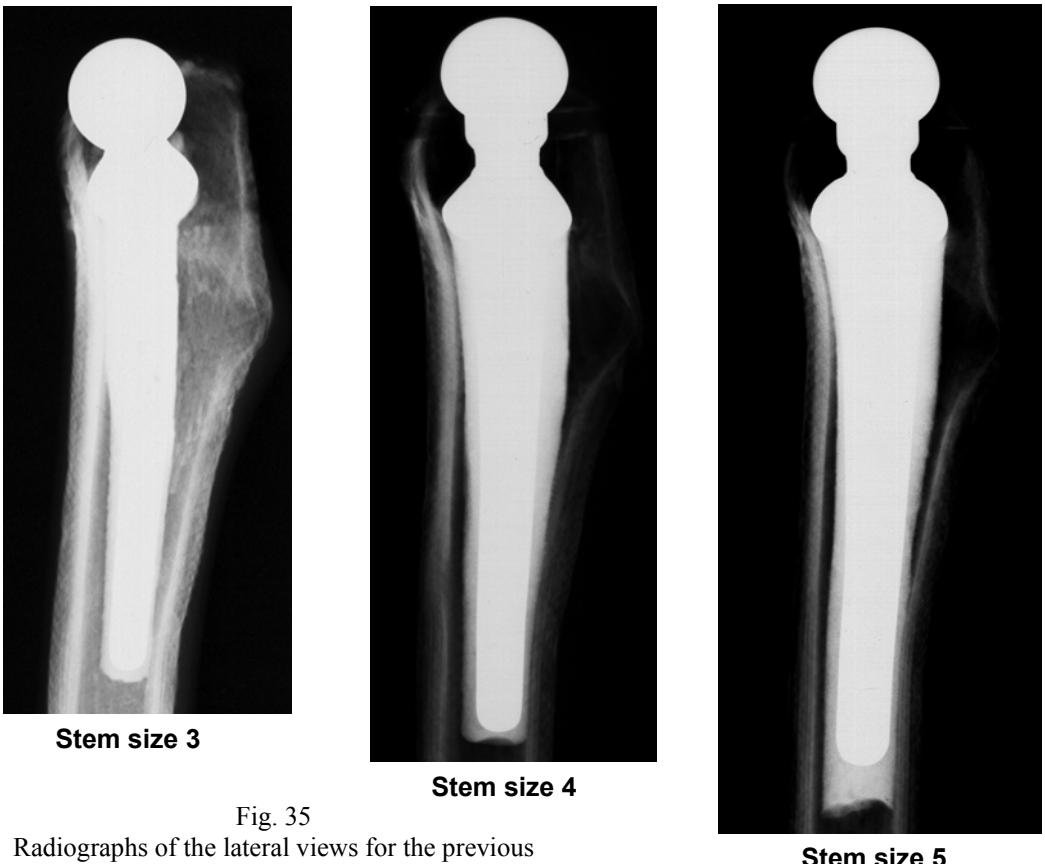

Fig. 35
Radiographs of the lateral views for the previous cemented stems.

10. 4. Results

By comparison of the strain test data of the implanted femurs and the strain data at the same position of the intact femurs, there were significant differences. It has been found that the strains on the implanted femur were markedly reduced, especially on the proximal femurs both on medial and lateral surfaces. The peak axial compressive and tensile strain was located in areas corresponding to the level of the stem tip, in both medial and lateral surfaces respectively. Non significant changes were detected on the anterior and posterior surfaces.

10. 4. 1. Comparison of the Strain Values Before and After Implantation of Cemented Stems with the Same Offset (46.5 mm)

<u>Comparison between implanted femur with GHE Size 3 and intact femur</u>

On the medial surface

At the calcar region, there was reduction in strain, in the range of -65.0% of the normal. At the mid of the stem in range of -17.3% of the normal. At the level of the stem tip, there were very small differences where the strain values in the implanted femur were higher about +1.8% than normal.

Table 6: Reduction of the strain on the medial surface of the implanted femur (stem size 3 = 110 mm) in percentage of the intact femur.

Calcar region Point (1)	Mid of the stem Point (6)	Tip of the stem Point (11)
-65.0%	-17.3%	+1.8%

On the lateral surface

Proximally there were reductions in the strain in the range of -61.1% of the normal. At the mid of the stem in the range of -31.4% of the normal. At the levels of the stem tip in the range of -12.5% of the normal.

Table 7: Reduction of the strain on the lateral surface of implanted femur (stem size 3 = 110 mm) in percentage of the intact femur.

Proximally Point (1)	Mid of the stem Point (6)	Tip of the stem Point (11)
-61.1%	-31.4%	-12.5%

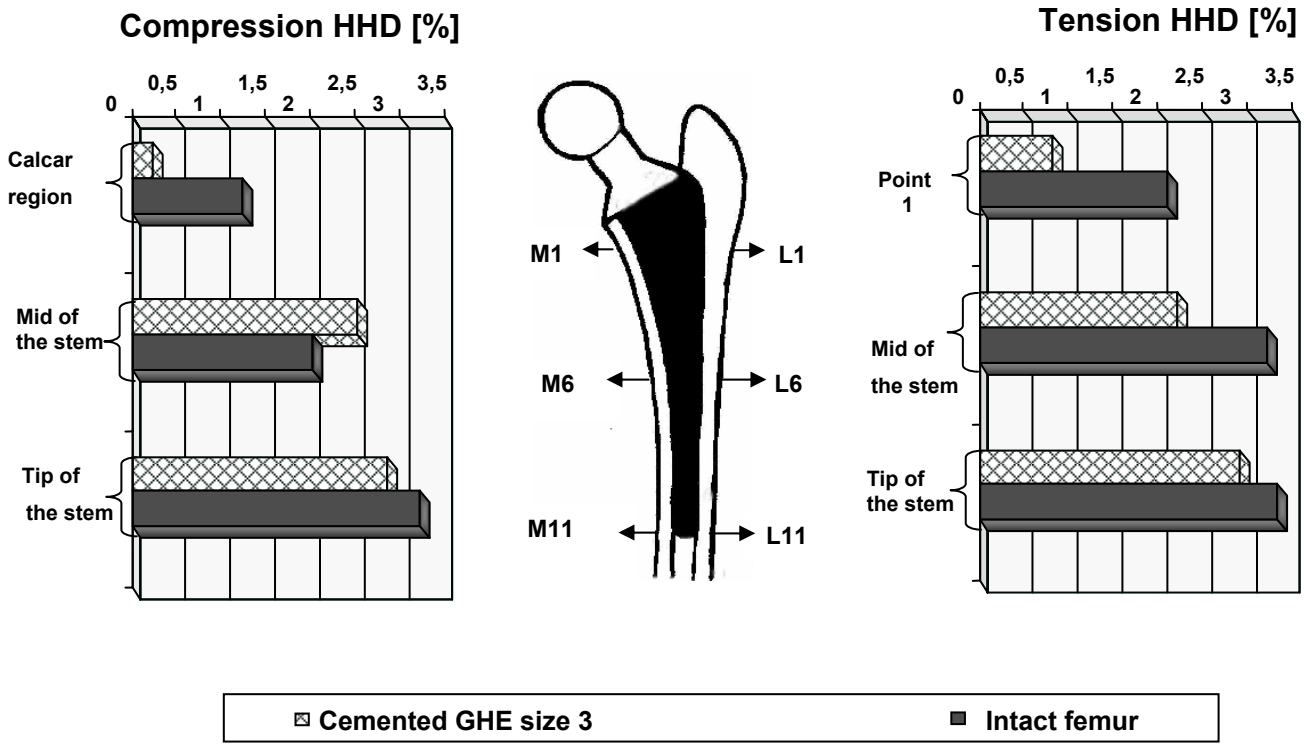

Fig. 36

Graphs showing bone strains at three locations along both medial and lateral surfaces of the implanted femur (cemented stem, size 3) and intact femur. The smallest strain values were proximally at the calcar region, but gradually increased distally where the maximum values were near the tip of the stem.

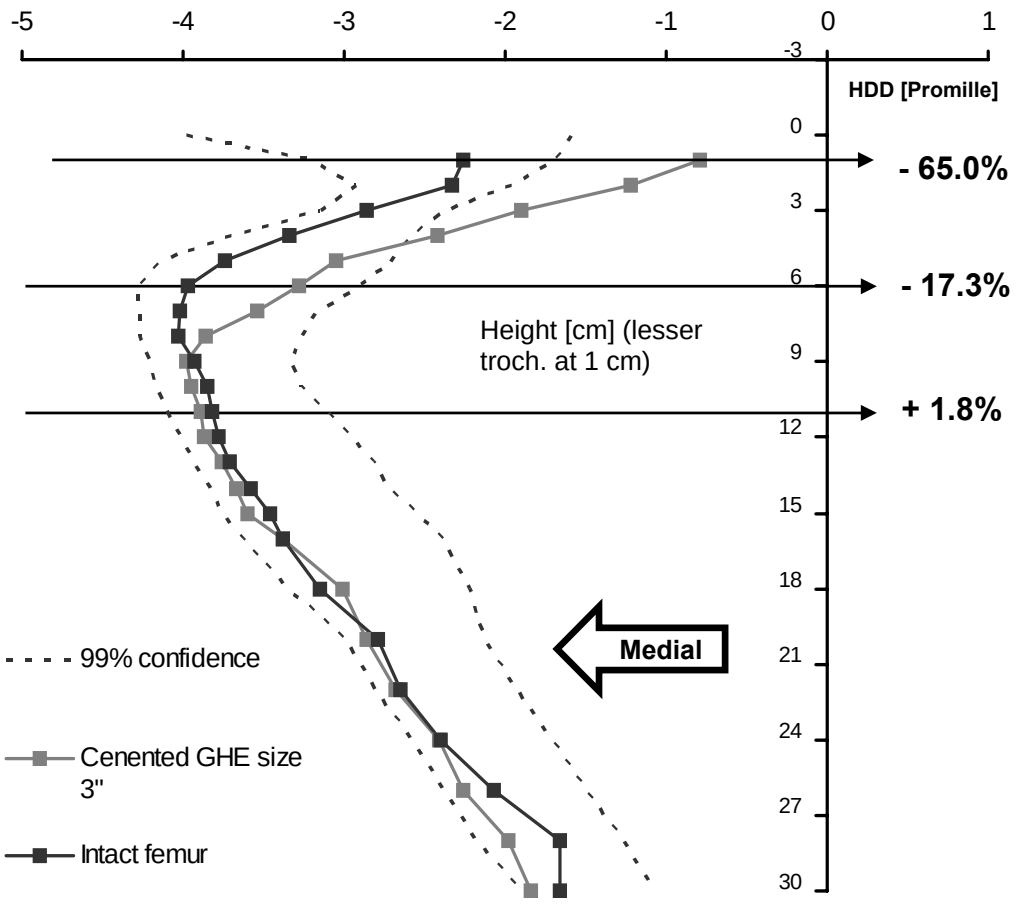

Fig. 37
Strain along the medial surfaces after implantation of stem size 3 In comparison with the intact femur.

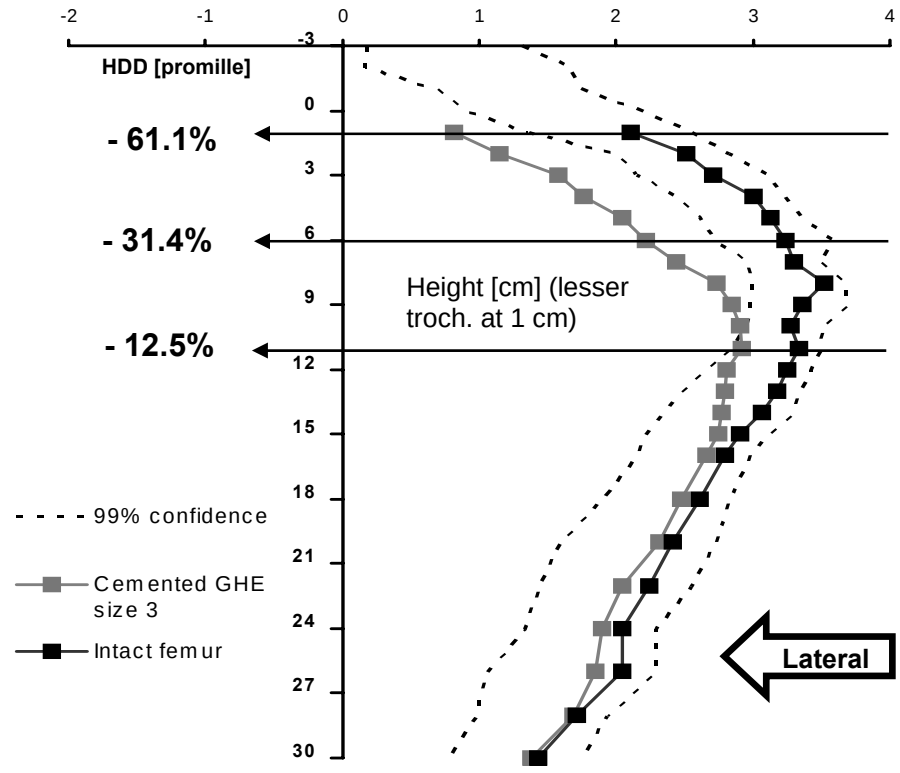

Fig. 38
Strain along the lateral surfaces after implantation of stem size 3 In comparison with the intact femur.

10. 4. 2. Comparison of the Strain Values Before and After Implantation of Cemented Stems with different Offsets (from 32.2 to 51 mm)

The strain pattern of the implanted femurs with different offsets from 32.2 mm (14.3 mm lower than the normal offset of the intact femur, that was 46.5 mm) to 51 mm (4.5 mm higher than the normal offset) was investigated. Measurements were done for each implanted femur. There were significant differences in the strain values of the implanted femur with different offset on both medial and lateral surfaces, especially near the distal end of the stems.

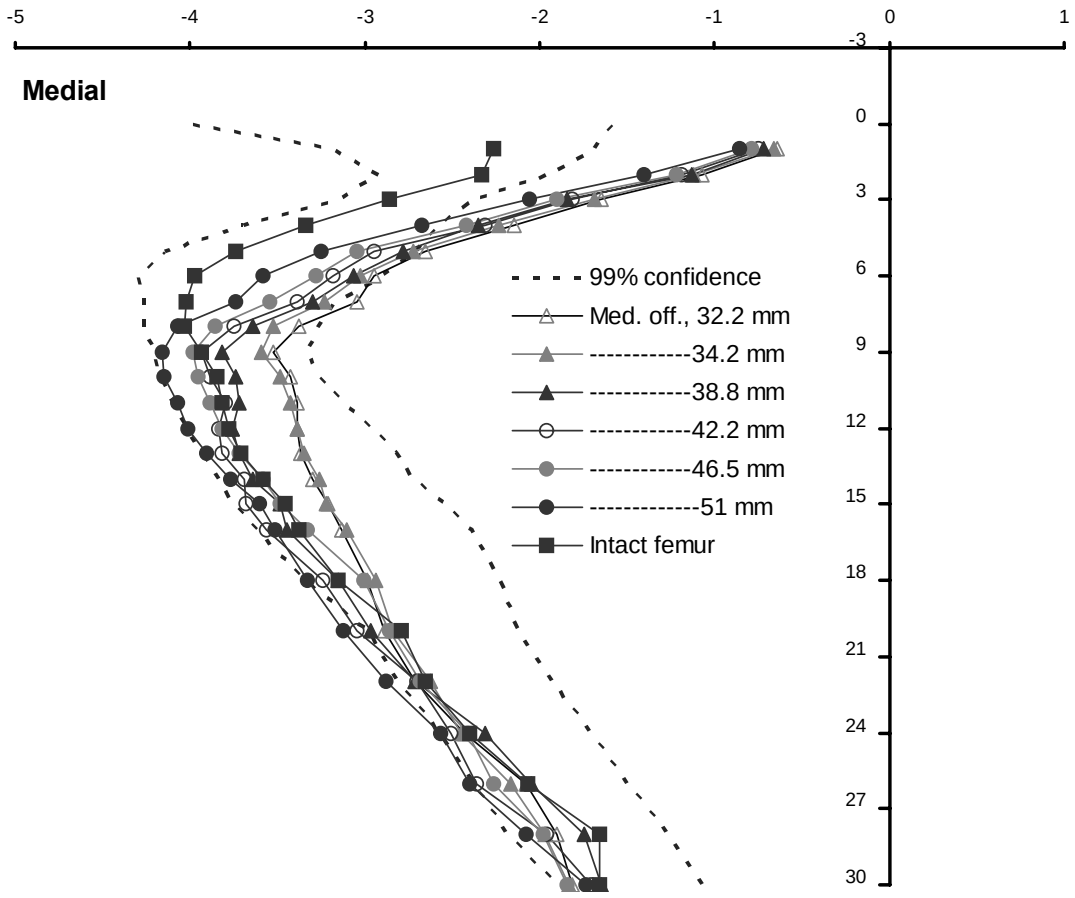

Fig. 39
Strains along the medial cortical bone after implantation of cemented stem size 3, with different offset.

Table 8: Effect of different offset (from 32.2 to 51 mm) on the medial femoral strain

Medial surface **Medial offset**	**Calcar region Point (1)**	**Mid of the stem Point (6)**	**Stem tip Point (11)**
32.2 mm	-71.6%	-25.6%	-11.2%
34.2 mm	-70.7%	-23.6%	-10.2%
38.8 mm	-68.1%	-22.6%	-2.6%
42.2 mm	-66.8%	-20.9%	-0.5%
46.5 mm (**normal offset**)	-65.0%	-17.3%	+1.8%
51 mm	-61.9%	-9.8%	+6.5%

Table 9: Effect of different offset (from 32.2 to 51 mm) on the lateral femoral strain

Lateral surface **Medial offset**	**The highest point proximally Point (1)**	**Mid of the stem Point (6)**	**Stem tip Point (11)**
32.2 mm	-68.8%	-49.6%	-33.6%
34.2 mm	-68.2%	-46.2%	-29.6%
38.8 mm	-64.4%	-42.5%	-20.0%
42.2 mm	-62.0%	-35.8%	-17.0%
46.5 mm **(normal offset)**	-61.1%	-31.4%	-12.5%
51 mm	-58.7%	-28.7%	-9.3%

On the medial surface

Increasing the medial femoral offset to 51 mm (4.5 mm higher than the normal offset) induced higher strains than the measured values of the implanted femur with the normal offset (46.5 mm). The previous table (8) shows that in comparison to the strain magnitude of the intact femur, there were reductions by -61.9% at the calcar region, -9.8% at the mid of the stem and +6.5% higher than the values of the intact femur at the distal tip of the stem.

A decreased medial offset to 32.2 mm (14.3 mm lower than the normal offset), produced marked decrease in the strain values in comparison to the measured values of the implanted femur with the normal offset and in comparison to the strain magnitude of the intact femur.

There were reductions by -71.6% at the calcar region, -25.6 % at the mid of the stem and -11.2% at the distal end of the stem.

On the lateral surface

Increasing the medial femoral offset higher than the normal offset produced higher strains than the measured values of the implanted femur with the normal offset. With 51 mm and in comparison to the strain magnitude of the intact femur, there were reductions by -58.7% at point (1), -28.7% at the mid of the stem, and -9.3% at the distal end of the stem.
Decreasing the medial offset produced marked decrease in the strain values. With 32 mm and in comparison to the strain magnitude of the intact femur there were reductions by -68.8% at point (1), -49.6% at the mid of the stem and -33.6% at the distal end of the stem.

10. 4. 3. Comparison of the Strain Values of the Three Implanted Femurs with Different Stem Sizes and the Confidence Interval of 12 Intact Bones

On the medial surface

There were marked differences in the medial femoral strain values after implantation of different stem sizes. In comparison to the mean values of the 99% confidence interval, the highest strain was produced by cemented stem size 3, then by size 4, and size 5, respectively. In the following table, the medial femoral strain reduction for each femur after implantation, along three locations as percentages of the mean values in 99% confidence is presented.

Table 10: Percentages of medial femoral strain reduction after implantation in relation to 99% confidence

Medial surface	Calcar region Point (1)	Mid of the stem Point (6)	Stem tip Point (11)
Stem size 3 (110 mm)	-67.7%	-8.8%	+7.7%
Stem size 4 (120 mm)	-80.4%	-22.2%	-12.7%
Stem size 5 (130 mm)	-89.8%	-29.4%	-23.5%

On the lateral surface

The highest strain was produced by stem size 3, then by size 4 and 5 respectively. In the following table, we presented the lateral femoral strain reduction for each femur after implantation, along three locations as percentages to the values of 99% confidence interval.

Table 11: Percentages of the lateral femoral strain reduction after implantation in relation to 99% confidence

Lateral surface	**The highest point proximally, Point (1)**	**Mid of the stem Point (6)**	**Stem tip Point (11)**
Stem size 3 (110 mm)	-57.9%	-29.5%	-7.5%
Stem size 4 (120 mm)	-65.1%	-36.5%	-17.4%
Stem size 5 (130 mm)	-71.2%	-46.0%	-19.9%

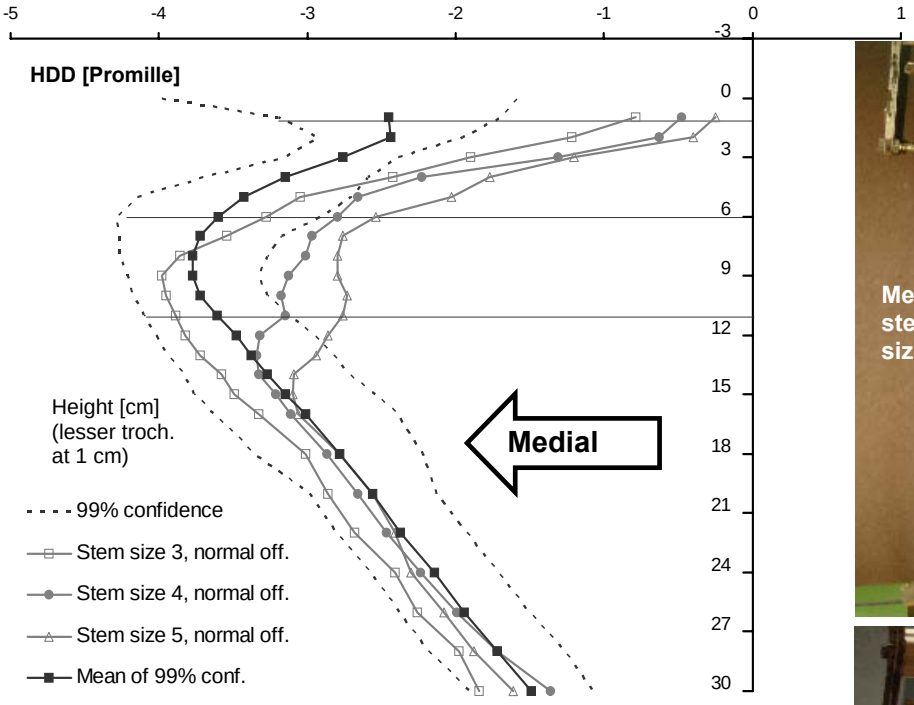

Fig. 41
Strains along the medial cortical bone after implantation of different stem sizes (cemented).

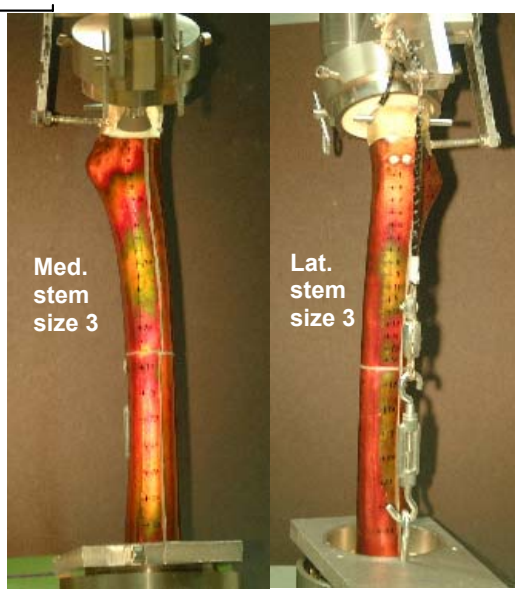

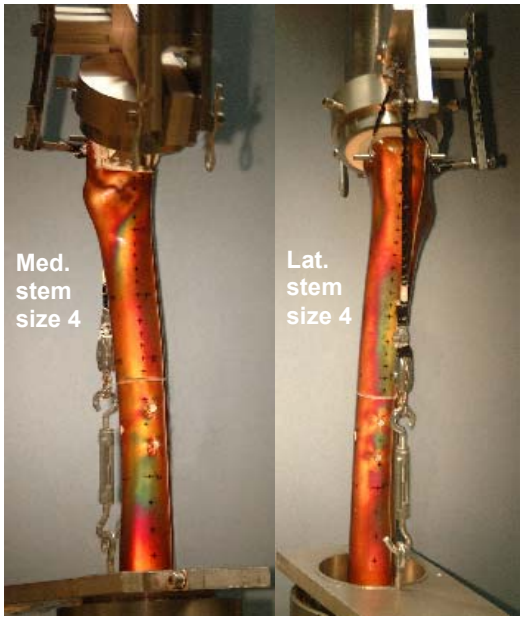

Fig. 42 ▶
Photographs showing the medial and lateral surfaces of loaded coated composite femurs after implantation of cemented stems size, 3, 4, and 5, respectively (viewed though a reflection polariscope).

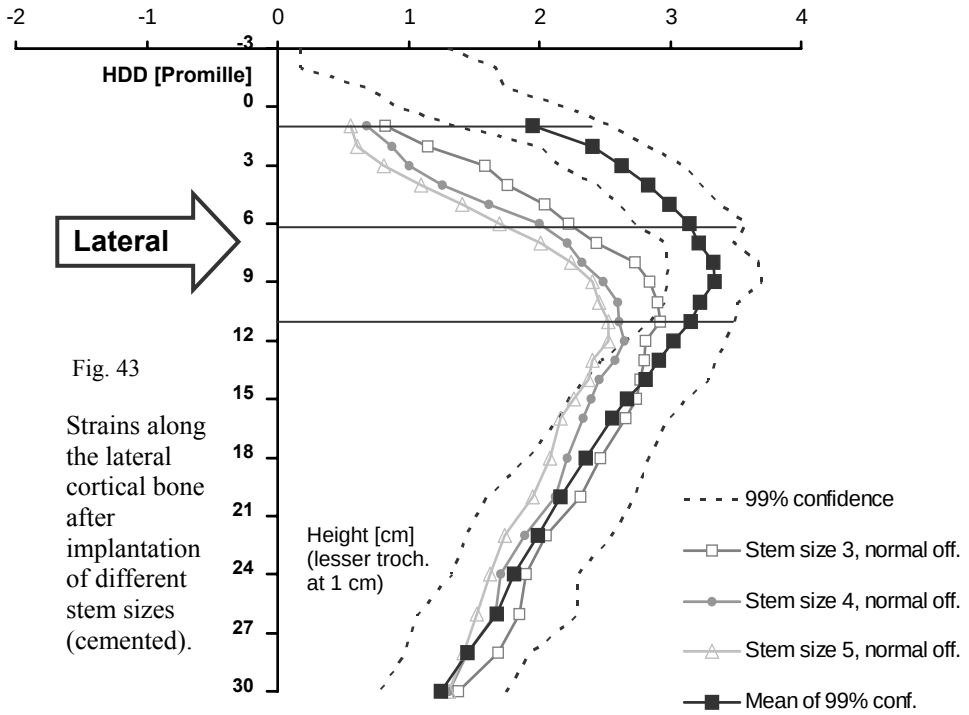

Fig. 43
Strains along the lateral cortical bone after implantation of different stem sizes (cemented).

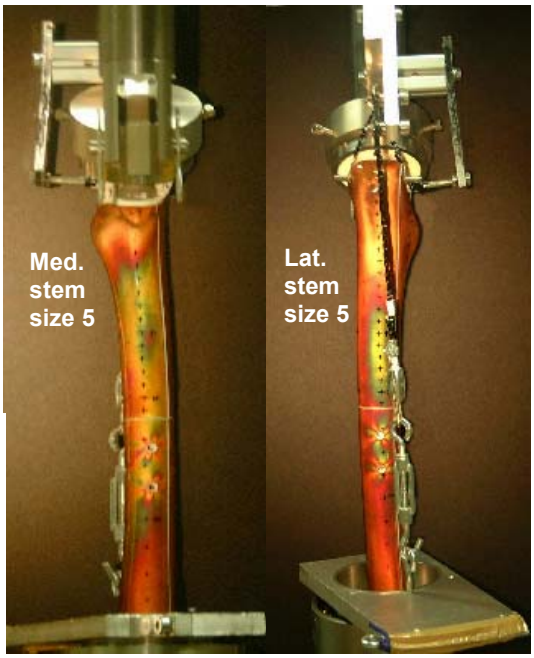

On the medial surface, in comparison to the results of stem size 3 (110 mm), stem size 4 (120 mm) produced more strain reduction about -12.7%, -13.4% and -20.4% at the calcar region, mid of the stem and stem tip respectively (table 10). Increasing of the stem size by 2 cm (stem size 5, 130 mm), produced more strain reduction about -22.1%, -20.6% and -31.2% at the calcar region, mid of the stem and stem tip respectively. Laterally, in comparison to the results of stem size 3, stem size 4, produced more strain reduction, about -7.2%, -7% and -9.9% at point (1), mid of the stem and stem tip respectively. With stem size 5, there were -13.3%, -16.5% and -12.4% at point (1), mid of the stem and stem tip respectively (table 11).

10. 5. Discussion

10. 5. 1. Femoral Strain Before and After Implantation

After total hip replacement the aim is to obtain stress distribution on the femur as close as possible to the normal physiological stress distribution for all loads that will be transferred across the hip joint [73 p. 1, 12].

In this project, after implantation of cemented stem size 3, there was reduction in the strain values at the calcar region in the range -65.0% of the normal values (table 6) and at the first and most proximal point laterally in the range of -61.1% of the normal values (table 7). It was found that the large stress shielding was in the proximal regions and the greatest strain values after implantation were at the level of the stem tip where it was +1.8% medially and -12.5% laterally [6 p. 91, 75 P. 71]. Addition of any implant to the femur will cause some degree of stress shielding. To be satisfied, it is better to create a situation in which the peri-implanted stresses are kept within acceptable values to the physiological condition to decrease bone resorption (Dr. Jo Miller, paradox of isoelasticity) [6 p. 94, 74 p. 25]. It was found that after femoral implantation the increased stiffness of the proximal parts of the femurs produced marked reductions of the strain magnitudes on the implanted femurs. This is due to “stress shielding” by the implant [75 p. 76, 61 p. 741, 68 p. 203].

The results are in agreement with the report by William Maloney and Jasty (1989) where they investigated the biological and mechanical changes that occur in vivo by examination of femurs retrieved at autopsy from 11 patients who died from 2 weeks to 17 years after having cemented THA. They have proved that after cemented THA there were marked strain reductions in the calcar region and that the peak axial compressive and tensile strains were at the level of the tip of the stems along the medial and lateral femoral surfaces, respectively in a reverse manner to the intact bone [39 p. 118, 49 p. 134, 58 p. 84, 68 p. 202, 75 p. 75]. In this project, the significant differences were on the medial and lateral aspects but not significant on both anterior and posterior surfaces. Luca Cristofolini et al. proved that significant differences were also on the medial and lateral aspects where the gluteal muscles increased the compression medially and tension laterally [13 p. 622]. Szivek noticed that there were strain variations on the anterior and posterior surfaces as a result of differences in the smaller bending moment on these surfaces. Because of high applied bending moments on the medial and lateral surfaces, strains were more consistent on the medial and lateral surfaces [70 p. 279].

10. 5. 2. Role of the Offset

Femoral offset is the distance from the centre of rotation of the femoral head to a line bisecting the long axis of the femur. In this study it was found that reducing of the medial offset by 14.3 mm below the normal offset of the intact femur (46.5 mm) reduced the bending moment and the femoral strain (fig. 39, table 8) [75 p. 74].

An increased femoral offset by 4.5 mm above the normal offset increased the bending moment and femoral strain pattern. Biomechanically, it is found that when the offset decreases, the abductor lever arm will decrease, resulting in an increase in both abductor muscle force and the resultant force across the hip joint, which could result in greater polyethylene wear and loosening over time. An increase in femoral offset decreases the abductor muscles force and the resultant force across the hip joint [18 p. 23]. Due to these significant stress changes with the different offsets, differentiation and comparison between implanted and intact femur should be done with the same bending moment (offset) [15 p. 443].

A decreased femoral offset moves the femur medially, resulting in potential impingement, soft tissue laxity, instability and possible dislocation. Increasing the femoral offset moves the femur laterally and will decrease incidence of impingement, improve soft tissue tension and better stability without lengthening the leg [18 p. 23]. When the joint forces and the abductor forces are the same, due to different offsets, different bending moments to the femur will occur [15 p. 437].

10. 5. 3. Effect of Different Implant Sizes on the Femoral Strain Patterns

In these results and in comparison of the strain values after implantation of different stem sizes and mean values of 99% confidence interval, there were significant differences. It was found that, the smaller the stem, the higher of the produced strain. The highest strains on both medial and lateral surfaces were with stem size 3, then size 4, and size 5 respectively (fig.41, 43). Stress shielding and risk of bone resorption with size 5 (larger and stiffer) should be expected more than that of size 4 and size 3 [68 P. 203].

It should expected that patients with the best bone quality have the smaller femoral canals and require smaller (more flexible) implants, whereas osteoporotic patients with larger canals need larger (stiffer) implants, thus they are predisposed towards more bone loss [6 P. 94].

Beside the stem sizes, thickness of the cement mantle constitutes an important role for the long-term implant survival and is affected not only by proper selection of stem size and canal preparation but also by proper position of the stem within the canal. Breusch et al. have identified typical areas of thin cement mantels (< 2 mm) anteroproximally and posterodistally especially with straight stems. Deficient cement mantles induced osteolysis and loosening [8 P. 652]. Neutral or near-neutral position of a stem with a mantle thickness of 2.5 mm near the tip will reduce the cement strain significantly while still maintaining a stem of sufficient size to withstand the increased strain that occurs within the prosthesis if the layer of the cement is thinner [24 P. 47]. For biomechanical analysis, it is very important to compare different implants with the same offset. It was found that large sized implants caused greater stress shielding. Because excessive stress-shielding is negative for the long-term fixation of an implant it is favourable to use smaller stems. But it has to be considered clinically that cement failure may occur by using very small stems. The results are in agreement with the results from Steinhauser (1998). By photoelastic analysis, he investigated the strain patterns on the femoral surfaces after implantation of special tumour prostheses with different stem lengths and materials. Regarding to the stem lengths, he used different stems with 80, 120, and 160 mm. He postulated that short stems produced strain patterns near to the physiological patterns and higher than those produced by the long stems [67 p. 52].

The results are in agreement with the clinical results from Charles Engh and Bobyn in 1988. In a roentgenographic study of 411 primary non cemented hip arthroplasties using the AML prostheses, they proved that using of a larger, structurally stiffer stem increased the risk of marked bone resorption. It was proven that there was a 10% incidence of marked bone resorption for the smaller stems with a distal diameter less than 13 mm and 44% incidence for the larger stem with a distal diameter larger than 13 mm [23 P. 18, 6 P. 83].
According to Bobyn (1992), stiffness = material modulus x geometric factor. A slight increase in the stem size causes relatively large increase in the stem stiffness. The correlation between stem stiffness and femoral bone remodelling in both canine and human studies proved that the use of more flexible implants should generally produce less bone resorption [6 P. 86, 87, 37 P. 125, 5 P.196, 205].

Crowninshield et al. found in 1980 that the stresses within the cement mantle near the tip of the prosthesis could be reduced by increasing the stem length, increasing the cross-sectional size of the stem, and decreasing the modulus of the stem [16 p. 72-74].

10. 6. Femoral Strain Patterns after Implantation of Cemented and Cementless GHE Stems

10. 6. 1. Materials and Methods

Two composite femurs were prepared and coated with photoelastic layers. The strain patterns on the femoral surfaces of the intact femurs were measured. Both femurs were implanted by cementless partial porous coated stems, type GHE, size 4 (see fig. 44, B). The femoral strain patterns after implantation were measured three times for each femur (measurements were done by Martin Ellenrieder, doctoral candidate). After removal of the cementless stems, both femurs were implanted by cemented GHE stems, one femur by stem size 4 and the other by stem size 5. The implanted femurs (with cemented and cementless stems) had the same offset similar to the intact femur (46.5 mm). Femurs were potted, fixed and loaded in the same manner as discussed before (see p. 47-49). We measured the strain patterns after implantation of cemented stems three times for each femur and compared the results with those of cementless stems in relation to the measurements of the intact femurs.

10. 6. 2. Characteristics of the Stems

See p. 54, 55

10. 6. 3. Geometrical Characteristics

Table 12: Lengths of the stems

	Cemented stem	Cementless stem
Stem length	120 mm	120 mm

Table 13: Medio-lateral diameter (see fig. 44)

	Cemented stem	Cementless stem
Point (1)	25.9 mm	31.5 mm
Point (6)	11.1 mm	14.1 mm
Point (12)	8.8 mm	10.3 mm

Table 14: Antero-posterior diameter

	Cemented stem	Cementless stem
Point (1)	15.8 mm	20.5 mm
Point (6)	11.2 mm	14.5 mm
Point (12)	8.8 mm	10.3 mm

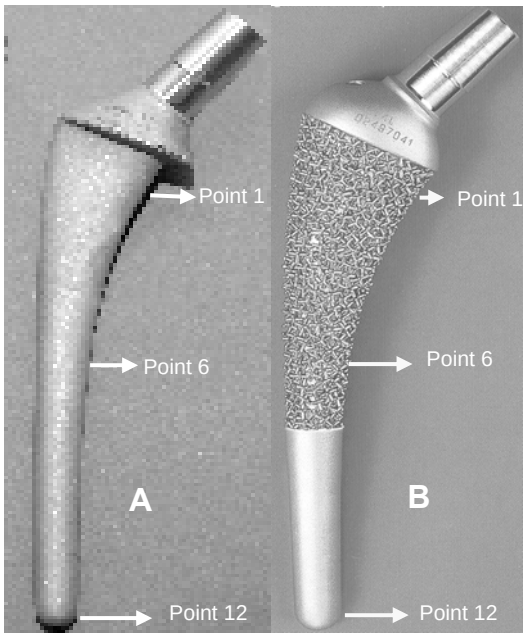

Fig.44

Photographs A and B showing the anterior surfaces of a cemented and a cementless GHE stem, size 4.

10. 6. 4. Results

10. 6. 4. 1. Comparison the Femoral Strain Patterns after Implantation of Cemented and Cementless Stems of the Same Size (4)

On the medial surface

It was found that the cemented stem produced at the calcar region and near the distal end of the stem more stress shielding than those of the cementless stem, but at the mid of the stem, the condition was reversed, where the cementless stem produced more stress shielding than the cemented stem (see fig. 45, 47).

- At the calcar region (point 1) there were reductions in the strain in the range of -79.0% of the normal values of the unresected femur for cemented stem and -57.2% for the cementless stem.
- At the mid of the stem in the range of -15.9% of the normal for the cemented stem and -32.1% for the cementless stem.
- At the distal region in the range of -7.3% of the normal for the cemented stem and -1.7% for the cementless stem.

Table 15: Reduction of the strains on the medial surfaces after implantation of cemented and cementless stems, (both had size 4) in relation to the strain values of the intact femur.

Region	Calcar region Point (1)	Mid of the stem Point (6)	Distally Point (11)
Cemented stem	-79.0%	-15.9%	-7.3%
Cementless stem	-57.2%	-32.1%	-1.7%

On the lateral surface

The overall strain values for the cementless stem were higher than those for the cemented stem, but the differences were not statistically significant (fig. 46, 47).

- Proximally there were reductions in the strain, in the range of -59.7% of the normal for the cemented stem and in the range of -56.2% for the cementless stem.
- At the mid of the stem in the range of -29.3% for the cemented stem and -22.6% for the cementless stem.
- At the distal region in the range of -6.1% of the normal for the cemented stem and -1.0% for the cementless stem.

Table 16: Reduction of the strains on the lateral surfaces after implantation of cemented and cementless stems, (both have size 4) in relation to the strain values of the intact femur.

Region	Proximally Point (1)	Mid of the stem Point (6)	Distally Point (11)
Cemented stem	-59.7%	-29.3%	-6.1%
Cementless stem	-56.2%	-22.6%	-1.0%

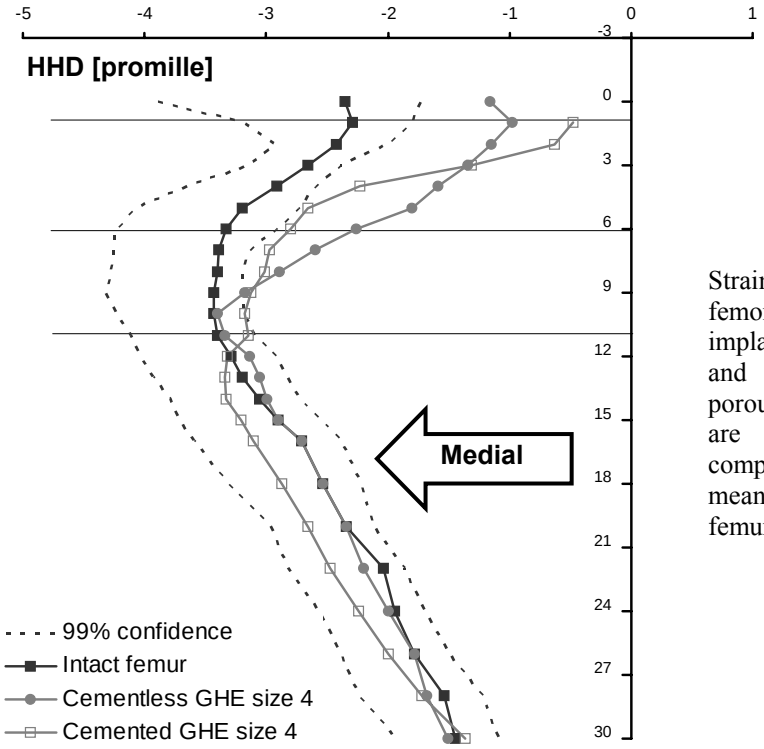

Fig. 45

Strains on the medial femoral surfaces after implantation of cemented and cementless partial porous coated stem (both are GHE size 4) in comparison to the strain mean values of the intact femur.

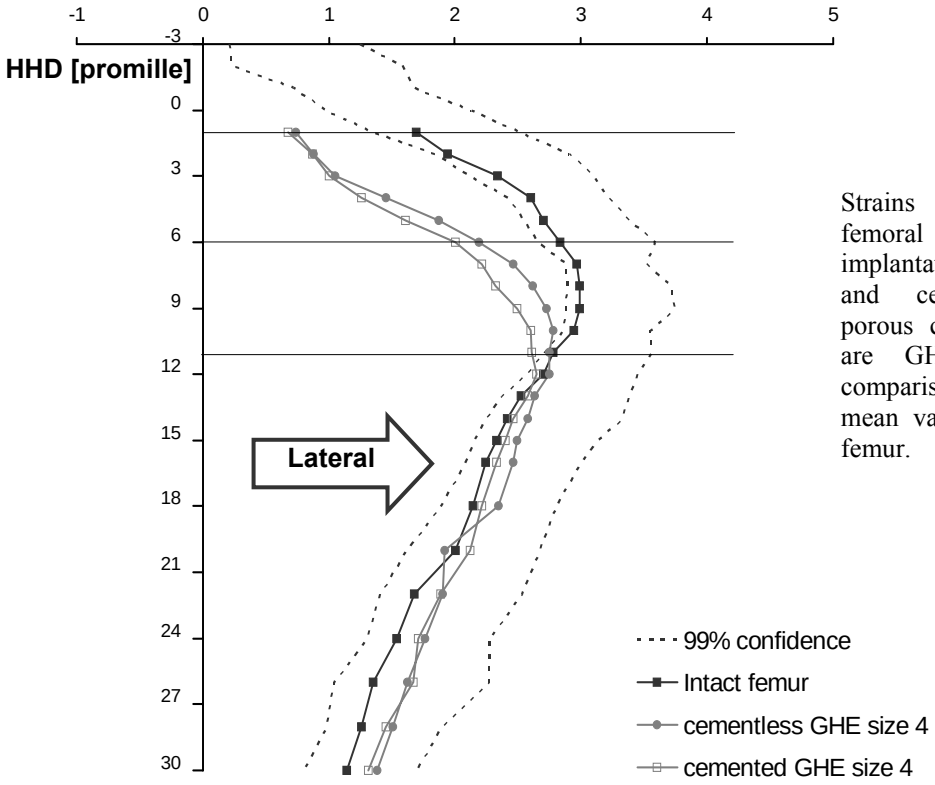

Fig. 46

Strains on the lateral femoral surfaces after implantation of cemented and cementless partial porous coated stem (both are GHE size 4) in comparison to the strain mean values of the intact femur.

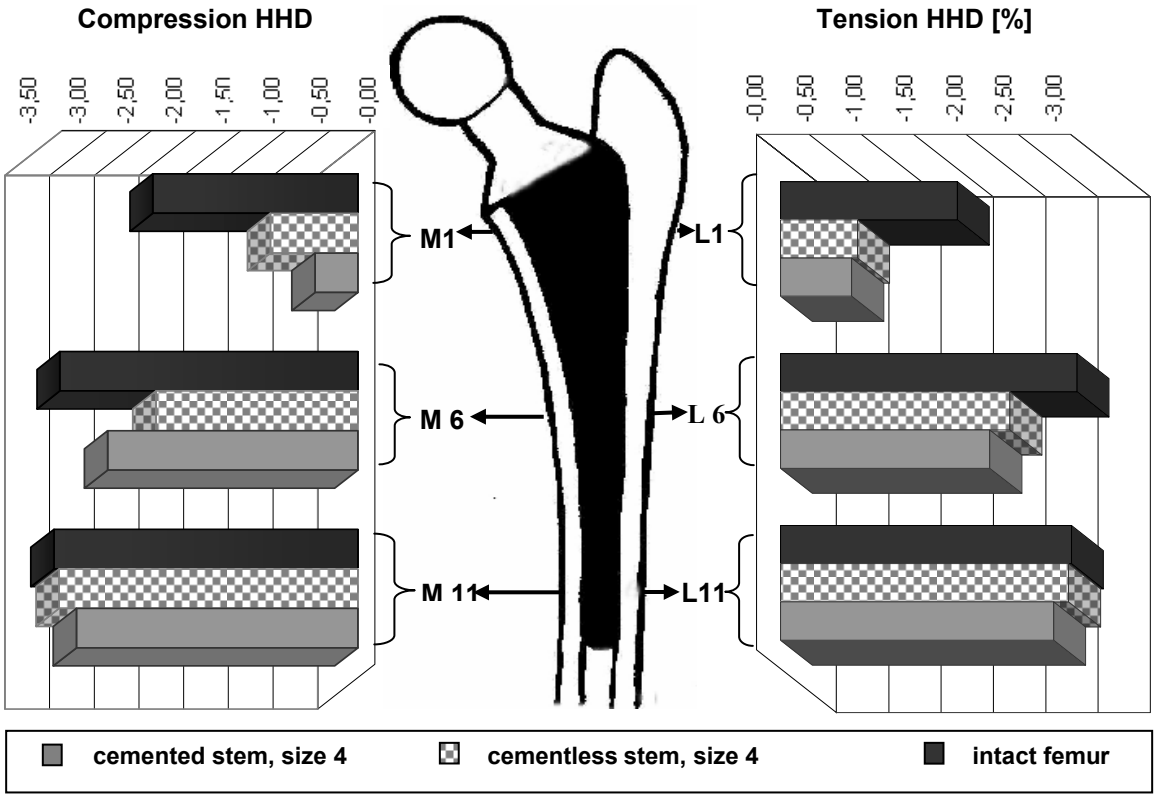

Fig. 47

Graphs showing, strains along three locations on the medial and lateral surfaces of the implanted femurs with cemented and cementless stem size 4 in relation to the strain values of the intact femur.

Fig. 48
Radiographs (AP views)
of both, cemented and cementless stems size 4.

10. 6. 4. 2. Comparison of the Femoral Strain Patterns after Implantation of a Cemented Stem, Size 5 and Cementless Stem, Size 4

On the medial surface

- At the calcar region (point 1) there were reductions in the strain, in the range of -89.5% of the normal for the cemented stem, size 5 and in the range of -47.6% for the cementless stem, size 4.
- At the mid of the stem in the range of -21.6% of the normal for the cemented stem, size 5 and -37.0% for the cementless stem, size 4.
- At the level of the stem tip, there were small differences where the strain values for the cemented stem, size 5 reduced in the range of -9.7% and minimally increased in a range of +1.8% for the cementless stem, size 4.

Table 17: Reduction of the strains on the medial femoral surfaces after implantation of a cemented stem, size 5 and a cementless stem, size 4 in percentage of the intact femur.

	Calcar region Point (1)	**Mid of the stem Point (6)**	**Tip of the stem Point (12)**
Cemented stem size 5	-89.5%	-21.6%	-9.7%
Cementless stem size 4	-47.6%	-37.0%	+1.8%

On the lateral surface

- Proximally there were reductions in the strain, in the range -68.0% of the normal for the cemented stem, size 5 and in the range of -52.5% for the cementless stem, size 4.
- At the mid of the stem, in the range of -43.5% for the cemented stem, size 5 and -24.5% for the cementless stem, size 4.
- At the level of the stem tip, reduced in the range of -7.3% for the cemented stem, size 5 and minimally increased in the range of +1.8% for the cementless stem, size 4.

Fig.18: Reduction of the strains on the lateral femoral surfaces after implantation of a cemented stem, size 5 and a cementless stem, size 4 in percentage of the intact femur.

	Proximally Point (1)	**Mid of the stem Point (6)**	**Tip of the stem Point (12)**
Cemented stem size 5	-68.0%	-43.5%	-7.3%
Cementless stem size 4	-52.2%	-24.5%	+1.8%

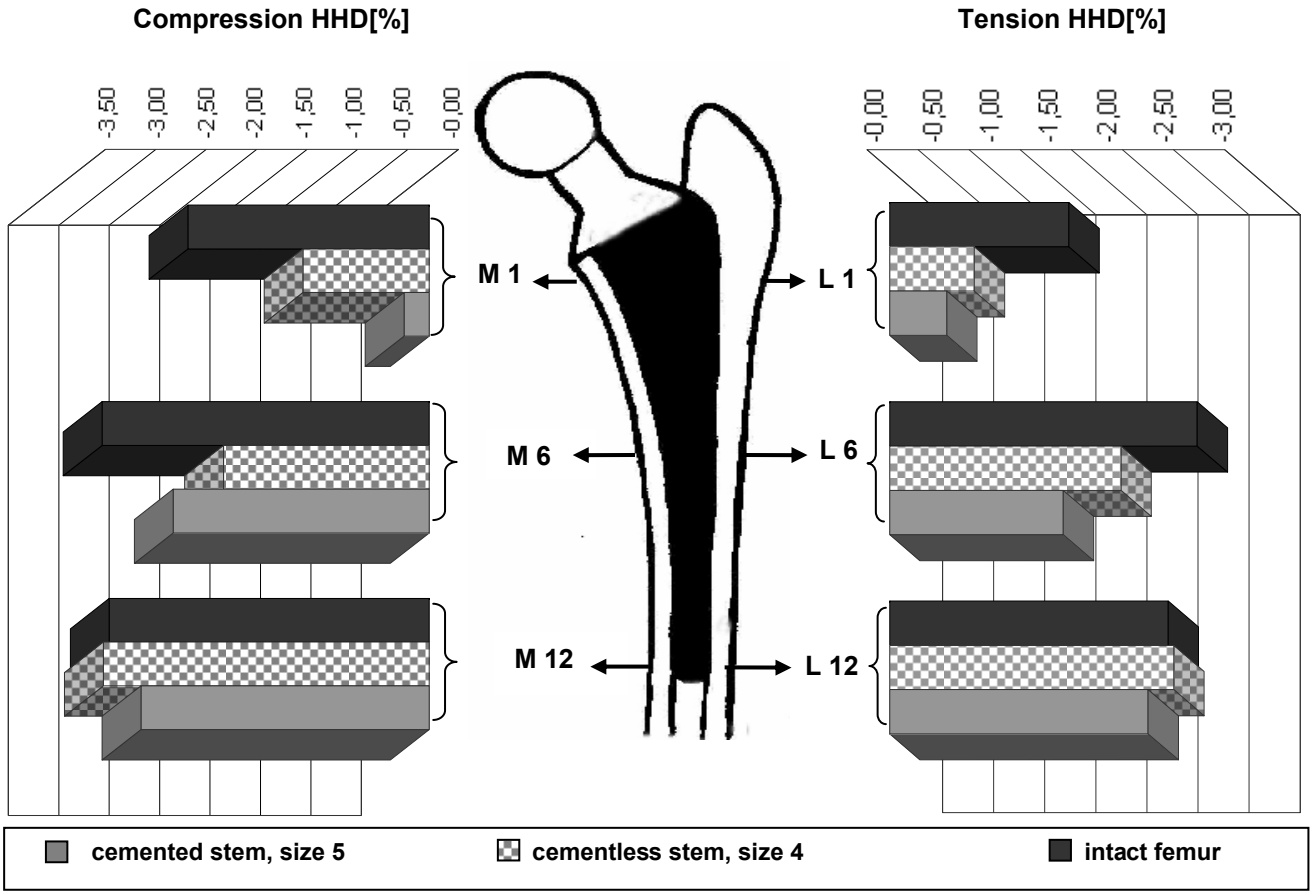

Fig. 49

Graphs showing strains along three locations on both medial and lateral surfaces of the implanted femurs with a cemented stem, size 5 and a cementless stem size, 4 in relation to the strain values of the intact femur.

10. 6. 5. Discussion

Because cement failure is one of the major problems in cemented hip arthroplasty, biologic fixation of the stem by means of bone ingrowth has become the focus of considerable interest among orthopaedic surgeons. Bone ingrowth has been demonstrated into porous metals, resulting in a strong interface between metal and bone providing stable fixation for the load-bearing prostheses [25 p. 293]. In the proximal femurs and by comparison of the stress test data of the implanted femurs (cemented and cementless) to the stress test data at the same positions of the intact femurs, there were significant reductions of the stresses and the strains on the implanted femurs whatever cemented or cementless, as a result of implantation [72 p. 889]. Distal to the stem tip, the strain patterns began to converge, indicating that distally there were little changes in bone loading after prosthetic implantation and that there were similarities of the loading tests for both cemented and cementless stems.

It is widely held that the remodelling changes seen around cementless stems tend to appear in a short period of time and tend to be more sever than those observed around cemented stems [28 p. 768, 40 p. 37].
In this study it was found that cementless stems created strains in the proximo-medial surfaces and near the distal end of the stem more than those of cemented stems which created higher strains only in the mid region (fig. 45, 47). Therefore, we expect less bone remodelling and better bone stock in the trochanteric region and distally with a cementless stem than with a cemented stem. The role of porous coating cannot be examined in this study but, it should be expected that, proximal bone ingrowth should force stress transfer at the proximal bone-implant interface, thereby helping to maintain proximal bone stock and decrease bone resorption [23 p. 8, 7 p. 393, 38 p. 707]. Laterally, the overall strain values for the cementless stem were higher than those for the cemented stem, but the differences were not statistically significant [35 p. 741]. These are in agreement with the clinical findings from Engh and Bobyn in 1988, where they have reported clinically the fact that most bone resorption was found in the proximo-medial area and less bone remodelling on the lateral side [23 p. 17].

The results are in agreement with the results from Sumner in 1992. He investigated bone remodelling and ingrowth of the bone in association with the use of cementless porous femoral stems at two years in a canine total hip arthroplasty model. He postulated that the amount of medullary bone increased proximally and distally [69 p. 248].

The results also are in agreement with the clinical assessment from Michael Torchia in 1990. He investigated bone remodelling in the femoral diaphysis following cemented and cementless hip arthroplasty. He found that there were localised stress transfer near the stem tip with cementless specimens and stress shielding in the stem tip region with cemented specimens. In his study, he interpreted increase in the cortical area and second moments of area of femoral cross section to indicate stress transfer, and reduction in these properties to indicate stress shielding [72 p. 889].

The results also are in agreement with the clinical results form Astor Reigstad (1993). He compared radiographically the femurs for 5 years after cemented and cementless hip arthroplasty for coxarthrosis in 120 patients. He concluded that incidence of distal cortical hypertrophy and proximal radio-opaque double line was higher around cementless stem. The remodelling processes with cementless stems tended to be self limited and the net bone loss seemed to be less than that around cemented stems [60 p. 415].

Amstutz et al., in 1989 have reported that the cortical hypertrophy around the distal part of the cementless press fit stems with a frequency as high as 66 percent is thought to be an indication of distal stress transfer to the cortical bone [3 p. 115]. Lintner et al., 1988 have confirmed by histological examination of autopsied cases that the distal hypertrophy is not associated with loosening [60 p. 415].

A histological analysis revealed that the porous metal serves as a matrix for bone ingrowth. Implants placed into experimental animals have subsequently shown that 30-40% of the porous surfaces are covered with new bone. The reactive changes have not been seen at the bone-metal interface, bone appears to exist uniformly in direct contact with the porous metal surfaces without the development of a fibrous membrane. The absence of any fibrous membrane formation strongly suggests of a highly compatible and stable biological system.
[25 p. 294, 34 p. 309]
In a few implants retrieved from osteoporotic patients, not only bone ingrowth was found, but new bone was found within the pre-existing cortical porosity. This suggested that the altered strain distribution in the surrounding cortex, produced by the presence of a metallic femoral stem, stimulated new bone formation [65 p. 171].

It was found that fixation of a fully porous-coated femoral component by osseous ingrowth results in massive osteolytic changes in the upper femur [9 p. 221, 65 p. 170, 50 p. 628].
It is postulated that the proximal bone loss was the same for both proximally and fully coated stems but distally where was no porous coating on the proximally coated stems, the extent of the cortical bone loss was somewhat less severe [28 p. 769, 7 p. 393, 408, 36 p. 1262].
Proximal bone ingrowths with the proximal coated stem minimises the possibility of predominantly distal stem fixation causing proximal stress shielding and bone resorption and forces proximal stress transfer between the interface bone and implant surface, thereby helping to maintain or possibly increase proximal bone stock. Both, the promotion of the supportive bone proximally and reduction of the tendency for rigid distal stem fixation that could promote fatigue failure, are factors that could be beneficial to long-term implant performance [7 p. 393].

N.B
In this project we did not give attention to the effect of the stem collar on the proximal femoral strain. It was out of our investigation and discussion. However, Jacob in 1980 proved that direct bearing of the collar of the prostheses neck on the cortical bone of the calcar does not bring significant changes in the general stress conditions within either the bone or in the prosthesis stem [42 p. 172].

11. Experimental Analysis with Three Cementless "Custom-Made" Stems with Different Sizes and Shapes (Adaptiva®-Indiviual Endprosthesis-System)

In this project, the strain values on the femoral surfaces after implantation of three different cementless stems were investigated and compared with the confidence interval.

1. Femoral neck prosthesis, NR. D 2108.
2. Femoral prosthesis with short shaft, NR. D 2077.
3. Standard prosthesis, NR. D 2076.

11. 1. Characteristics of the Stems*

- Cementless prosthesis, made of Ti6Al4V (titanium alloy).
- Euro taper 12/14 mm.
- They are straight stems without collar.
- They have rectangular cross section with contact to the medial and lateral cortex with rotational and primary stability where a customised stem can be shaped to fill the medullary canal with respect to obtain maximum stability without migration to varus or valgus.
- For primary hip replacement with individual adjustment to the femur, on the basis of CT pictures in a computer-aided 3D-construction procedure.
- By customisation of the stem, the surgeon can restore the normal geometry of the hip by correction of the following biomechanical parameters:

    1. Leg length.
    2. Rotation of lower extremity.
    3. Position of the femur in relation to the centre of rotation.
    4. Abductor lever-arm.

- They are bone saving stems and have a minimal invasive procedure during implantation that is required especially in younger individuals, where good amount of bone will be saved for revision.

---

* endoPro medical GmbH (2003), Hip Stem Adaptiva® individual endoprosthesis, Product Properties http://www.endopro.de/Adaptiva/Adaptiva-Arzt/Info/adaptiva-arzt-info.html, Stand: 24.01.2003

11. 2. Manufacturing of the Implants

- Designing and manufacturing of the customised implants depend on computer tomography (CT) scan. The CT data are used for the three dimensional reconstruction of the femoral canal. The implants are reconstructed using computer-assisted design technology (CAD) and computer-assisted manufacturing (CAM) techniques. The implant is manufactured in titanium alloy (Ti-6Al-4V) according to ASTM (American Society for Testing and Materials) standard for using this alloy in implants (ASTM F 1472). Surgical implants are coated by ceramic hydroxyapatite according to standard specification for composition of ceramic hydroxyapatite (ASTM F 1185).

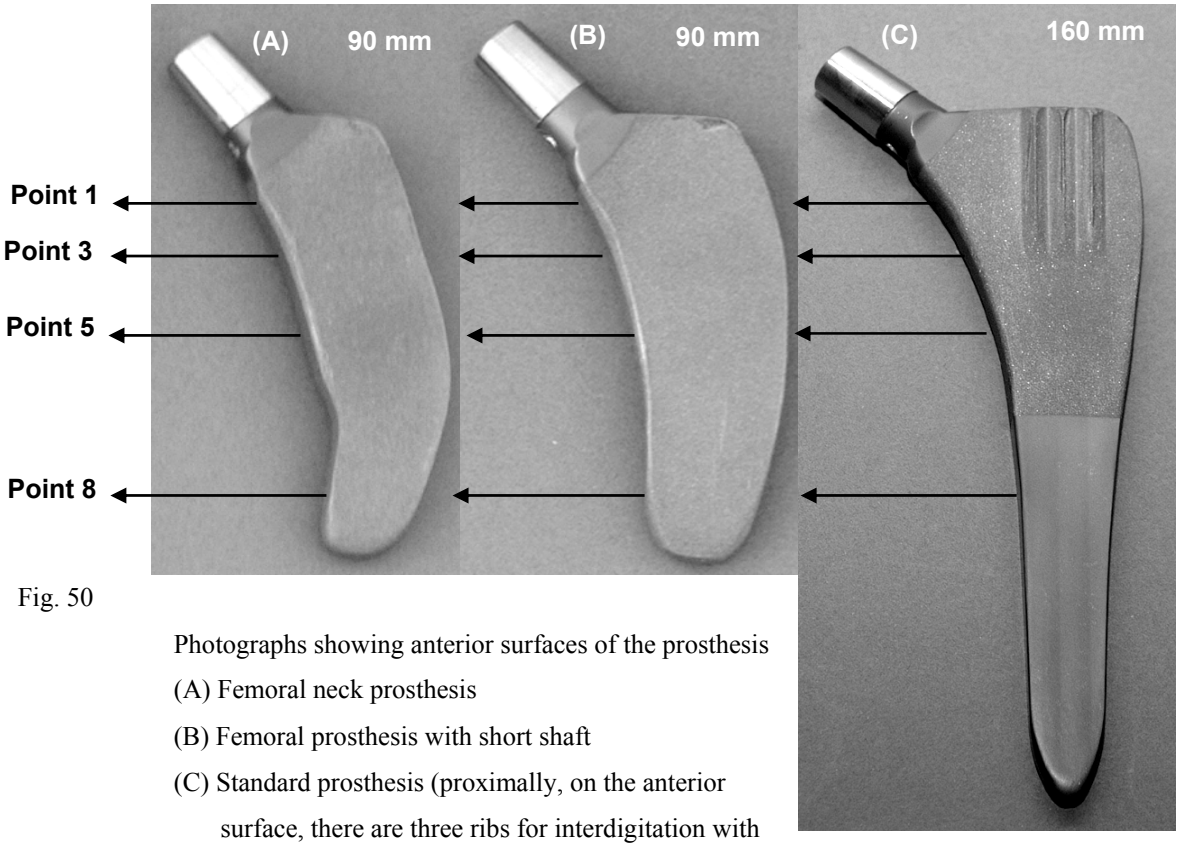

Fig. 50

Photographs showing anterior surfaces of the prosthesis
(A) Femoral neck prosthesis
(B) Femoral prosthesis with short shaft
(C) Standard prosthesis (proximally, on the anterior surface, there are three ribs for interdigitation with the metaphyseal cancellous bone)

11. 3. Geometrical Differences of the Stems

Table 19: Lengths of the stems

(A)	(B)	(C)
Femoral neck prosthesis	Femoral prosthesis with short shaft	Standard prosthesis
90 mm	90 mm	160 mm

Table 20: Medio-lateral diameter (see fig. 50)

	(A)	(B)	(C)
Point (1)	28.0 mm	33.0 mm	45.0 mm
Point (3)	26.3 mm	32.5 mm	38.8 mm
Point (5)	25.0 mm	29.0 mm	31.0 mm
Point (8)	17.0 mm	21.0 mm	22.0 mm

Table 21: Antero-posterior diameter

	(A)	(B)	(C)
Point (1)	11.6 mm	11.6 mm	11.6 mm
Point (3)	11.2 mm	11.2 mm	11.2 mm
Point (5)	10.4 mm	10.4 mm	10.2 mm
Point (8)	9.1 mm	9.2 mm	9.3 mm

N.B:

Stems (A) and (B) have the same length (90 mm) but (B) has medio-lateral diameter wider than (A) (about 4 mm).

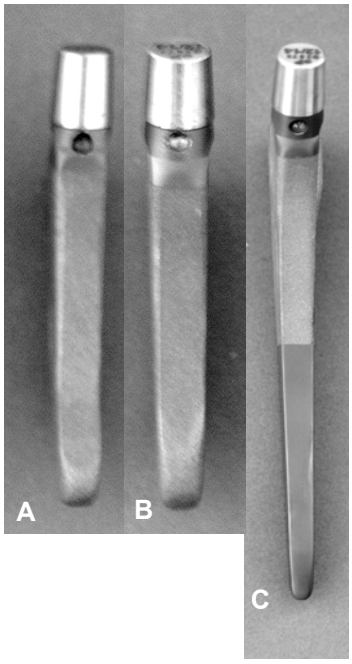

Fig. 51

Photographs showing medial surfaces of the prosthesis:

(A) Femoral neck prosthesis
(B) Femoral prosthesis with short shaft
(C) Standard prosthesis

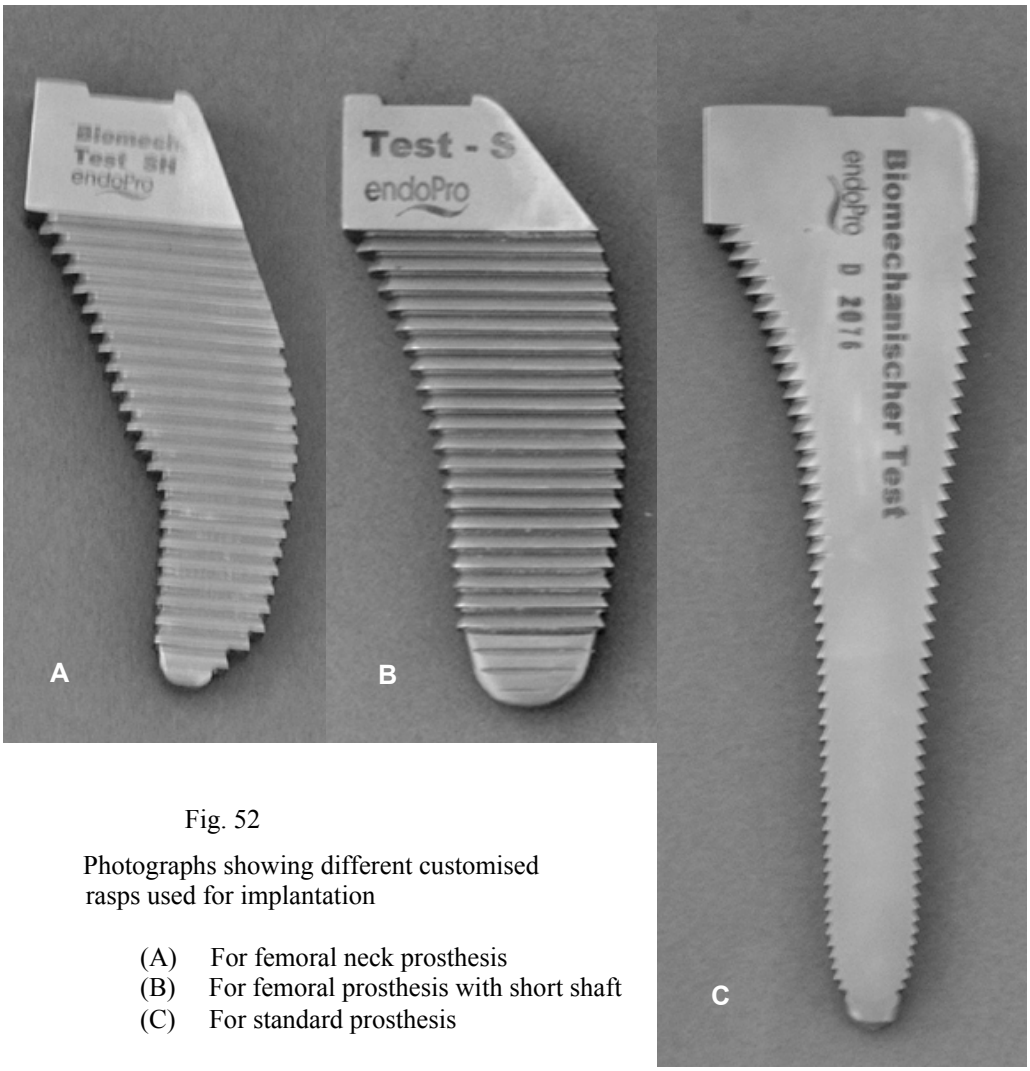

Fig. 52

Photographs showing different customised rasps used for implantation

(A) For femoral neck prosthesis
(B) For femoral prosthesis with short shaft
(C) For standard prosthesis

11. 4. Materials and Methods

Three composite femurs were prepared and coated by photoelastic coating layers. Each femur was tested stepwise by the three different types of cementless stems (fig. 50).

Cutting of the femoral neck, reaming of the femoral canal and stem implantation were done for all femurs in the same situation and by an experienced orthopaedic surgeon (G. G.), using the instruments recommended by endoPro medical Company (supplier of the prosthesis) to avoid any technical variations during implantation.

Roentgenograms were then done for each femur after implantation as documents for the position of the implanted stem (fig. 53, 54).

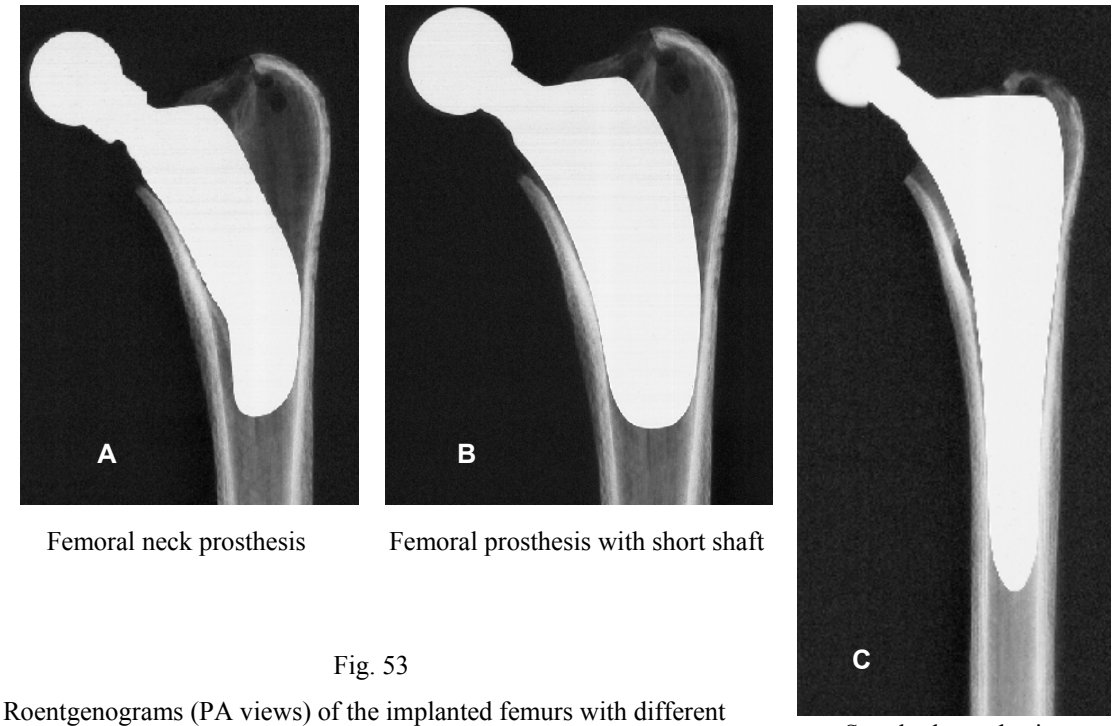

Femoral neck prosthesis

Femoral prosthesis with short shaft

Standard prosthesis

Fig. 53

Roentgenograms (PA views) of the implanted femurs with different cementless, custom-made stems.

.

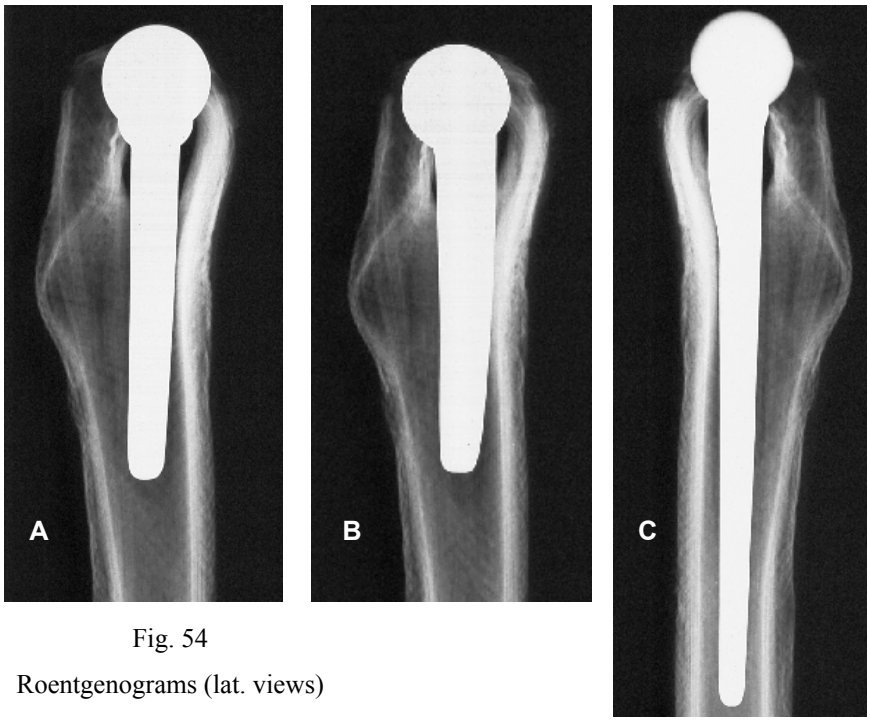

Fig. 54

Roentgenograms (lat. views)

11. 5. Results

Comparison between the strain values on the femoral surfaces after implantation of the previous three different cementless stems and the mean of 99% confidence interval of 12 unresected bones.

On the medial surfaces

By comparison of the strain test data of the implanted femurs and the strain test data at the same position of the mean of confidence interval, there were significant differences and reductions in the strain patterns with the three different stems as a result of implantation.

Proximally (point 3)

There were strain reductions in the range of -22.1%, -56.9%, and -69.5% of the mean confidence for the femoral neck stem, short shaft stem, and the standard stem, respectively.

At the mid of the stem (point 5)

There were strain reductions in the range of -10.5%, -17.5% and -82.5% of the mean confidence with the femoral neck stem, short shaft stem, and the standard stem, respectively.

At the stem tip (point 9)

The strain values increased in the range of +10.0%, and +9.0% of the mean confidence with the femoral neck stem and the short shaft stem, respectively. With standard stem, there was reduction in a range of -3.7%.

Table 22: Strain values on the medial surfaces, in a percentage to the mean of confidence interval.

Medial surface→	Proximally (Point 3)	Mid of the stem (Point 5)	Tip of the stem (Point 9)
Femoral neck stem	-22.1%	-10.5%	+10.0%
Stem with short shaft	-56.9%	-17.5%	+9.0%
Standard stem	-69.5%	-82.5%	-3.7%

On the lateral Surfaces

Proximally (point 1)

There were strain reductions in the range of -74.8%, -83.0%, and -51.8% of the mean confidence with the femoral neck stem, the short shaft stem and the standard stem, respectively.

At the mid of the stem (Point 5)

There were strain reductions in the range -68.2%, -75.2%, and -80.9% with the femoral neck stem, the short shaft stem and the standard stem, respectively.

At the stem tip (point 9)

There were strain reductions in the range -25.4%, -33.2%, and -62.2% with the femoral neck stem, the short shaft stem and the standard stem, respectively.

Table 23: Strain reductions on the lateral surfaces, in a percentage to the confidence interval

Lateral surface→	Proximally (Point 1)	Mid of the stem (Point 5)	Tip of the stem (Point 9)
Femoral neck stem	-74.8%	-68.2%	-25.4%
Stem with short shaft	-83.0%	-75.2%	-33.2%
Standard stem	-51.8%	-80.9%	-62.2%

Proximally on the lateral surface (trochanteric region) it was found that the standard stem produced higher strain pattern than the others. This strain is assembly strain indicating areas of local contact between the stem and the endosteal cortical surfaces (see fig. 55, 58, 59).

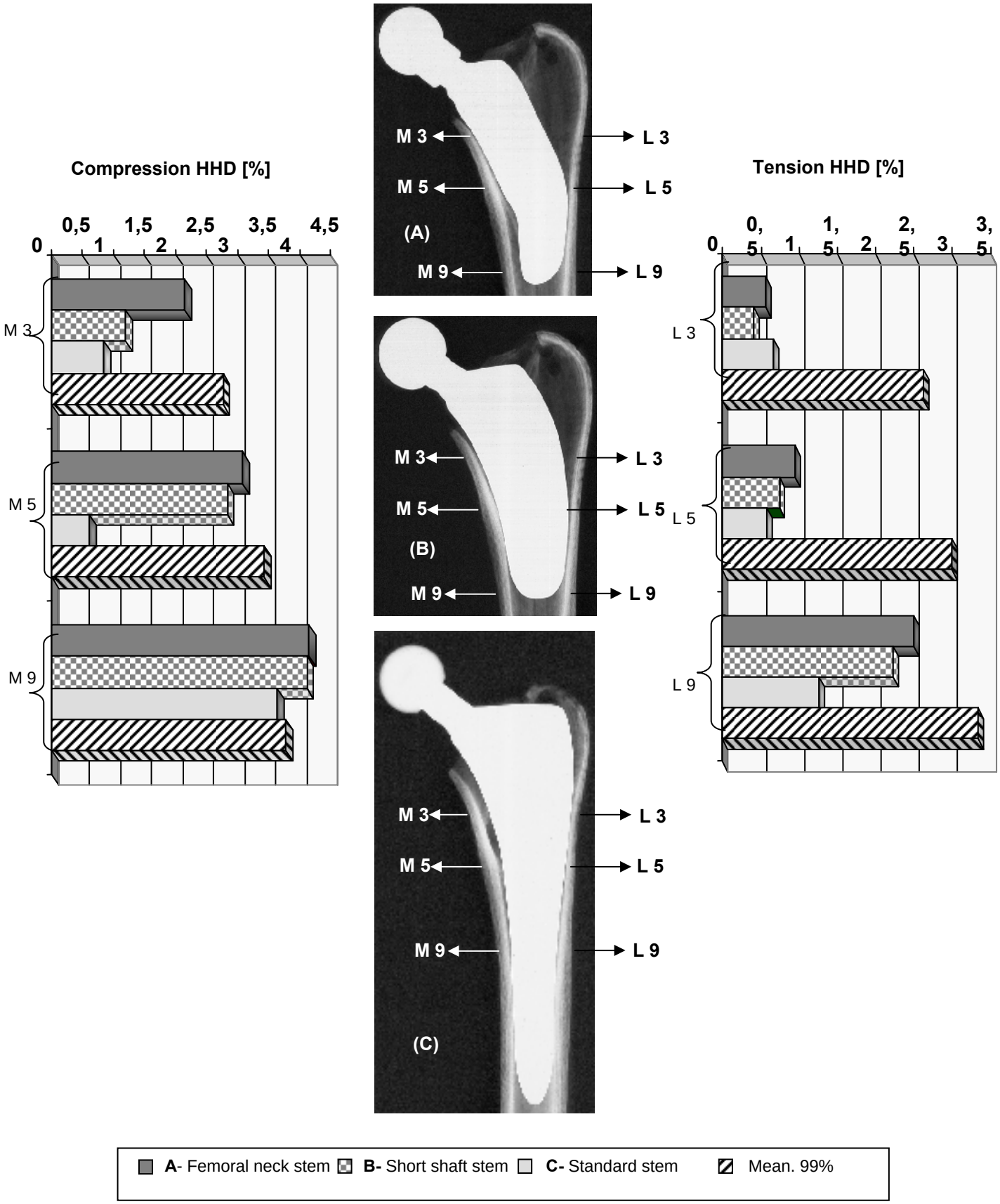

Fig. 55
Roentgenograms and graphs showing, strain reductions along three different locations on both medial and lateral surfaces of implanted femurs with different custom-made stems.

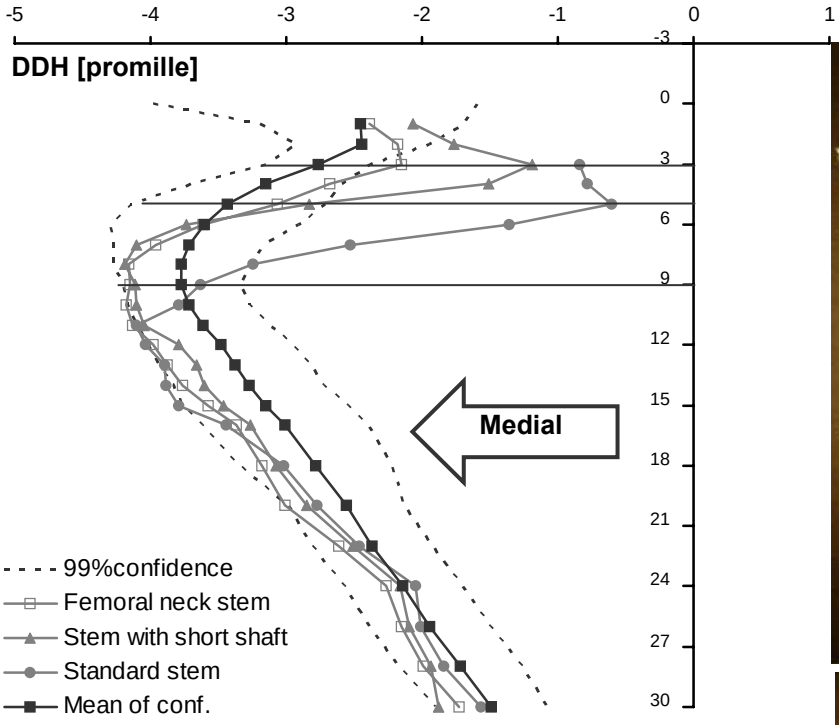

Fig. 56
Strains on the medial surfaces of implanted femurs with three different custom-made stems.

Fig. 57
Photographs showing the medial and the lateral surfaces of the loaded coated composite femurs after implantation with cementless three different custom-made stems (A) femoral necks stem (B) femoral stem with short shaft (C) standard stem, respectively.

(Viewed through a reflection polariscope)

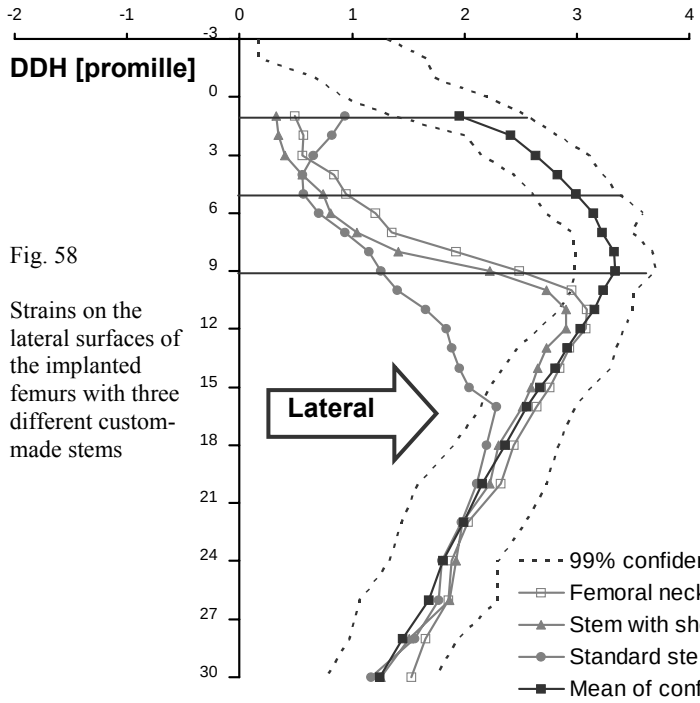

Fig. 58

Strains on the lateral surfaces of the implanted femurs with three different custom-made stems

11. 6. Discussion

Customised stems have been developed to overcome the geometrical mismatch between the femoral canal and cementless stems [2 p. 927, 30 p. 272]. Adaptiva custom-made stems are bone saving stems and can have a minimal invasive procedure during implantation, which is required especially in younger individuals. Conservation of the bone stock is very important, especially when considering that cementless implants are typically used in younger patients where there is high incidence of revision during his lifetime [6 p. 90]. Femoral neck stem which has medio-lateral diameter about 4 mm smaller than the short shaft stem (table 19-21), produced higher strain and smaller stress shielding than the other (see fig. 55, 57).

The standard stem in comparison to the other two stems enlarged in its proximal part (see fig. 50) produced stress shielding more than the other 2 stems. Laterally, there were assembly strains [fig. 59]. If these strains are too high, they can lead to femoral fracture and prosthetic loosing where the pressure-fit occurs between the medial and lateral cortex.

In this study it was found that larger diameter stems produced more stress shielding thus they are expected to cause more pronounced bone loss. This is because the axial rigidity of the implant increases directly with the cross-sectional area or square of the stem diameter, and flexural rigidity increases directly with the area moment of inertia or fourth power of the stem diameter. Thus, a small increase in stem diameter can greatly increase its rigidity. Since, in a composite structure, load is preferentially carried by the more rigid material, the less rigid surrounding bone is relieved of stress to a greater degree with a larger stem [22 p. 54].

Fig. 59

Photographs of unloaded coated composite femur implanted with cementless, custom-made standard stem, showing assembly strains.
Viewed through reflection polariscope
(lateral and medial surfaces from left to right)

There were colourful patches of fringes (assembly strains) on the proximal femoral cortex without loading of the femur. These patches extended till point 16, corresponding to the distal end of the stem. The inserted press-fit of the femoral stem was close to the cortical wall [75 p. 75]. Also micro fracture may occur at strain levels lower than that needed to produce visible fracture. With a cementless total hip arthroplasties, the incidence of femoral fractures has been reported to be as high as 20% in clinical studies [43 p. 479, 486].

Fixation of the implants depends on press-fitting technique and insertion of the stem is critical as long as the degree of the press fitting cannot be controlled. Because the stability of the implant and the load transfer are affected by the insertion forces, we have to accept a certain risk of fracturing the femur to achieve a primary stable implant [15 p. 464].
To obtain a stable fit stem in cementless hip arthroplasty without femoral fracture and compromising stability of the stem, great care is required for preparing the femoral canal to the appropriate size as determined from preoperative templating, using accurate instrumentation and proper selection of the suitable stem size.

Jasty et al. 1993, investigated assembly strains of cementless femoral arthroplasty using photoelastic technique. Insertion of an optimal-size prosthesis after preparing the femoral canal with instruments the same size as the prosthesis produced moderate assembly strains, up to 1,100 micro strains. Half a millimetre press-fit of optimal prostheses produced larger assembly strains, up to 2,000 micro strains. Half a millimetre press-fit of a prosthesis that was also one size (1.0 mm) larger than that determined to be optimum produced even larger assembly strains up to 6,000 micro strain) and longitudinal linear fractures in the femoral cortex. In this project, the standard custom-made stem was evaluated and the data form Jasty apply also purely to a prosthesis of specific design. Therefore, the results cannot be generalized to all cementless stems where many different cementless prosthetic designs rely on press-fit to provide initial stability [43 p. 485, 486].

12. Comparison Between Custom-made and ESKA Implants

12. 1. Characters and Geometrical differences of the Stems

The two femoral components which we used were a standard custom-made stem (Adaptiva, EndoPro medical Company) and a cementless GHE, size 4 (ESKA implants). Aim of this study was to compare the changes in the pattern of the principle strains after implantation of the previous stems in composite femurs. Similarities of the stems included type of fixation (cementless, press-fit), proximal HA coating and no collar.

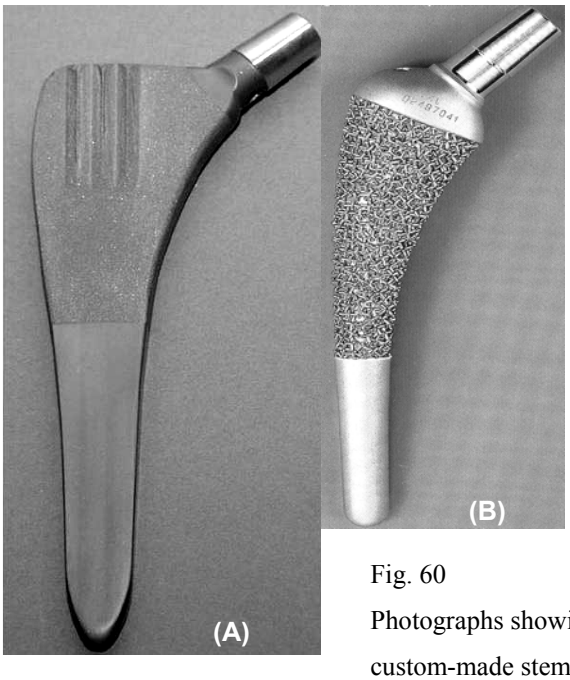

Fig. 60
Photographs showing the standard
custom-made stem (A) and the GHE stem, size 4 (B)

Table 24: Comparison between a standard custom-made stem and a GHE stem, size 4 (see p. 54, 55, 81).

Standard custom-made stem	GHE stem, size 4
Made of titanium alloy Ti6Al4V. Cementless. Collarless. Euro taper 12/14 mm. Length: 160 mm. Straight. Coated by ceramic hydroxyapatite.	Made of cobalt chromium. Cementless. Collarless. Euro taper 12/14 mm. Length: 120 mm. Anatomical. Partial porous coated (can be covered by ceramic hydroxyapatite).

12. 2. Materials and Methods

Each stem was implanted in three coated composite femurs. The set-up and loading protocol were the same for each femur as employed for the intact femur (see page 47). The femoral strain patterns after implantation were measured three times for each femur. The results from both stems were compared with the mean of 99% confidence-interval.

12. 3. Results

Both stems induced significant stress shielding on both medial and lateral femoral cortical surfaces. On the lateral surfaces and proximally on the medial surfaces, the deviation from the physiological strains was pronounced after insertion of the custom-made stem. Distally on the medial surfaces, the custom-made stem induced higher strains than those from the GHE stem (fig. 61, 62).

On the medial surfaces

Proximally, the significant changes were obviously from point 3 till point 7. Strain reductions were in the following forms for the custom-made and the GHE stems respectively. At point 4, were -75.2% and -49.5%. At point 6, were -62.2% and -37.2%. At point 12, increased strain values in the range of +16.0% for custom-made stem and decreased in the range of -9.7% for the GHE stem.

Table 26: Strain changes on the medial cortical surfaces after implantation of the stems.

	Point (4)	Point (6)	Point (12)
Standard custom-made	-75.2%	-62.2%	+16.0%
Cementless GHE, size 4	-49.5%	-37.2%	-9.7%

On the lateral surfaces

Proximally from point 2 till the end of the stems, there were significant strains reductions in the following forms for the custom-made and the GHE stem respectively. At point 2, were - 65.9% and -63.5%. At point 6, were -77.7% and -30.5%. At point 12, were -39.3% and -9.2%.

Table 25: Strain changes on the lateral cortical surfaces after implantation of the stems.

	Point (2)	Point (6)	Point (12)
Standard custom-made	- 65.9%	-77.7%	-39.3%
Cementless GHE, size 4	-63.5%	-30.5%	-9.2%

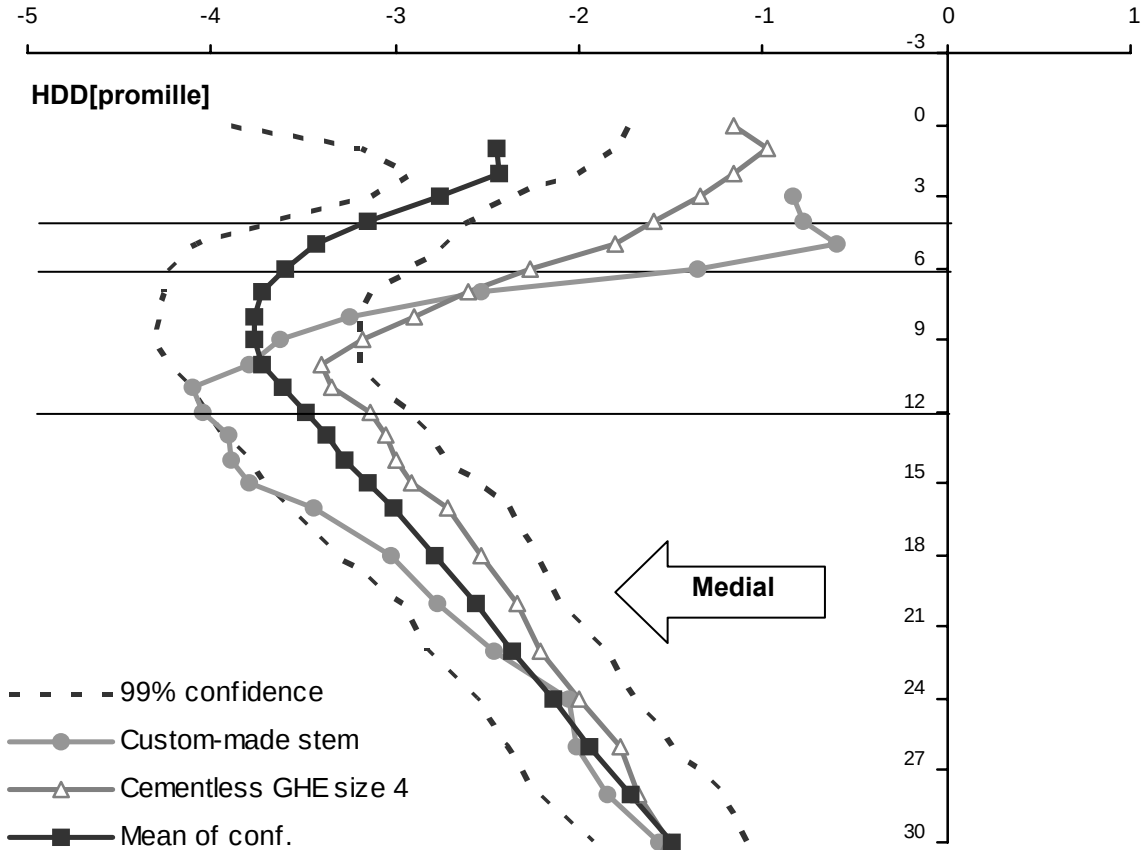

Fig. 61

Strains along the medial cortical bone after implantation of the custom-made and GHE size 4 stems
In comparison with the mean of 99% confidence-interval, determined by unresected femurs.

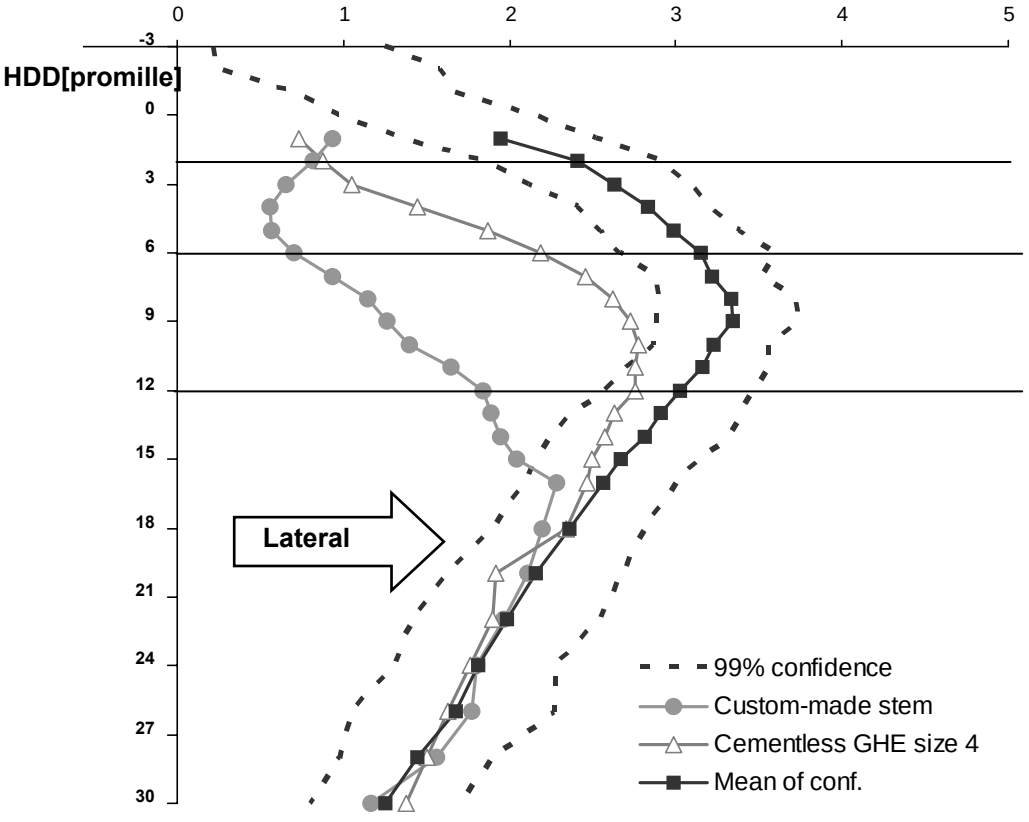

Fig. 62

Strains along the lateral cortical bone after implantation of the standard custom-made and the GHE size 4 stems
In comparison with the mean of 99% confidence-interval, determined by unresected femurs.

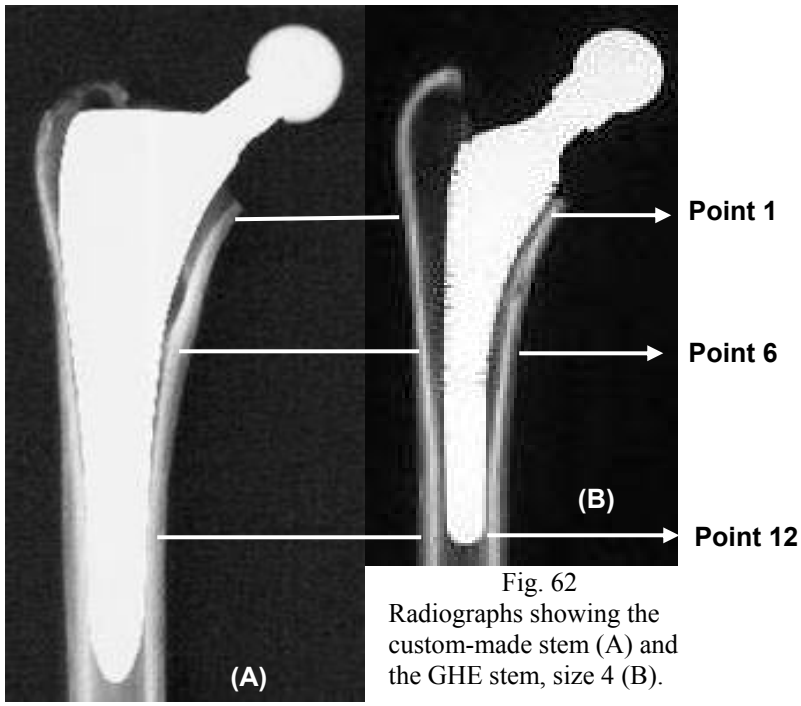

Fig. 62
Radiographs showing the custom-made stem (A) and the GHE stem, size 4 (B).

12. 4. Discussion

In this study, it was found that the custom-made stem induced significant stress shielding more than those induced by the anatomical stem, especially on the proximomedial and lateral regions. The custom-made stem induced higher strain on the distal region, medially.

Aamodt et al. investigated the proximal femoral strain in human cadaver femurs after insertion of a cementless, anatomical stem (Profile; DePuy, Leeds, UK) and a custom-made stem (SCP as., Trondheim, Norway). It has been shown in their study a consistently more physiological pattern of the strain in the proximal femur after insertion of customised stem compared with standard anatomical stem. They investigated stems of specific designs and identical composition (titanium) and suggested that stem sizes and stiffness are not major determinants for stress shielding [1 p. 928]. However, the effect of the stem size and stiffness were dominant design features controlling stress shielding, in our experimental results and in many experimental studies [67 p. 52, 68 p. 203, 6 p. 86, 87, 37 p. 125, 5 p. 196, 205, 22 p. 54].

In this study, the different stem sizes have to be considered were the custom-made stem length was 160 mm and the GHE stem length was 120 mm. The relationship between stem length and canal filling in cementless custom-made total hip arthroplasty was investigated

clinically and it was concluded that superior filling at both the proximal and the distal levels can be obtained by using 100 mm custom made components [63 p. 219, 222]. Hence the custom-made stem was a large canal-filling stem (fig. 62) and had a large cross-sectional area and therefore was stiffer than the anatomical GHE stem and thus induced more stress shielding.
The results are in agreement with the results of the analytical study from Huiskes (1989) which predict extensive stress shielding around canal-filling implants [36 p. 1265]. Engh et al. in the clinical studies have been shown, that the femoral shaft is maximally relieved of stress by a stem that fills the canal [22 p. 54, 23 p. 7].

Distally on the medial surfaces, it has been found that the custom-made stem induced higher strains compared with both the anatomical GHE stem and the mean of the confidence interval. Beside lengths and contouring of the stems, coating geometry and the young's modulus of the material have to be considered because all act in concert relative to the load-transfer mechanism. The role of the proximal porous coating and subsequent bone ingrowth cannot be examined in composite femurs. The lower-modulus material in custom-made stem (titanium) may reduce the stress shielding below the lower proximal region [36 p. 1260]. It has been shown in a clinical study that cortical hypertrophy was most evident in zones 3 and 5 (distal regions) in patients with a tight canal fill, suggesting that it may be an indication of stress transfer to the surrounding cortex [3 p. 115]. It was proved in a post operative radiological study that the straight stem with tight diaphyseal fit transfers strains distally and induced stress shielding proximally [45 p.184, 188].

From a biomechanical point of view, it should be expected with the straight custom-made stem that the proximal bone resorption induces more load transfer to the highly strained distal region. Such a mechanism may eventually cause mechanical failures, especially in young active patients [36 p. 1262].

13. Summary

After femoral implantation, the increased stiffness of the proximal part of the femur will produce marked reductions of the strain magnitudes on the implanted femurs, consequently leading to bone remodelling and resorption. Some degree of stress shielding will occur after any implantation, without regarding to the stem size or method of fixation.

In our study it was found that reducing of the medial offset below the normal offset of the intact femur (46.5 mm) reduced the bending moment and the femoral strains.
Therefore for biomechanical analysis, it is very important to compare different implants with the same offset. It was found that large sized implants induced greater stress shielding. Because excessive stress-shielding is negative for the long-term fixation of an implant it is favourable to use smaller stems to create a situation in which the postoperative femoral strains are kept within acceptable values to the physiological condition to decrease bone resorption. But it has to be considered clinically that cement failure may occur by using very small stems.

It was found in this study that a cementless proximally structured stem, induced strains in the trochanteric region and near the distal end of the stem more than those of a cemented stem which created higher strains only in the mid region. Therefore less adverse bone remodeling may be expected the cementless stem, which could be reflected in increased longevity. With a cementless stem it should be expected that proximal bone ingrowths should force stress transfer at the proximal bone-implant interface, thereby helping to maintain the proximal bone stock and decrease bone resorption.

Investigation of the three different custom-made stems has shown that the standard stem (the largest stem) induced more stress shielding in comparison to the other stems (femoral neck stem and femoral stem with short shaft). Proximally on the lateral surface (trochanteric region) it was found that the standard stem induced higher strain patterns than the others. This strain partially was assembly strain, indicated by areas of local contact between the stem and endosteal cortical surfaces. If these stresses are high, a femur may fracture during impaction of the stem. To obtain a stable fit stem in cementless hip arthroplasty without femoral fracture and compromising stability of the stem great care is required for preparing the femoral canal to the appropriate size as determined from preoperative templating, using accurate instrumentation and proper selection of the suitable stem size.

In comparison between the standard custom-made stem and the anatomical GHE stem, it was found that the changes in the cortical strains were less pronounced for the anatomical stem and this prosthesis consistently achieved a more physiological pattern of strain in the proximal femur than did the standard custom-made stem.

14. References

[1] Aamodt A, Lund-Larsen J, Eine J, Andersen E, Benum P, Husby OS: Changes in proximal femoral strain after insertion of uncemented standard and customised femoral stems. An experimental study in human femora. J Bone Joint Surg 83 (2001) 921-929

[2] Amont A, Lund-Larse J, Eine J, Andersen E, Benum P, Husby OS: In vivo Measurements show tensile axial strain in the proximal lateral aspect of the human femur. J Orthop Res 15 (1997) 927-931

[3] Amstutz H.C, Nasser S, More R.C, Kabo J.M: The anthropometric total hip Femoral prosthesis, preliminary clinical and roentgenographic findings of exact-fit cementless application. Clin Orthop Rel Res 242 (1989) 104-119

[4] Bergmann G, Graichen F, Rohlmann A: Hip joint loading during walking and running, measured in two patients. J Biomech 26 (1993) 969-990

[5] Bobyn JD, Glassman AH, Goto H, Krygier JJ, Miller JE, Brooks CE: The effect of stem stiffness on femoral bone resorption after canine porous-coated total hip arthroplasty. Clin Orthop Relat Res 261 (1990) 196-213

[6] Bobyn JD, Mortimer ES, Glassman AH, Engh CA, Miller JE, Brooks CE: Producing and avoiding stress shielding. Laboratory and clinical observations of noncemented total hip arthroplasty. Clin Orthop Rel Res 274 (1992) 79-96

[7] Bobyn JD, Pilliar RM, Binnington AG, Szivek JA: The effect of proximally and fully porous-coated canine hip stem design on bone modelling. J Orthop Res 5 (1987) 393-408

[8] Breusch SJ, Luboschek M, Kreutzer J. Brocai D, Gruen TA: Dependency of cement mantle thickness on femoral stem design and centralizer. J Arthroplasty 16 (2001) 648-657

[9] Brown I.W, Ring P.A: Osteolytic changes in the upper femoral shaft following porous-coated hip replacement. J Bone and Join Surg 67-B (1985) 218-221

[10] Callaghan JJ, Forest EE, Olejniczak JP, Goetz DD, Johnston RC: Charnley total hip arthroplasty in patients less than fifty years old. A twenty to twenty-five-year follow-up note. J Bone and Join Surg 80 (1998) 704-714

[11] Charnley J, Pusso R: The recording and analysis of gait in relation to the surgery of the hip joint. Clin Orthop Rel Res 58 (1968) 153-164

[12] Cristofolini L, Viceconti M, Cappello A, Toni A: Mechanical validation of whole bone composite femur models. J Biomech 29 (1996) 525-535

[13] Cristofolini L, Viceconti M, Toni A, Giunti A: Influence of thigh muscles on the axial strains in a proximal femur during early stance in gait.
J Biomech 28 (1995) 617-624

[14] Cristofolini L, Viceconti M: In vitro stress shielding measurements can be affected by large errors. affected by large errors.
J Arthroplasty 14 (1999) 215-219

[15] Cristofolini L: A critical analysis of stress shielding evaluation of hip prostheses. Crit Rev Biomed Eng. 25 (1997) 409-483

[16] Crowninshield RD, Brand RA, Johnston RC, Milroy JC: An analysis of femoral component stem design in total hip arthroplasty. J Bone Joint Surg 62 (1980) 68-78

[17] Crowninshield RD, Johnston RC, Andrews JG, Brand RA: A biomechanical investigation of the human hip. J Biomech 11 (1978) 75-85

[18] Davey J.R, O'Connor D.O, Burke D.W, Harris W.H: Femoral Component Offset, It's Effect on Strain in Bone-Cement. J Arthroplasty 8 (1993) 23-26

[19] Davey JR, Harris WH: A preliminary report of the use of a cementless acetabular component with a cemented femoral component. Clin Orthop Rel Res 245 (1989) 150-155

[20] Davy DT, Kotzar GM, Brown RH, Heiple KG, Goldberg VM, Heiple KG, Berilla J, Burstein AH: Telemetric force measurements across the hip after total arthroplasty. J Bone Joint Surg 70 (1988) 45-50

[21] Duda GN, Heller M, Albinger J, Schulz O, Schneider E, Claes L: Influence of muscle forces on femoral strain distribution. J Biomech 31 (1998) 841-846

[22] Engh C.A, Bobyn J.D, Glassman A.H: Porous-coated hip replacement. The factors governing bone ingrowth, stress shielding, and clinical results. J Bone and Joint Surg 69-B (1987) 45-55

[23] Engh CA, Bobyn JD: The influence of stem size and extent of porous coating on femoral bone resorption after primary cementless hip arthroplasty. Clin Orthop Rel Res 231 (1988) 7-28

[24] Estok DM, Orr TE, Harris WH: Factors affecting cement strains near the tip of a cemented femoral component. J Arthroplasty 12 (1997) 40-48

[25] Evarts C M: Biologic fixation. Journal of arthroplasty 1 (1986) 293-296

[26] Finlay JB, Chess DG, Hardie WR, Rorabeck CH, Bourne RB: An evaluation of three loading configurations for the in vitro testing of femoral strains in total hip arthroplasty. J Orthop Res 9 (1991) 749-759

[27] Finlay JB, Rorabeck CH, Bourne RB, Tew WM: In vitro analysis of proximal femoral strains using PCA femoral implants and a hip-abductor muscle simulator. J Arthroplasty 4 (1989) 335-345

[28] Galante JO, Lemons j, Spector M, Willson P D Jr, Wright T M: The biologic effects of implant materials. J Orthop Res 9 (1991) 760-775

[29] Gerlach UJ, Lierse W: Functional construction of the superficial and deep fascia system of the lower limb in man. Acta Anat (Basel) 139 (1990) 11-25

[30] Götze C, Steens W, Vieth V, Poremba C, Claes L, Steinbeck J: Primary stability in cementless femoral stems: custom-made versus conventional femoral prosthesis. Clin Biomech (Bristol, Avon) 17 (2002) 267-273

[31] Grecula MJ, Morris RP, Laughlin JC, Buford WL, Patterson RM: Femoral surface strain in intact composite femurs: a custom computer analysis of the photoelastic coating technique. IEEE Trans Biomed Eng 47 (2000) 926-933

[32] Harman MK, Toni A, Cristofolini L, Viceconti M: Initial stability of uncemented hip stems, an in-vitro protocol to measure torsional interface motion. Med Eng Phys 17 (1995) 163-171

[33] Harris WH: Will stress shielding limit the longevity of cemented femoral components of total hip replacement? Clin Orthop Rel Res 274 (1992) 120-123

[34] Hedley AK, Clarke IC, Kozinn SC, Coster J, Gruen T, Amstutz HC: Porous ingrowth fixation of the femoral component in a canine surface replacement of the hip. Clin Orthop Rel Res 163 (1982) 300-311

[35] Hua J, Walker PS: A comparison of cortical strain after cemented and press-fit proximal and distal femoral replacement. J Orthop Res 10 (1992) 739-744

[36] Huiskes R, Weinans H, Dalstra M: Adaptive bone remodeling and biomechanicaldesign considerations for noncemented total hip arthroplasty. Orthopedics 12 (1989) 1255-1267

[37] Huiskes R, Weinans H, van Rietbergen B: The relationship between stress shielding and bone resorption around total hip stems and the effects of flexible materials. Clin Orthop Rel Res 274 (1992) 124-134

[38] Huiskes R: Failed innovation in total hip replacement, diagnosis and proposals for a cure. Acta Orthop Scand 64 (1993) 699-716

[39] Huiskes R: Stress shielding and bone resorption in THA, clinical versus computer-simulation studies. Acta Orthop Belg 59 (1993) 118-129

[40] Huiskes R: The various stress patterns of press-fit, ingrown, and cemented femoral stems. Clin Orthop Rel Res 261 (1990) 27-38

[41] Husikes R. Biomechanics of artificial-joint fixation. In: Mow V. C., Hayes W.C. Basic Orthop Biomech New York, Raven Press (1991) 375-442

[42] Jacob HA, Huggler AH: An investigation into biomechanical causes of Prosthesis stem loosening within the proximal end of the human femur. J Biomech 13 (1980) 159-173

[43] Jasty M, Henshaw RM, O'Connor DO, Harris WH: High assembly strains and femoral fractures produced during insertion of uncemented femoral components. A cadaver study. J Arthroplasty 8 (1993) 479-487

[44] Joshi M G, Advani S G, Miller F, Santare M H: Analysis of a femoral hip Prosthesis designed to reduce stress shielding. J Biomech 33 (2000) 1655-1662

[45] Laine HJ, Puolakka TJ, Moilanen T, Pajamaki KJ, Wirta J, Lehto MU: The effects of cementless femoral stem shape and proximal surface texture on 'fit-and-fill' characteristics and on bone remodelling. Int Orthop 24 (2000) 184-190

[46] Lewallen DG, Cabanela ME: Hybrid primary total hip arthroplasty, a 5- to 9-year follow-up study. Clin Orthop Rel Res 333 (1996) 126-133

[47] Ling RSM, O'Connor JJ, Lu TW, Lee AJC: Muscular activity and the biomechanics of the hip. Hip Int 6 (1996) 91-105

[48] Madey SM, Callaghan JJ, Olejniczak JP, Goetz DD, Johnston RC: Charnley total hip arthroplasty with use of improved techniques of cementing. The results after a minimum of fifteen years of follow-up. J Bone Joint Surg 79 (1997) 53-64

[49] Maloney WJ, Jasty M, Burke DW, O'Connor DO, Zalenski EB, Bragdon C, Harris WH: Biomechanical and histologic investigation of cemented total hip arthroplasties. A study of autopsy-retrieved femurs after in vivo cycling. Clin Orthop Rel Res 249 (1989) 129-140

[50] Mc Namara BP, Cristofolini L, Toni A, Taylor D: Relationship between bone-prosthesis bonding and load transfer in total hip reconstruction. J Biomech 30 (1997) 621-630

[51] McLeish RD, Charnley J: Abduction forces in the one-legged stance. J Biomech 3 (1970) 191-209

[52] Measurements Group, Inc., USA: Instruction for Casting and Contouring Photoelastic Sheets. Instruction Bull IB-221-C (1982)

[53] Measurements Group, Inc., USA: Instructions for bonding flat and contoured photoelastic sheets to test-part surfaces. Instruction Bull IB-223-E (1982)

[54] Measurements Group, Inc., USA: Instructions for mixing type PL-1 liquid plastic. Instruction Bull IB-233-3 (1993)

[55] Measurements Group, Inc., USA: Instructions for using PC-10 Adhesive. Instruction Bull IB-227 (1982)

[56] Morris R P, Grecula M J, Buford W L, Jr., Patterson R M: Biomechanical and photoelastic evaluation of a new synthetic composite femur bone for use in hip prosthesis studies. Bioengineering conference ASME 50 (2001) 249-250

[57] Nordin M, Frankel V H: Biomechanics of the hip. Basic biomechanics of the musculoskeletal system. Williams & Wilkins. Baltimore.
Philadelphia. London. Second Edition (1989) 135-149

[58] Oh I, Harris WH: Proximal strain distribution in the loaded femur. An in vitro comparison of the distributions in the intact femur and after insertion of different hip-replacement femoral components.
J Bone Joint Surg 60 (1978) 75-85

[59] Otani T, Whiteside LA, White SE: Strain distribution in the proximal femur with flexible composite and metallic femoral components under axial and torsional loads. J Biomed Mater Res 27 (1993) 575-585

[60] Reigstad A, Rokkum M, Bye K, Brandt M: Femoral remodelling after arthroplasty of the hip. Prospective randomized 5-year comparison of 120 cemented/uncemented cases of arthrosis.
Acta Orthop. Scand 64 (1993) 411-416

[61] Rohlmann A, Mössner U, Bergmann G, Kolbel R.: Finite-element-analysis and experimental investigation in a femur with hip endoprosthesis.
J Biomech 16 (1983) 727-742

[62] Rohlmann A, Mössner U, Bergmann G, Kolbel R: Finite-element-analysis and experimental investigation of stresses in a femur.
J Biomed Eng 4 (1982) 241-246

[63] Sakai T, Sugano N, Nishii T, Haraguchi K, Ochi T, Ohzono K: Stem length and canal filling in uncemented custom-made total hip arthroplasty.
Int. Orthop. 23 (1999) 219-223

[64] Sobotta J: Atlas of Human Anatomy, Volume 2 Thorax, Abdomen, Pelvis, Lower Limbs. Edited by J. Staubesand - Translated by A. N. Taylor - Urban & Schwarzenberg, Munich-Vienna-Baltimaore Engl Ed 11 (1989)

[65] Spector M: Historical review of porous-coated implants. J Aarthroplasty 2 (1987) 163-177

[66] St. Terry Canale: Campebell's Operative Orthopaedics, Mosby, St.Louis. Baltamore. Bosten. Carlsbad. Chicago. Ninth edition (1998)

[67] Steinhauser E: Faserverstärkte Kunststoffe in der Tumorendoprothetik des proximalen Femurs. Hieronymus, München, ISBN 3-933083-91-5 (1998)

[68] Sumner DR., Galante J O: Determinants of stress shielding: design versus material versus interface. Clin Orthop Rel Res 274 (1992) 202-212

[69] Sumner DR, Turner TM, Urban RM, Galante JO: Remodelling and ingrowth of bone at two years in a canine cementless total hip-arthroplasty model. J Bon Joint Surg 74 (1992) 239-250

[70] Szivek JA, Gealer RL: Comparison of the deformation response of synthetic and cadaveric femora during simulated one-legged stance. J Appl Biomater 2 (1991) 277-280

[71] Taylor M E, Tanner K E, Freeman M A, Yettram A L: Stress and strain distribution within the intact femur: compression or bending? Med Eng Phys 18 (1996) 122-131

[72] Torchia M E, Ruff C B: A quantitative assessment of cross- sectional cortical bone remodelling in the femoral diaphysis following hip arthroplasty in elderly females. J orthop Res 8 (1990) 883-891

[73] Vander Sloten J, Labey L, Van Audekercke R, Van der Perre G: The development of a physiological hip Prosthesis: evaluation of the strains after implantation of a prototype of hip implant: experiment in a dry femur. Biomed Mater Eng 3 (1993) 1-13

[74] Walker PS, Robertson DD: Design and fabrication of cementless hip stems. Clin Orthop Relat Res 235 (1988) 25-34

[75] Zhou XM, Walker PS, Robertson DD: Effect of press-fit femoral stems on strains in the femur.A photoelastic coating study. J Arthroplasty 5 (1990) 71-82

15. Acknowledgments

I would like to thank

- Prof. Dr. R. Gradinger, medical director of the "Klinik für Orthopädie und Unfallchirurgie der Technischen Universität München" for giving me this fellowship doctoral study and for his being doctor thesis supervisor.

- Dr.-Ing. E. Steinhauser, director of the Biomechanical Laboratory of the "Klinik für Orthopädie und Unfallchirurgie" for his professional technical guide and invaluable help during this study and correction of the thesis.

- Prof. Dr. W. Mittelmeier and PD Dr. G. Gruber for implantation of the femoral stems.

- M. Ellenrieder (doctoral candidate) for his technical supports during coating of the bones, measurements and giving the measurement results for cementless GHE stems.

- All stuff colleges in the Biomechanical Laboratory for their kindly support, especially Dr. med. Dipl.-Ing. R. Bader.

- ESKA Implants GmbH, for the financial support of my scholarship for one year and further for the supply of the implants.

- Endopro GmbH, for supply of Adaptiva implants.

ISBN 978-3-89791-364-6